THE UNIVERSITY OF MICHIGAN

INDUSTRY PROGRAM OF THE COLLEGE OF ENGINEERING

SOME PROPERTIES OF SPRAYS FORMED BY THE DISINTEGRATION OF A SUPERHEATED LIQUID JET

William L. Short

A dissertation submitted in partial fulfillment
of the requirements for the degree of
Doctor of Philosophy in the
University of Michigan
Department of Chemical and Metallurgical Engineering
1962

October, 1962

IP-583

ACKNOWLEDGEMENTS

The author is particularly indebted to many people who rendered assistance during the course of the doctoral program. Sincere appreciation and thanks should go to:

Professor J. Louis York, the chairman of the doctoral committee, for his guidance, assistance and suggestions throughout the course of the work.

Professors A. G. Hansen, R. B. Morrison, M. R. Tek, and G. B. Williams, the other committee members, for their help in interpretive work and in the preparing of this dissertation.

Mr. Gordon Ringrose, who constructed much of the electronic equipment used in the research.

The Allied Chemical Company for their support during the second year of study.

E.I. du Pont de Nemours and Company, who very generously donated the Freons used in this study.

D. P. Kessler who, as a CM 690 project, wrote a portion of one of the computer programs used.

The Industry Program of the College of Engineering who prepared the final form of this dissertation.

TABLE OF CONTENTS

TABLE OF CONTENTS (CONT'D)

LIST OF TABLES

LIST OF TABLES (CONT'D)

LIST OF FIGURES

LIST OF FIGURES CONT'D

LIST OF FIGURES CONT'D

LIST OF APPENDICES

NOMENCLATURE

A_c	Acceleration modulus
A	Area
C	Growth rate constant [see Equation (5.4)]
C	Dimensionless variable [see Equation (5.8)]
C_D	Drag coefficient
C_f	Skin friction coefficient
C_p	Specific heat
D	Diameter of jet or drop
D	Dimensionless variable [see Equation (5.8)]
D_m	Molecular diffusivity
D_t	Thermal diffusivity
D_{mn}	Mean drop diameter
$dw/d\Theta$	Evaporation rate
E	External force
f(x)	Probability distribution function
F(x)	Probability density function
g_c	Conversion factor
h_c	Convective heat transfer coefficient
I	Integral [see Equation (C-8)]
k	Thermal conductivity
k'	Constant [see Equation (5.5)]
k_c	Correction factor [see Equation (7.16)]
k_g	Mass transfer coefficient
K	Evaporation constant [see Equation (6.10)]

m_k	k-th moment about origin
M	Mean molecular weight
M^o	Mass
n	Number of droplets
N	Total diffusion rate
P	Pressure
P_f	Vapor pressure
P_r	Prandtl number
r	Radial distance [see Equation (7.21)]
R	Radius
R	Gas law constant
R	Rosin-Rammler distribution
Re	Reynolds number
s	Radial distance [see Equation (7.21)]
S_c	Schmidt number
t	Time
T	Temperature
T	Dimensionless variable [see Equation (7.5)]
t_m	Mean temperature difference
V	Velocity
W_e	Weber number
$\overline{X}$	Mean of X
Z	Ohnesorge number

Greek

ρ	Density
λ	Wavelength

Θ	Time, spray cone angle
λ_s	Latent heat
μ	Viscosity
σ	Surface tension
ΔT	Superheat
α	See Equation (5.5)
τ	Dimensionless time
β	Dimensionless radius
$\Gamma_\alpha(\ell)$	$\int_0^\infty t^{\ell-1} e^{-t}\, dt$
δ	Uniformity parameter
ϵ	Strain [see Equation (C-3)]

Subscripts

l	**Liquid**
o	**Initial** value
v	Vapor
x	X direction
y	Y direction

ABSTRACT

Classically sprays are formed by pressure atomization, spinning disks and air atomization. The purpose of this study was to study the properties of sprays formed by the flashing of superheated liquid jets and to investigate the variables which control the breakup of a superheated liquid jet.

Sprays were produced by the flashing of superheated water, Freon 11 and Freon 113 using simple orifice type nozzles, having small length to diameter ratios.

The breakup of the superheated jets, as characterized by a shattering temperature, was found to correlate using a simple model relating a shatter temperature group to a function of the Weber number, Ohnesorge number and a vapor to liquid density ratio. The drop size distributions may be satisfactorily represented either by a log normal or a Rosin-Rammler distribution. Mean drop diameters are strongly dependent upon the surface tension of the fluid injected. Spray evaporation rates were calculated using the method of Probert with satisfactory results. The drop velocities were found to asymptotically approach a limiting value which is equal to the induced air velocity.

The breakup mechanism is described in terms of the growth of a vapor bubble in a superheated liquid. The most important variables are surface tension and nozzle diameter. It is pointed out that viscosity likely plays an important role but the range over which the viscosity may be varied at the breakup point is necessarily small.

CHAPTER I

INTRODUCTION

The purpose of any atomization or spray process is to break up a continuous liquid jet into a discontinuous series of liquid droplets of varying sizes. Spray formation is most commonly carried out by pressure injection, by a swirl chamber nozzle or by air atomization. In the first two of these processes the liquid is broken into droplets by the creation of an unstable jet or an unstable sheet of liquid which must disintegrate under the action of pressure and surface tension forces. The sprays studied in this investigation were created, at least in part, by the flashing or vaporizing of a portion of the liquid jet, after it issued from the nozzle.

The purpose of this study is threefold. Firstly, to investigate the effect of fluid properties on the breakup of a superheated liquid jet, and to discover what properties of the injected fluid are most important to the breakup mechanism; secondly, to investigate the drop size distributions which arise from this method of spray creation; and finally to study the effect of distance from the nozzle and position in the spray, upon the average drop diameter; i.e., to determine the effect of evaporation on the drop size distribution and on the average diameter.

Thermodynamically, flashing of a liquid occurs when it is at a temperature greater than the equilibrium temperature corresponding to the pressure of the surroundings. For example, in this sense, liquid water at a temperature above 212 degrees Fahrenheit will "flash" when it is exposed to atmospheric pressure. Under truly adiabatic conditions all of

the vapor formed will receive its heat by conduction through the liquid, at the expense of the enthalpy of the unvaporized portion of the liquid phase. Equilibrium will be reached when the residual liquid phase has cooled to its saturation temperature (212 degrees Fahrenheit for water at atmospheric pressure). Flashing, in the sense defined above, could also result from the vaporization of a gas dissolved in the liquid phase. It has, however, been demonstrated experimentally and with some theoretical justification[5] that this method of spray formation is not as effective as flashing by superheating techniques.

Sprays formed by the "flashing" technique have much different characteristics than sprays formed by pressure injection at a comparable pressure level. The sprays resulting from flashing contain many more small droplets and have a narrower drop size distribution. For example, at an injection pressure of 120 psig, a typical linear average drop diameter reported in this study might be 50 microns, with 90 per cent of all of the drops included within the range of 20 to 120 microns. As a consequence of the larger number of smaller drops, one would expect that the spray would evaporate more rapidly at a given set of conditions of the surroundings than a spray formed by pressure injection and hence one which contained larger drops.

The results reported here consider the breakup of three liquids: water, trichloromonofluoromethane ("Freon 11") and trichlorotrifluoroethane ("Freon 113"). The breakup mechanism is described by the measurement of a "shatter temperature." The meaning of this term and a description of its measurement will be given in considerable detail. A measure of the effectiveness of the breakup of a liquid jet is given by the drop size distribution.

These distributions were analyzed by a photographic technique. The variation of diameter throughout the spray results directly from the study of the drop size distribution throughout the spray.

The flashing process occurs in at least one application since it is likely that the fuel injected into the afterburner of a jet engine is superheated before it leaves the nozzle. An application of a very similar technique is the "aerosol bomb" in which the material to be sprayed is stored in a pressure vessel with a portion of propellant. When the mixture of the material and propellant is injected into the atmosphere, a fine spray results from flashing of the propellant.

CHAPTER II

THEORY AND MECHANISM OF LIQUID JET BREAKUP BY PRESSURE ATOMIZATION

1. The Breakup Regimes

In the past fifty years many excellent papers have been published on the mechanism of spray formation and on the influence which the various fluid properties, such as density or viscosity, have on the breakup of liquid jets. It is not the purpose to present here a complete or even a semi-complete summary of the literature of spray formation. Such literature surveys are available.[9,43] It will be useful to review briefly some of the pertinent references relating to sprays formed by pressure or hydraulic atomization.

Pressure or hydraulic atomization may be defined as a process in which the liquid is forced through an orifice or a nozzle to form an unstable liquid jet or sheet which disintegrates upon leaving the atomizer. Holfelder and Haenlein[20] have observed liquid jet disruption using spark photography, and reported four stages of jet disintegration.

(1) At very low injection velocities the breakup into drops is caused by rotationally symmetric oscillations of the jet surface due to the effect of primary disturbances and surface tension forces.

(2) At higher jet velocities the breakup into drops results from oscillations with the additional effect of air friction.

(3) At larger velocities the breakup occurs through waviness of the jet assisted by air friction.

(4) Finally at still larger velocities there is immediate and complete disruption of the jet, which takes place at or near the orifice. The exact breakup mechanism in this regime is still not known, although one or two theories will be discussed later.

Nukiyama and Tanasawa[37] in a similar photographic study of spray formation distinguished these stages of jet disintegration:

(1) Dropwise splitting of the jet due to surface tension forces.

(2) Twisted, ribbon-like atomization which corresponds to (2) and (3) above.

(3) Filmwise atomization corresponding to (4) above. All of these three regions were observed with the jet velocity increasing from an initially low value.

Ohnesorge[38] found similar stages of jet disintegration and hypothesized that the different stages occur at different values of the Reynolds number and that these values are determined by a characteristic viscosity number. This number is sometimes called the Ohnesorge number, Z, and is given by

$$Z = \frac{\mu}{\sqrt{\rho \sigma D}} \qquad (2.1)$$

where

μ is the liquid viscosity

ρ is the liquid density

σ is the interfacial tension

D is the jet diameter.

Figure 1 is a plot of his relationship between the Ohnesorge and Reynolds numbers. The regimes in this figure labeled I, II and III correspond approximately to the three regions of breakup described by Nukiyama and Tanasawa. Although the boundaries between the regimes have been shown in Figure 1 as having a sharp division, in actual fact there is no sharp or clear cut transition from one breakup mechanism to another. The loci of the transition points could perhaps be more accurately described as a band rather than as a line. For illustrative purposes, the injection conditions for the nozzles and fluids used in this study are shown in the shaded regions of Figure 1. The information portrayed in this figure is taken from Ohnesorge's paper, and it will be utilized later in the description of the breakup of flashing liquid jets.

2. The Breakup Mechanism

The mechanism of the disintegration of a mass of liquid into small drops has been the subject of many theoretical and experimental investigations since the pioneer work of Rayleigh.[46] His efforts were mainly confined to a study of the stability of low speed, non viscous jets; i.e., region (1) described above. Rayleigh concluded that surface tension would cause a small disturbance on the jet surface to propagate and that the wave length of these disturbances having the maximum growth rate would be about 4-1/2 times the jet diameter, and that the drops formed would be slightly less than twice the diameter of the jet itself. His solution neglects any aerodynamic or viscous forces and he therefore has only dealt with the injection of "inviscid liquids" at low velocities.

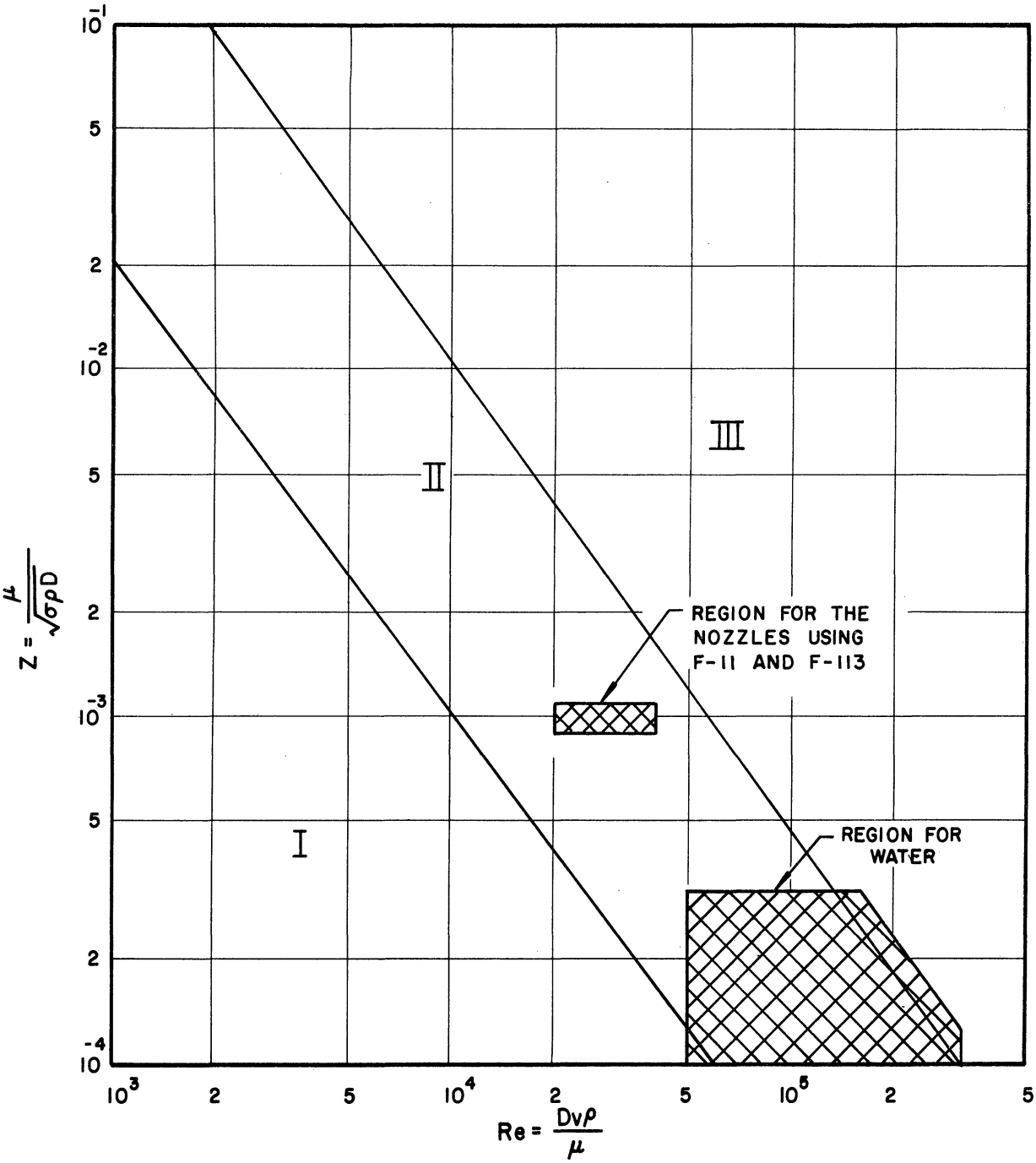

Figure 1. Stages of Jet Disintegration in Relation to the Reynolds Number and the Ohnesorge Number.

Haenlein,[20] among others, showed experimentally that for very viscous liquids the wavelength of the disturbance with the maximum growth rate would be much larger than that predicted by Rayleigh (for example, up to 30 or 40 times the jet diameter for the case of caster oil). Weber[59] studied the same problem theoretically and was able to show that with the inclusion of viscous effects the wavelength of the disturbance with the maximum growth rate is:

$$\lambda = \pi D \sqrt{2\left(\frac{\mu}{\sqrt{\rho D \sigma}} + 1\right)} \qquad (2.2)$$

where

λ is the wavelength

D is the jet diameter

μ is the viscosity

ρ is the density

σ is the interfacial tension.

In the limit of zero viscosity this gives excellent agreement with Rayleighs' results.

Haenlein's experiments were confirmed theoretically by Weber for the first three stages of jet breakup (two stages according to the description of Nukiyama and Tanasawa), but not for the final stage of random and immediate disruption. Weber, from a study of the aerodynamic forces acting on the jet, demonstrated that the breakup time (length) decreases with increasing jet velocity. He also showed that the critical value of the wave length of the disturbance decreased with a dimensionless

constant, which is now called the Weber number. It is

$$N_{We} = \frac{\rho_G V^2 D}{2 g_c \sigma} \qquad (2.3)$$

where

ρ_G is the density of the receiving medium

V is the jet velocity

D is the jet diameter

σ is the interfacial tension

g_c is a conversion factor to engineering units (in an F,M,L,T system)

The liquid velocity at which the aerodynamic forces become important depends upon the physical properties of the liquid and is given, for instance, by Haenlein[20] as 26 feet per second for water.

The third breakup regime, often called wave-like breakup, has been the study of few experimental and/or theoretical investigations. The limited evidence available indicates that it first becomes important at a velocity of about 80 feet per second for water. This critical velocity is dependent upon the physical properties of both the injected and receiving fluids.

Miesse,[34] in a survey of his own and other data, concluded that the last stage of disintegration was determined chiefly by the Weber number and very slightly by the jet Reynolds number.

The theoretical studies described above assume some slight imperfection in the liquid surface, at which point the instability propagates itself to eventually cause the jet disintegration. Some workers have claimed that the important mechanism in atomization is the manner in

which these originally small imperfections are formed. Mehlig[33] cited the importance of the radial components of the velocity arising from turbulent flow through the injector. Thiemann[56] held forth that liquid turbulence is a primary factor in jet disruption. In fact, Schweitzer[50] has shown that a jet can disintegrate without air action, if the turbulence level on leaving the orifice is sufficiently high.

To date, the only theory suggested for the last, and most important region of jet breakup, is the ligament theory first suggested by Castleman.[6] He proposed that disturbances on the liquid surface are acted on by the air stream and that the disturbance is caught up and drawn out as a fine ligament, one end of which remains anchored to the liquid jet. The ligament is then "cut off" by a rapid growth of a dent in its surface and the small detached mass quickly collapses to form a drop. Thus atomization occurs at the gas liquid interface due to the relative velocity between the two phases. Castleman also proposed that in high velocity gas streams ligaments collapse as rapidly as they are formed. A consequence of this line of argument is that a continuing increase in relative velocity will at some point cause no further decrease in the size of the drop formed. Littaye,[28] while agreeing with the theory of Castleman in most respects, does <u>not</u> report a minimum drop size in an atomization process. Hinze[22] has pointed out that even though turbulence may cause the initial disturbances in the jet, these disturbances are most likely amplified by air friction to form ligaments which are torn off to form drops. Thus he, in effect, agrees with the ligament theory.

3. Other Drop Formation Processes

The above discussion has not included two other possible mechanisms of drop formation: secondary atomization and coalescence. While neither of these two methods of drop formation is too important in spray analyses, they will be discussed briefly.

3.1 Secondary Atomization

Secondary atomization may be defined as the formation of drops from drops which have previously been broken off liquid jets. It is a well known fact that a spherical drop, when subjected to a relative velocity in an air stream can, under certain conditions, be unstable and shatter to form two or more smaller drops. The mechanism of secondary atomization has been studied by Lane,[26] Baron,[3] Balje and Larson,[1] Littaye,[29] Siestrunck,[52] Hinze,[21] and Dodd.[10]

Lane, in a photographic study, observed that liquid drops were blown into the shape of a liquid ring with a thin film in the center. This film then expanded to form a hollow bag with a liquid torus rim, and the bag finally shattered to form fine droplets. This was followed by the disintegration of the torus to form larger droplets. Whether or not a drop will be blown into this shape and disintegrated depends upon interfacial tension, drop size, air velocity and the nature of the exposure of the drop to the air (transient or steady flow).

The hollow bag shape observed by Lane was predicted theoretically by Baron. Dodd developed a similar theory to predict the distortion of a water drop exposed to a stream of air with a continuously increasing relative velocity. Probably the most important conclusion to

arise from all of these investigations was the result that a drop will be unstable if its Weber number exceeds a certain limiting value. The numerical values reported for this critical Weber number vary somewhat from investigator in investigator. Richardson[48] reports a value of about 20 and Hinze[22] a value of about 22 for the critical value for water.

Two difficulties arise when attempting to apply the critical Weber number concept to the stability of drops normally encountered in sprays. Firstly, all of the above studies were carried out with drop sizes in excess of one thousand microns, and secondly all of the critical Weber numbers cited refer to non viscous liquids. Certainly an increase in viscosity should make a drop more stable, but no quantitative studies have been made on this point.

3.2 Drop Coalescence

It is possible that at some point fairly far removed from the spray nozzle that the droplets may be moving slowly enough that any "large" drop formed by this mechanism would prove stable. Collision of drops can occur as a result of eddy diffusivity or through varying axial velocities. Very little experimental or theoretical work has been done on the problem of coalescence. The major difficulty lies in the fact that even if a good manner of describing the collision frequency is found, that one still must find some additional information which will determine whether or not drops which do collide in actual fact coalesce. Gorbatschew[18] has shown that the coalescence of colliding liquid drops is dependent upon the liquid properties and the drop size and also upon the angle and velocity of impact.

CHAPTER III

EXPERIMENTAL APPARATUS AND PROCEDURES

In the preceding chapter an outline of the present state of knowledge of spray formation by pressure atomization was given. It is clearly evident that the theories and mechanisms discussed can not apply to sprays formed by a flashing liquid jet, at least not without major modifications.

It is then necessary to devise experimental methods which can be used to investigate this type of spray formation. Three distinct areas of study immediately suggest themselves:

(1) The mechanism of disintegration of a superheated liquid jet. Brown[5] has suggested a theory for this breakup, but because he studied only one system (water), his theory is not of general use.

(2) The heat source for evaporation of sprays formed by this method will be different from those generally reported in the literature and for this reason the means of handling this problem analytically should be investigated.

(3) The drop size distributions and drop velocities should be analyzed and the results compared to any existing data.

With these points in mind the experimental equipment described below was developed. Also various analytical techniques were considered and it was found that photographic analysis would be most suitable for the purposes of this study. The reasons for this choice will be brought out in the succeeding pages.

1. The Injection System

A diagram of the liquid injection system is shown in Figure 2. The system is designed so that "hot" liquids (in this case superheated water) and "cold liquids" (Freon 11 and Freon 113) may all be injected. In both cases the liquid to be injected is fed into the ten gallon tank, and injected as follows:

(a) Superheated Water

The tank is filled to about the mid point with water and steam passed into the tank until the pressure is raised to the pressure of the steam line (about 130 psig). The superheated water is then passed through the double-pipe heat exchanger and out of the nozzle. The spray temperature is controlled by means of the heat exchanger, using cooling water. The nozzle is connected to the piping by means of a heavily insulated flexible coupling.

(b) Freon 11 and Freon 113

These two liquids are injected in essentially the same manner as water, except that the driving pressure is maintained by a nitrogen supply, as indicated in Figure 2. The Freon is superheated as it passes through the heat exchanger, using 130 psig steam as the heating medium.

The flow rate of the injected fluid may be metered using a Fischer-Porter variable area flow meter having a range of 0.026 gallons per minute to 0.211 gallons per minute, or the flow rate may be calculated from the well known orifice equation and from a knowledge of the

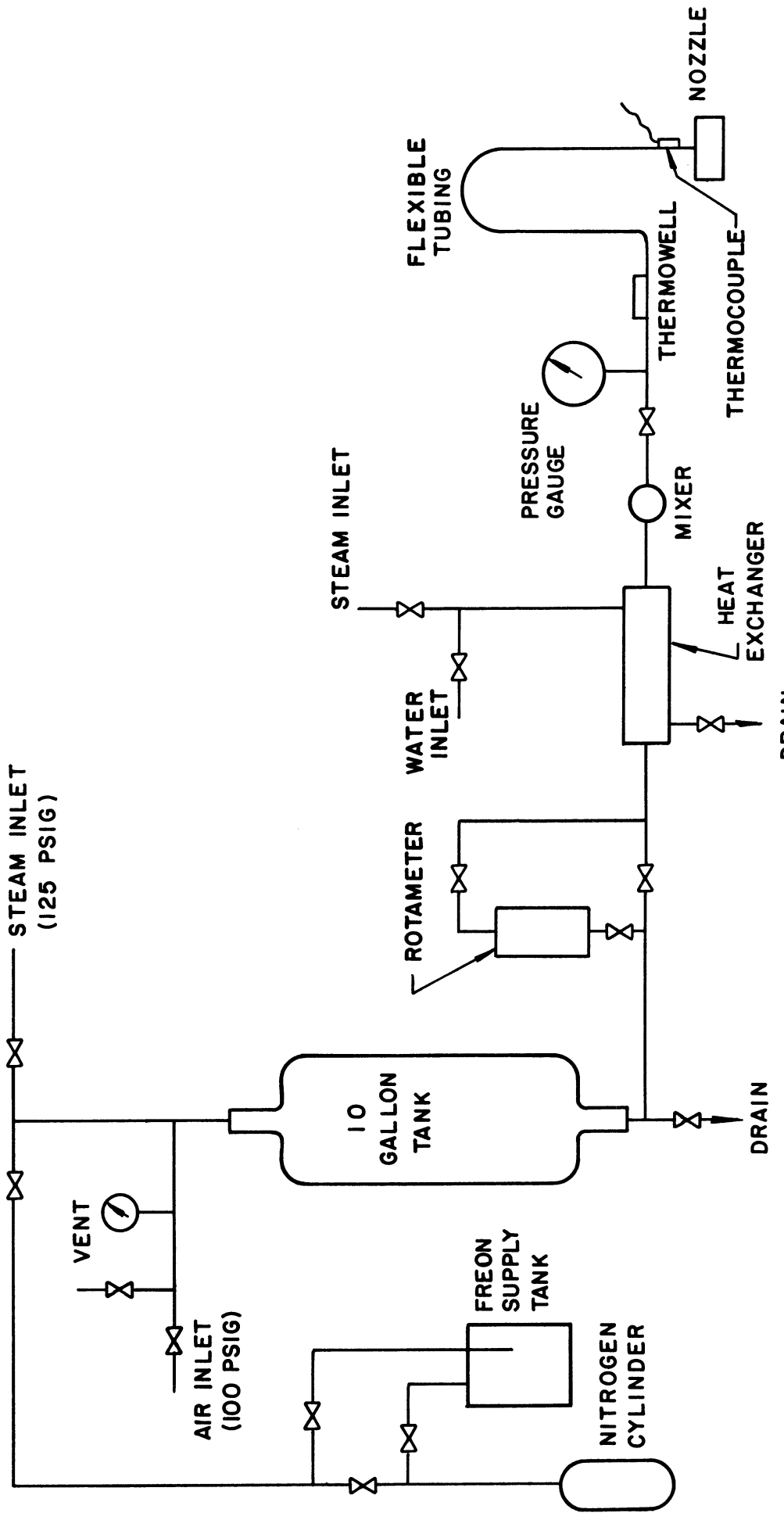

Figure 2. Liquid Injection System.

discharge coefficient. This latter method was nearly always employed. The value of the discharge coefficient was determined experimentally to be about 0.8. The injection pressure is measured with a J. P. Marsh Mastergauge Type 103, which was calibrated by Brown[5] using a dead weight tester. By means of this gauge it was possible to determine the injection pressure to the nearest one half pound. Injection temperatures are measured by a copper-constantan thermocouple, which makes contact with the pipe about one half inch above the nozzle. Both the pipe and as much of the nozzle as possible are heavily insulated to reduce the experimental error to a minimum. In addition, a thermowell is located just downstream from the pressure gauge which can be used as a check on the accuracy and reliability of the thermocouple.

2. Spray Analysis

There have been many attempts made to develop a completely satisfactory method of spray analysis. The large concentration of effort in this area is due, in part, to the very great and numerous experimental difficulties involved. The methods which are normally used can be separated into the following groups.

(a) Slide and cell collection

(b) Size discriminating collectors

(c) Photographic methods

(d) Other optical methods

The most commonly used method for collecting and analyzing drops is coated slides. Such slides are coated with a soft material such as magnesium oxide and are then exposed to the spray for a short

period of time. When the drops strike the coating they leave an impression whose diameter is related to the drop diameter. Analysis may then be carried out by use of a microscope. The primary disadvantage of this method of drop size analysis is that if the spray is carried by a gas which is moving relative to the slide, the slide discriminates against collecting small drops. Hence, the measured average drop diameter will always be too large. A second and obvious difficulty arises from the fact that the impressions left on the slide are not the true drop diameters, and the relationship between the impression diameter and drop diameter must be determined by experiment. A third disadvantage is that some of the large drops may shatter upon contact with the slide. Two other important drawbacks are the problems of coalescence on the slide and evaporation of drops from the slide before the actual counting takes place, if some material other than magnesium oxide is used to coat the slide.

A similar technique is the use of a collection cell. It simply consists of a receptacle filled with a liquid into which the spray droplets fall. This method of analysis has most of the drawbacks associated with a coated slide, but their magnitude is usually decreased.

As pointed out above, the major disadvantage of slides and cells is their tendency to discriminate against collecting small droplets. This phenomenon, known as collection efficiency, is made use of in a sampling device called a jet impactor. This method is not too widely used and it will not be described here.

Aside from photography there are several other optical methods available for the sampling of sprays. One of the very well known of

these techniques is the photometer method of Sauter.[49] By means of this method the volume to surface mean diameter is determined by measuring the decrease in intensity of a light beam passing through the spray. This method gives no information concerning the drop size distribution. In addition to the method of Sauter, there have been attempts to analyze spray droplet sizes by light scattering techniques. These have not proved to be effective for other than a few specialized cases.

The method used in this investigation is photographic analysis. This technique was first successfully used by York[60] in 1949, and has been further developed and utilized by York and Stubbs[61] and Brown,[5] among many others. This method of analysis was chosen for the following reasons:

(a) It is possible to obtain drop velocity measurements which is essential if one is to carry out a study of the spray evaporation. In addition, the drop size distribution should be velocity weighted so that it will be representative of the temporal rather than the spatial distribution.

(b) The analytical technique of counting drops on a photographic negative does not discriminate against small drop sizes (except perhaps for drops below a diameter of ten microns) and the sprays investigated contain a very large number of drops below fifty microns in diameter.

The camera arrangement for the high speed photographs is shown in Figure 3. Light illumination is supplied by two General Electric catalog number 9364688G photolights. These give an extremely intense

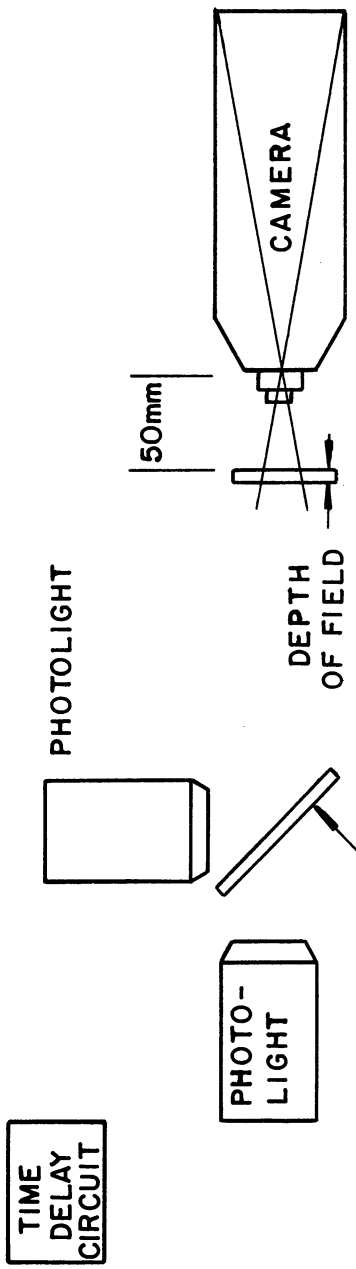

Figure 3. Camera Arrangement for High Speed Photographs.

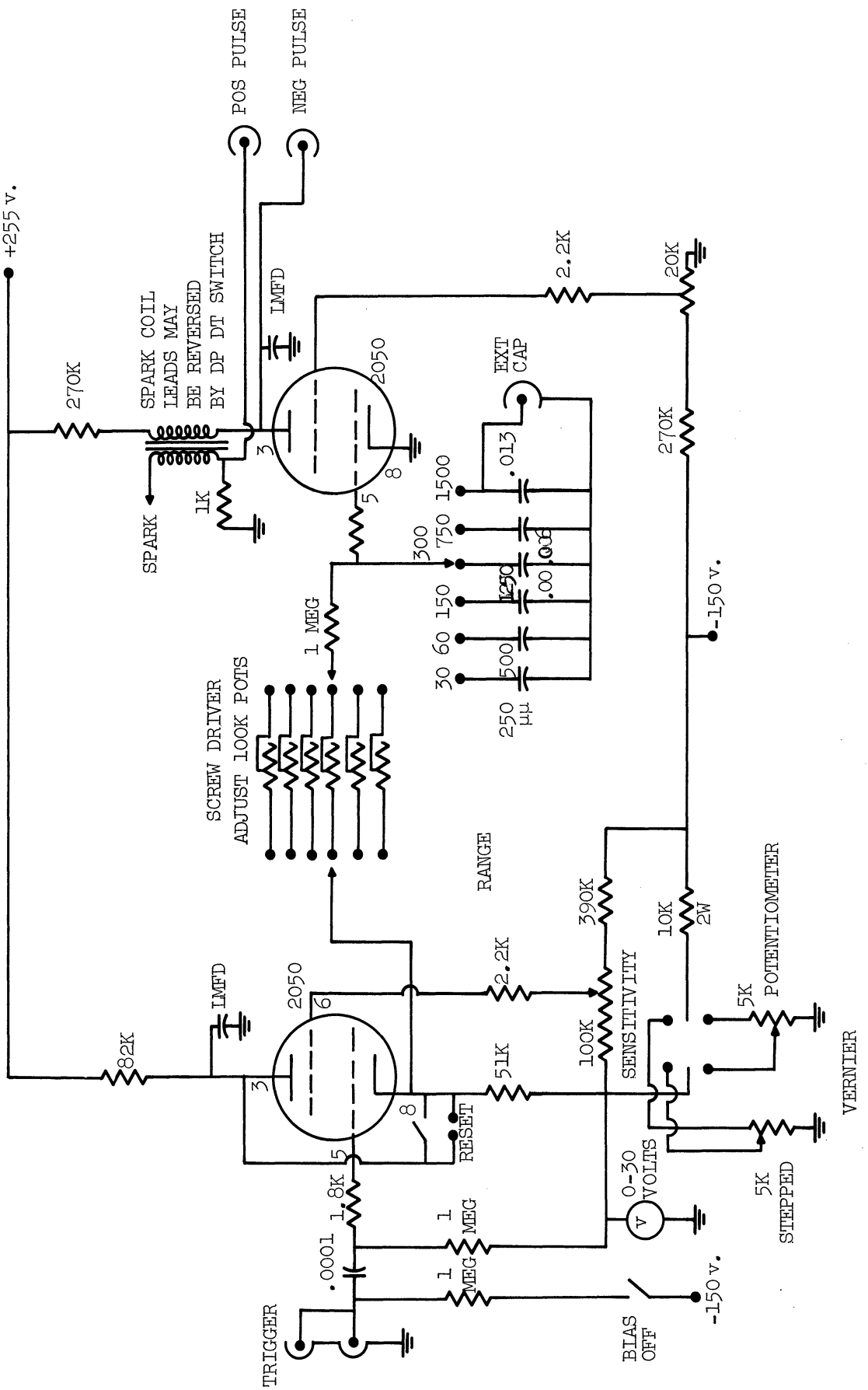

Figure 4. Time Delay Unit.

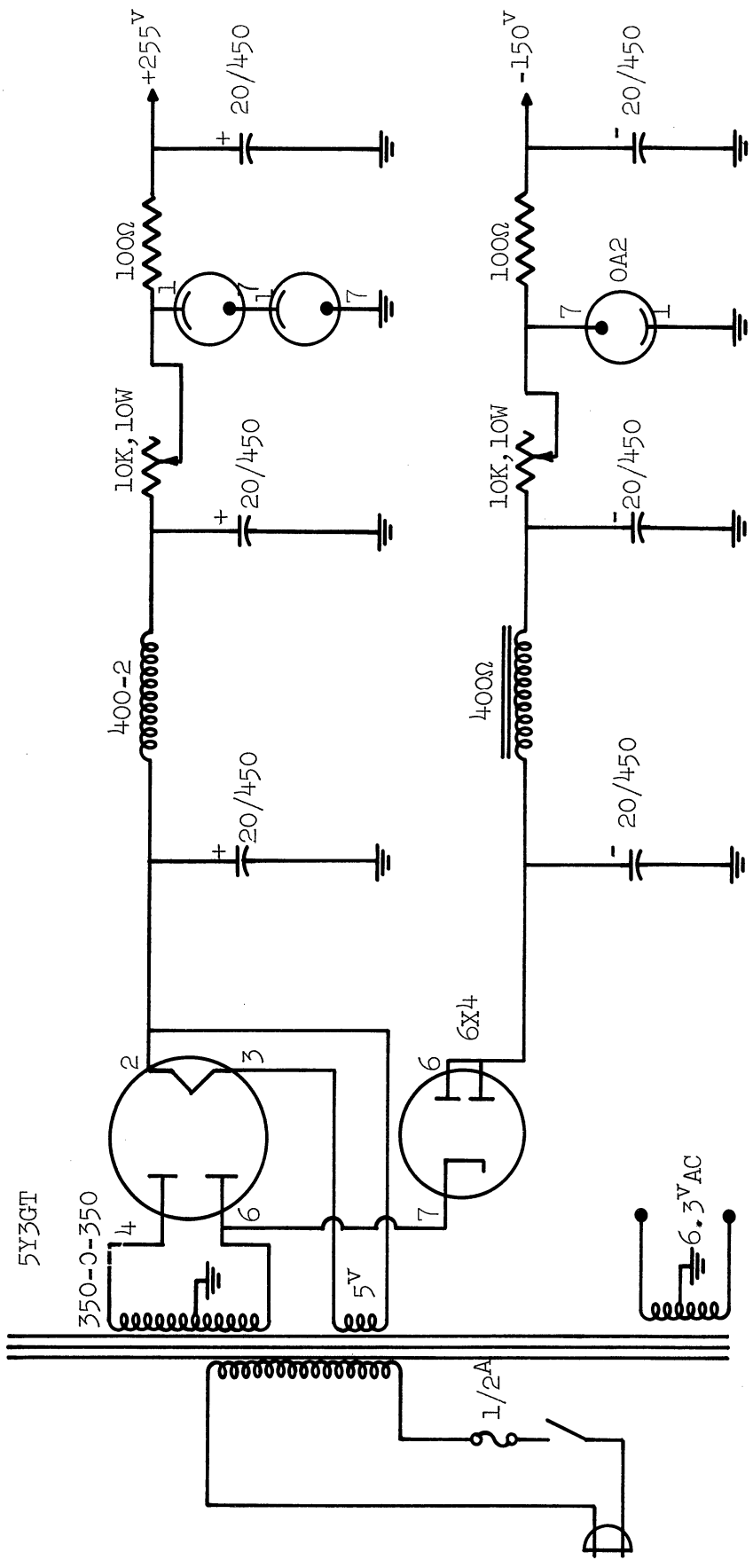

Figure 5. Power Supply for Time Delay Unit.

flash which has a duration of one or two microseconds. The lights are fired by means of the two time delay units shown in Figures 4 and 5. The firing source is a number 2050 thyraton and the time delay may be varied from about 5 to 1500 microseconds. The two delay units are wired in series with the first unit firing the first light and simultaneously supplying an impulse to the second unit which in turn fired the second light. The desired time interval between the two light flashes was set on the second delay unit.

The time delay units were calibrated by photographing the moving teeth on a band saw. Since the linear velocity of the saw blade was known it was a very simple calculation to measure the actual time delay. In order to ensure that the delay circuits remained accurate at all times the time delay was measured for each double flash picture using a Hewlett Packard Model 524B counter (with a model 52CB time interval unit). Also checks were made using photocells to ensure that the response times of the lights were small compared to the time interval between receipt of the high voltage impulse and the flash.

The two lights are placed at right angles to each other, with a half-silvered mirror positioned to provide silhouette illumination from each light. As explained above, if a double flash picture is required, they are discharged with a controlled and measured time interval between flashes. On the other hand only one light is triggered if a single flash picture is required. The latter are used to measure the drop size distributions while the double-flash pictures are used to determine the drop velocities. Double-image negatives were never used to measure drop size distribution.

The camera used was fitted with a 50-mm, f 3.5 lens which had a magnification of 10 X. Each photograph provides an image of the spray in a finite volume, which is about 0.4 X 0.5 X 0.06 inches. The film used in all cases was Kodak Contrast Process Ortho.

In the spray analyses, the nozzle is placed on a movable stand so that samples may be photographed at various spray locations. These locations are shown in Figure 6.

3. Dark Room Procedure

In order to ensure results that are as reproducible as possible, the developing technique was very carefully controlled. The developing tanks were immersed in a bath of running water maintained at 68°F. The films were developed for five minutes in Kodak D-11 developer with fairly continuous agitation, particularly during the first minute. After a 30 second rinse in water they were immersed in Kodak Acid Fix for ten minutes. Following another 30 second water rinse they were placed in a tank of Kodak Hypo Clearing agent for two minutes and then into a water bath for five minutes. All of the solutions were renewed in accordance with the manufacturers' recommendations. A Wratten series 2 red safelight filter was used to control illumination in the dark room.

4. Drop Analysis and Counting

An analysis of a spray location consists of four single-flash and four double-exposure photographs. Only the single-exposure photographs are employed to provide drop size distributions since the double exposure reduces the resolution of the smaller drops. The negatives are projected at an additional magnification of 10 X onto the ground glass

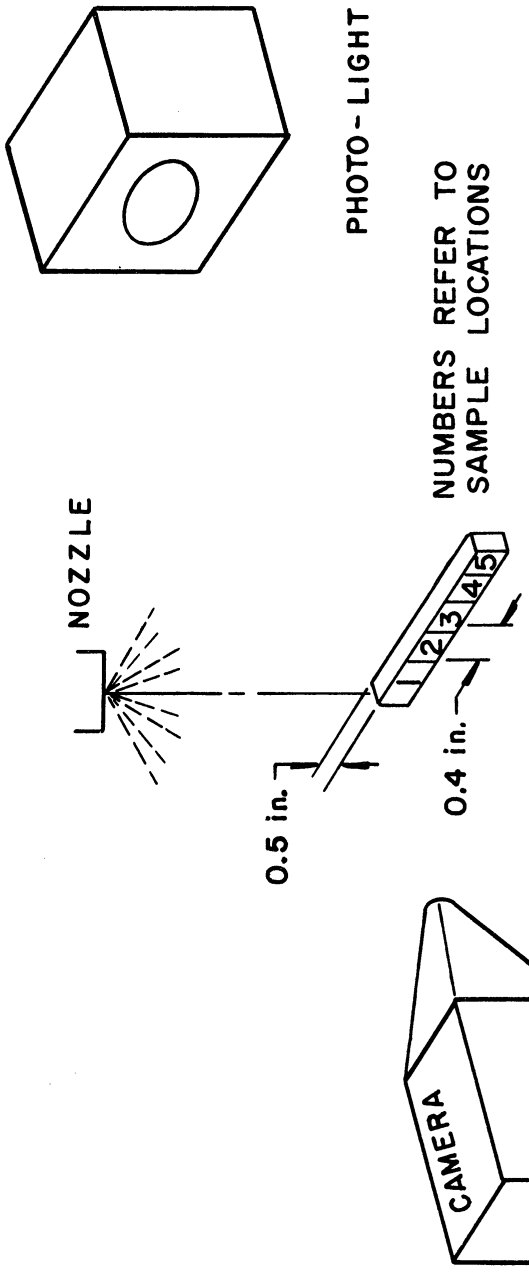

Figure 6. Sample Locations.

screen of an optical comparator, making a total image magnification of 100 X. Since each photograph contains drops which are in sharp focus and drops which are blurred because of displacement just outside the sample volume, a judgment must be made of which drop images are to be considered as part of the sample. To help overcome this difficulty a series of standard drop images has been developed to determine whether individual drop images on the negatives are to be counted. These standard drop images were prepared by Brown(5) and are fully discussed by him.

A word should be said here about the determination of the drop velocities. When measuring the velocity of a particular drop only the linear distance was determined without regard to its actual direction; i.e., no correction was made if the drop was not moving vertically downwards.

The drop count by sizes provides a spatial distribution of the spray, which can be multiplied by the velocities in each size range to obtain a temporal distribution. From this information the surface area flow, volume flow (which may be checked against measured flow rates) and various mean diameters were calculated. A computer program for use with the IBM 709 at the University Computing Center was used for the numerical calculations mentioned above. This program is described in Appendix A.

The question naturally arises, whether the average diameters are dependent upon the number of drops counted; i.e., how many drops must be counted in order to have a statistically meaningful sample? This problem was investigated by Brown(5) and he reached the conclusion that

spray analyses data of this type would be meaningful, in a statistical sense, if a minimum of 200 to 300 drops were counted. Nearly all of the data taken here reports drop counts well in excess of the minimum. The exceptions are for the outer periphery of the spray where the drop number density is too low to fulfill the above requirement with a reasonable number of photographs.

5. Experimental Determination of Shatter Temperatures

The term "shatter temperature" as used here may be defined in the following manner. When the superheated jet leaves the nozzle, its temperature will decrease because of vaporization of part of the liquid and because of convective heat transfer. After a vapor bubble is first formed it will continue to grow as long as the liquid temperature is above the equilibrium temperature. There are then two possible cases:

(1) The vapor bubble will not grow large enough to disrupt the jet and will undergo the so-called growth-collapse phenomenon described by Bankoff and Mikesell.[2]

(2) The vapor bubble will grow large enough to completely disrupt the jet. The lowest temperature at which this occurs is defined to be the shatter temperature of the jet.

In order to measure experimentally the shatter temperature the following procedure was adopted. The fluid to be used was loaded into the receiving tank and it was then ejected through the orifice at the desired pressure but initially at a temperature below the shatter

temperature. The temperature of the fluid was then slowly raised. The occurrence of the shatter temperature was marked by an abrupt change from a continuous liquid jet to a discontinuous liquid jet, i.e., a spray. This change occurred over a range of about five degrees and for this reason the location of a shatter temperature is somewhat arbitrary. The shatter temperatures were all measured using the thermocouple located at the nozzle. In no case was it possible to observe the growth-collapse phenomenon, even though the temperature may be below the shatter temperature. The entire procedure was repeated several times in order to get the best possible estimate of the true shatter temperature. Great care was taken to raise the fluid temperature as slowly as possible to ensure that the thermocouple reading was as accurate as could be obtained.

CHAPTER IV

DISCUSSION OF RAW DATA

In this study three fluids, water, Freon 11 (trichloromonofluoromethane, CCl_3F) and Freon 113 (trichlorotrifluoroethane, $CCl_2F\text{-}CClF_2$) were used. The first two of these were used in the work on velocity profiles, drop size distributions and evaporation effects. All three were used in the investigation of the shatter temperature (this term is defined in a preceding section). The choice of fluids was, in the main, governed by the following considerations:

(1) The fluids must not be flammable or present an explosion hazard.

(2) The fluids must not be toxic.

(3) They should exhibit as wide a range as possible of the significant fluid properties (surface tension, viscosity, density, etc.).

The three fluids used are consistent with these requirements. The selection of the important variables a priori, is a very difficult problem and is best done by good hindsight. The relative roles of the variables will be brought forth in succeeding chapters. Let it suffice to say at this point that the fluids do have a large range of all of the important variables except for viscosity. The reason for this last statement is fully developed in Chapter V.

1. Range of Variables Studied

Table I summarizes the values of the physical properties of water, Freon 11 and Freon 113. It should be noted that in some cases the

TABLE I

PHYSICAL PROPERTIES OF WATER, FREON-11, FREON-113

Property	Water	Freon-11	Freon-113
Liquid Density (lb/ft3)	62.4	91.38	96.96
Viscosity (μ)(20°C)	1.00	-	-
Viscosity (B. Pt.)	0.21	0.405	0.619
Surface Tension (Dynes/cm)	72 (77°F)	19 (77°F)	19 (77°F)
Specific Heat (liquid)(Btu/lb°F)	1.00	0.209	0.218
Thermal Conductivity (Btu ft/hr ft^2°F)	0.394	0.0609	0.0521
Heat of Vaporization (Btu/lb)	970.3	78.31	63.12
Vapor Density at B. Pt. (lb/ft^3)	0.0373	0.365	0.461

TABLE II

EXPERIMENTAL NOZZLE DIAMETERS

Nozzle Number	Diameter, Inches
1	0.0124
2	0.0577
3	0.0425
4	0.0247
5	0.0166
6	0.0183
7	0.0322
8	0.0216
9	0.0168
10	0.0662
11	0.0161
12	0.0310

values of the properties are given at the normal boiling point as well as at room temperature.

Table II depicts the range of nozzle diameters used in the study of the shatter temperature. Only one nozzle diameter was used in the evaporation studies (number 12, 0.031 inches diameter). The nozzle diameters were determined using a Bausch and Lomb microscope equipped with a fylar eyepiece.

2. Size Distribution Data

Table III shows a typical set of raw data which was used to calculate the size distributions and the various mean diameters. The data shown are for the water system injected at a temperature of 287°F and a pressure drop across the nozzle of 120 psi. The data were taken at a distance of four inches from the nozzle. The number of drops and their average velocities are given for the drops which lie within any given size range. The size ranges referred to are those given in Table XXI of Appendix B. The sample locations are those shown in Figure 6. All of the additional data of this type is included in Appendix B.

3. Shatter Temperature Data

Table IV depicts all of the measurements of the shatter temperatures for the three fluids under various flow conditions and using the various nozzles. A part of the data is taken from Brown[5] and is repeated here in order to include it in the correlative and interpretative work, which is discussed in the next chapter.

As can be seen from Table IV, the shatter temperatures were measured for as wide a variation of flow conditions as was possible using the existing experimental equipment.

TABLE III

TYPICAL DROP SIZE AND VELOCITY DATA, WATER SYSTEM
AT A DISTANCE OF 4 INCHES FOR 120 PSIG INJECTION

Location	Photos	Number of Drops in Each Size Range											
		1	2	3	4	5	6	7	8	9	10	11	12
1	2		5	32	123	193	92	28	22	14	2		
2	2		12	78	231	256	100	46	24	20	11	2	
3	2		44	238	304	182	135	53	22	7	1		
4	4		5	34	71	70	96	103	22	6			
		Average Velocities in Each Size Range (Ft/Sec)											
1	4				21.6	31.8	39.9	41.6	97.3		117.5	127	133
2	4			13.9	18.3	33.4	38.4	48.3	83.2	106	110	123	125
3	4			7.44	13.4	18.3	22.0	36.6	55.8	83.7	93.9		
4	4			4.35	7.17	11.3	16.9	27.3	47.3	64.8			

TABLE IV

MEASURED SHATTER TEMPERATURES

Run	Fluid	Measured Nozzle Diameter (inches)	Pressure Difference (Psi)	Shatter Temperature °F
1	F-11	.0161	60	158
2	F-11	.0161	90	153
3	F-11	.0425	78	108
4	F-11	.0425	45	110
5	F-11	.0247	60	152
6	F-11	.0247	89	147
7	F-11	.0247	40	155
8	F-11	.0662	48	85
9	F-11	.0577	45	93
10	F-11	.0310	80	141
11	F-11	.0310	120	134
12	F-11	.0250	94	152
13	F-11	.0577	78	90
14	F-11	.0124	74	164
15	F-11	.0577	62	92
16	F-11	.0577	35	105
17	F-113	.0124	55	150
18	F-113	.0124	75	145
19	F-113	.0247	79	138
20	F-113	.0247	46	144
21	F-113	.0322	58	133
22	F-113	.0322	38	138
23	F-113	.0322	80	135
24	F-113	.0425	80	125
25	F-113	.0425	60	132
26	F-113	.0577	55	123
27	F-113	.0577	80	120
28	F-113	.0577	70	122
29	F-113	.0667	58	120
30	F-113	.0667	80	119
* 31	W	.0247	120	280
32	W	.0247	131	280
33	W	.0322	100	272
34	W	.0322	120	268
35	W	.0322	130	266
36	W	.0662	80	237
37	W	.0662	120	215
38	W	.0310	120	273
39	W	.0310	93	272
40	W	.0310	134	270
41	W	.0350	84	268
42	W	.0350	128	237
43	W	.0557	60	270
44	W	.0557	80	258
45	W	.0557	96	235
46	W	.0557	120	223

* Runs 31 to 46 are from R. Browns data and were experimentally verified in this study.

CHAPTER V

THE BREAKUP MECHANISM

In Chapter II a brief review was given of the theory of the disintegration of liquid jets and it was pointed out that Ohnesorge has presented a convenient graphical method of summarizing the location of the various breakup regimes. Figure 1 depicts this relationship expressed as the Ohnesorge number as a function of the Reynolds number. The approximate positions of the injection conditions for the nozzles used in this study are shown on this figure. Most of the locations corresponding to the injection conditions are seen to be either in region II or on the "boundary" between regions II and III. In other words, the jets will not disintegrate at or very near to the orifice. If disintegration does occur at all, it will result from wavelike breakup at some fairly large distance away from the nozzle. This was borne out experimentally in all cases as none of the jets did disintegrate without the addition of some superheat, but the amount of heat required is strongly dependent upon the nozzle diameter. One must therefore search for a different mechanism of disintegration.

1. The Breakup Mechanism

For the range of nozzle diameters and flow rates studied the controlling mechanism of breakup is bubble growth resulting from the superheat of the liquid, or in other words, "flashing" of the superheated liquid jet.

Thermodynamically, flashing occurs when the liquid is at a temperature above the saturation temperature corresponding to the

pressure of the surroundings. Under truly adiabatic conditions all of the vapor formed will receive its heat by conduction through the liquid, at the expense of the enthalpy of the unvaporized phase. Equilibrium will be reached when the residual liquid phase has cooled to its saturation temperature. Bubble growth can also result from vaporization of a dissolved gas, but it has been shown that this means of breakup is not as effective as superheat.(5)

When the superheated liquid jet leaves the nozzle, its temperature will decrease because of convective heat transfer and vaporization of part of the liquid. The heat loss by convection is small relative to that due to vaporization. The vaporization process generates two types of bubbles: surface bubbles which are easily observed and bubbles which grow in the interior of the liquid jet and which are not observable.

Figures 7, 8 and 9 are photographs of a Freon 11 jet taken just below its shatter temperature. The jet diameter is .031 inches and the injection pressure is 90 psig. The temperatures are 135, 138 and 140°F, respectively. It is easy to see that there are a large number of bubbles present on the jet surface and that the number density of these bubbles increases as the temperature increases. These bubbles do not play a major role in the breakup of the liquid jet. Despite their high frequency of occurrence, their only role seems to be to tear off small ligaments of liquid from its surface, by means of small explosions. These ligaments then form a fine spray or mist which surrounds the remaining, intact portion of the liquid jet. This mist may also be seen on the three photographs. The vapor bubbles appear on the surface (at

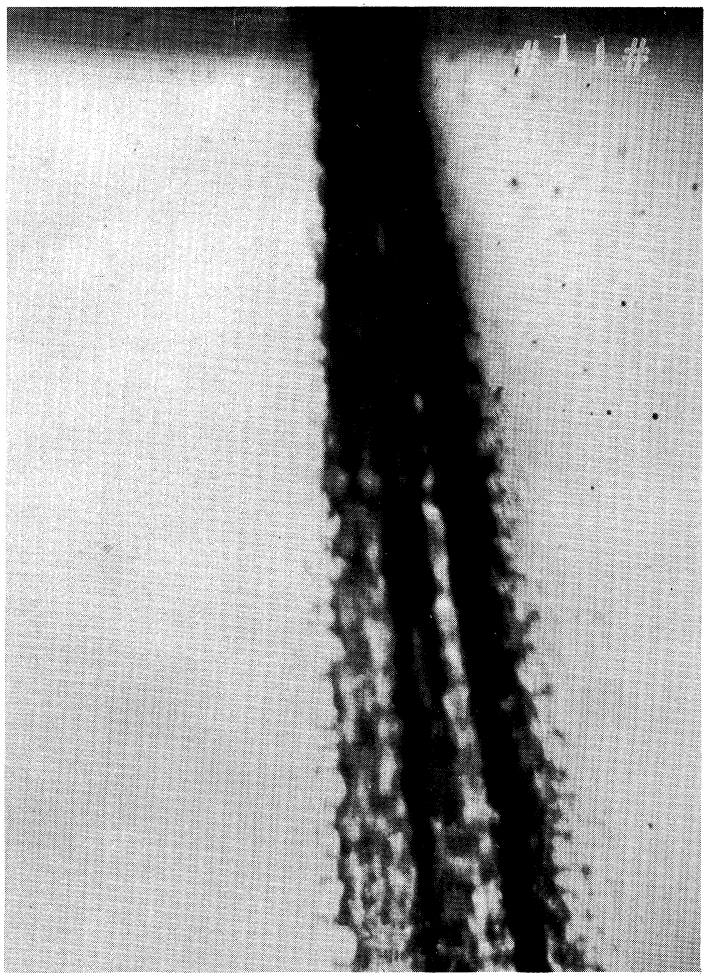

Figure 7. Flashing Jet (10X), 135°F.

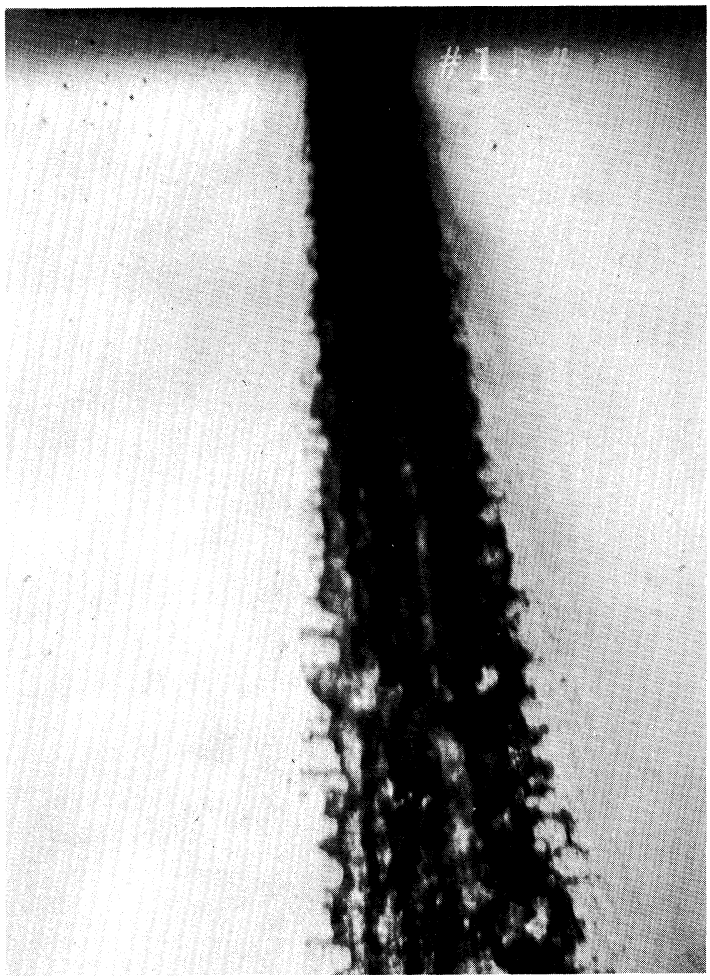

Figure 8. Flashing Jet (10X), 138°F.

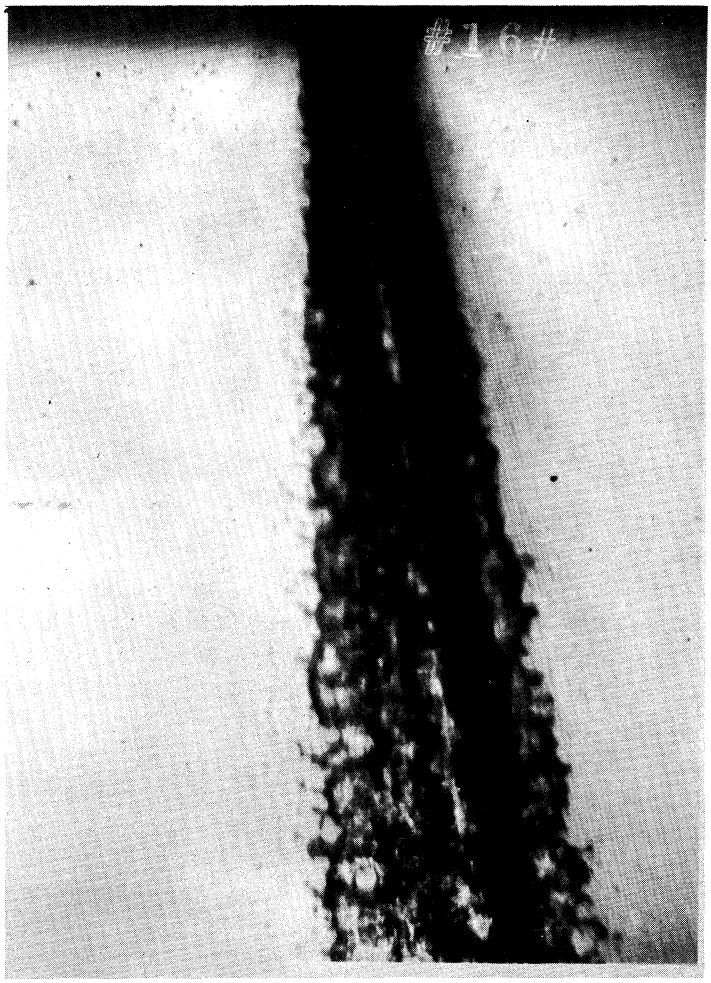

Figure 9. Flashing Jet (10X), 140°F.

least only visually) over a very small temperature range. This temperature range usually extends from the shatter temperature downwards for five or so degrees.

From observation of the surface bubbles it appears most likely that their growth is initiated by some micro disturbance on the jet surface, perhaps due either to roughness or vibration in the nozzle orifice. This supposition is supported in part by the observations of Brown[5] who reported that their occurrence was much less frequent for a sharp edged orifice than for any other type, all other conditions being equal. These bubbles were observed for all three fluids, water, Freon 11 and Freon 113.

The bubbles which are nucleated within the liquid jet and which grow to the required size are those which cause the disintegration of the liquid jet. Considering only these interior bubbles, after one is first formed it will continue to grow as long as the liquid temperature is above the equilibrium temperature. As previously discussed there are two possible cases, and the minimum temperature necessary to shatter the jet is the variable used to define the disintegration point. When the fluid is sprayed into the atmosphere with an initial temperature which is above the shatter temperature, vapor bubbles which are nucleated will grow to a sufficient size to "explode" the liquid jet and form a very fine cloud of liquid droplets.

2. Effect of Fluid Properties on the Breakup Mechanism

If one were to write down, a priori, the various fluid properties which affect this breakup mechanism, the following would certainly

be included--interfacial tension, liquid density, liquid thermal conductivity, vapor density, latent heat of vaporization, degree of superheat (this can be measured in many ways), liquid viscosity and specific heat of the liquid. The most useful manner in which to illustrate the relative role of each of these fluid properties would be to formulate and solve the appropriate differential equation which describes the growth of a vapor bubble in a superheated cylindrical jet. To do this at the present state of knowledge of this problem is exceedingly difficult. Much useful information may be gained from a study of an associated problem--the growth of a vapor bubble in a semi-infinite liquid which has a constant temperature. It is obvious that this immediately rids us of two difficulties:

(1) the non-uniformity of the temperature field

(2) the necessity of having a knowledge of the bubble spacing in the liquid jet.

In recent years a great deal of work has been published in the literature on the growth of vapor bubbles in a superheated liquid. Theoretical studies have been carried out by Plesset and Zwick,[40] Forster and Zuber,[15] Griffith,[19] Poritsky[41] and Shu.[51]

Plesset and Zwick and Forster and Zuber have attacked the problem in essentially the same manner, although the mathematical details are different. They both began with the Rayleigh equation for the motion of a bubble in a non viscous, incompressible liquid,

$$R\frac{d^2R}{dt^2} + \frac{3}{2}\left(\frac{dR}{dt}\right)^2 = \frac{\Delta P}{\rho} \qquad (5.1)$$

where

R is the bubble radius

t is the time

ΔP is the pressure difference between the bubble cavity and the surroundings at an "infinite" distance

ρ is the density of the liquid

and extended it to include the effects of surface tension

$$R\frac{d^2R}{dt^2} + \frac{3}{2}\left(\frac{dR}{dt}\right)^2 = \left(\Delta P - \frac{2\sigma}{R}\right)\frac{1}{\rho} \qquad (5.2)$$

where

σ is the surface tension.

In order to solve Equation (5.2) the pressure difference must be related to the temperature difference. This may be done by assuming that the temperature at the expanding vapor surface is the same as the temperature within the bubble cavity. Both of the authors conclude that there are two distinct regions of bubble growth. In the first of these the bubble radius is of the same order of magnitude as the initial radius and the growth is quite rapid. In the second stage (asymptotic stage) the surface tension and dynamic effects become less important and the growth rate is controlled by the rate of heat conduction from the bulk of the liquid to the bubble wall. They concluded that this growth rate is given by

$$R = R_o + C t^{\frac{1}{2}} \qquad (5.3)$$

where

R_o is the bubble radius at the beginning of the second stage

C is a proportionality constant.

The proportionality constant C in Equation (5.3) is known as the growth rate constant and contains most of the important fluid properties

$$C = \left(\frac{\Delta\tau\, C_p}{H_{fg}}\right)\left(\frac{\rho_L}{\rho_v}\right)\left(\pi \frac{k}{\rho_L C_p}\right)^{\frac{1}{2}} \qquad (5.4)$$

where

Δ_T is the superheat

H_{fg} is the latent heat of vaporization at the saturation temperature

k is the thermal conductivity

C_p is the specific heat

and the subscripts refer to liquid or vapor. It will be noted that the first term in brackets in the above equation is equal to the weight percent flashing.

This solution assumes a perfect fluid and negligible compressibility effects, as is reflected by the terms which appear in the bubble growth rate constant.

Griffith formulated a mathematical model for the growth of vapor bubbles on a heated surface, assuming hemispherical bubbles. His approach was to investigate the problem of conductive heat transfer from the liquid to the growing bubble. Assuming a laminar flow field and

constant fluid properties surrounding the bubble, the equation for the heat transfer process is

$$\nabla^2 T = \frac{\rho_L C_p}{k} \left(\frac{\partial T}{\partial t} + \vec{V} \cdot \nabla T \right) \tag{5.5}$$

where

$\vec{V}$ is the velocity vector.

Griffith solved the problem numerically with the result that

$$R = k' t^{\alpha}$$

where

k' is a constant

α is a number between 1/3 and 1/4.

He also concluded that the average growth rate of a bubble decreased with increasing maximum size and decreased with increasing pressure. At high pressures the maximum size of the bubble was found to be independent of pressure and primarily a function of the thickness of the superheated layer near the surface. This latter is in agreement with Forster and Zuber who state that the thickness of the thermal boundary layer is a very important consideration.

Poritsky has approached the problem in a much different manner, and for demonstrating the role of the fluid properties, a more useful one. Beginning with the Navier-Stokes equations he derived the equation below for the growth of a vapor bubble in a superheated <u>viscous</u> liquid.

$$R \frac{d^2 R}{dt^2} + \frac{3}{2} \left(\frac{dR}{dt} \right)^2 + \frac{4\mu}{\rho R} = \left(\Delta P - \frac{2\sigma}{R} \right) \frac{1}{\rho} \tag{5.6}$$

where

μ is the liquid viscosity.

It is of interest to note in passing, that with a suitable choice of the pressure difference term in Equation (5.6), that it may be also used to describe the collapse of a vapor bubble (i.e., cavitation).

Equation (5.6) may be expressed in the equivalent form

$$(P_o - P_\infty)(R_o^3 - R^3) - \sigma(R_o^2 - R^4)$$

$$+ \frac{\rho R^3}{2}\left(\frac{dR}{dt}\right)^2 + 4\mu \int_o^t R\left(\frac{dR}{dt}\right)^2 dt = 0 \qquad (5.7)$$

where

$P_o - P_\infty = \Delta P$,

and the subscript "o" refers to the initial conditions.

By defining the dimensionless variables

$$\tau = \frac{t}{R_o}\sqrt{\frac{P_o - P_\infty}{\rho}}$$

$$\beta = \frac{R}{R_o}$$

$$C = \frac{4\mu}{R_o\sqrt{\rho(P_o - P_\infty)}}$$

$$D = \frac{\sigma}{R_o(P_o - P_\infty)}$$

Equation (5.7) becomes

$$\frac{\beta^3-1}{3} - D(\beta^2-1) - \frac{\beta^3}{2}\left(\frac{d\beta}{d\tau}\right)^2 - C'\int_0^\tau \beta\left(\frac{d\beta}{d\tau}\right)^2 d\tau = 0 \qquad (5.8)$$

The "C'" in Equation (5.8) is not to be confused with the C previously defined to be the bubble growth rate constant. Equation (5.8) was solved by the method of isoclines for the three fluids, water, Freon 11 and Freon 113. In order to do so a value of $(P_o - P_\infty)$ must be assigned. This was done by using the arithmetic average between the shatter temperature and the saturation temperature for each of the three fluids. For illustrative purposes a nozzle diameter of 0.031 inches and an injection pressure of 120 psig was chosen. This corresponds to the temperatures given in Table V. The mathematical details leading up to Equation (5.8), and for the solution by the method of isoclines is given in Appendix C.

TABLE V

TEMPERATURES FOR USE WITH EQUATION (5.8)

Fluid	Shatter Temp.	Saturation Temp.	Assumed* Temp.
Water	270	210	240
Freon 11	134	72	103
Freon 113	134	116	125

* These temperatures were used in Equation (5.8) to arrive at the curves in Figure 10.

Figure 10 shows the results of the calculations. This is a plot of dimensionless time (τ) versus dimensionless radius (β) for the assumed conditions in Table V. Figure 11 shows the conversion of this plot to a more understandable one of bubble radius versus time. From this it will be observed that the vapor bubble grows most rapidly in the Freon 113 and least rapidly in the Freon 11 fluids at the temperature which is assumed to describe its growth throughout its lifetime. The curves on Figure 10 correspond to the values of C and D given in Table VI below.

TABLE VI

VALUES OF DIMENSIONLESS CONSTANTS IN EQUATION (5.8) FOR FIGURE 10

Fluid	C	D
Water	.0445	.201
Freon 11	.140	.1345
Freon 113	.0661	.0728

Changes in the constants C and D reflect a change of viscosity and surface tension as well as other fluid properties. A value of C = 0 represents an inviscid fluid and a value of D = 0 a fluid with negligible surface tension. From a study of the properties of the solutions to Equation (5.8) Poritsky has shown that an increase in D merely decreases the initial growth rate but after a short period of time the bubble growth rate becomes equal to that of a fluid having the same value of C, but a lower value of D. An increase in C causes an abrupt decrease in the rate of growth of the vapor bubble. Poritsky has presented

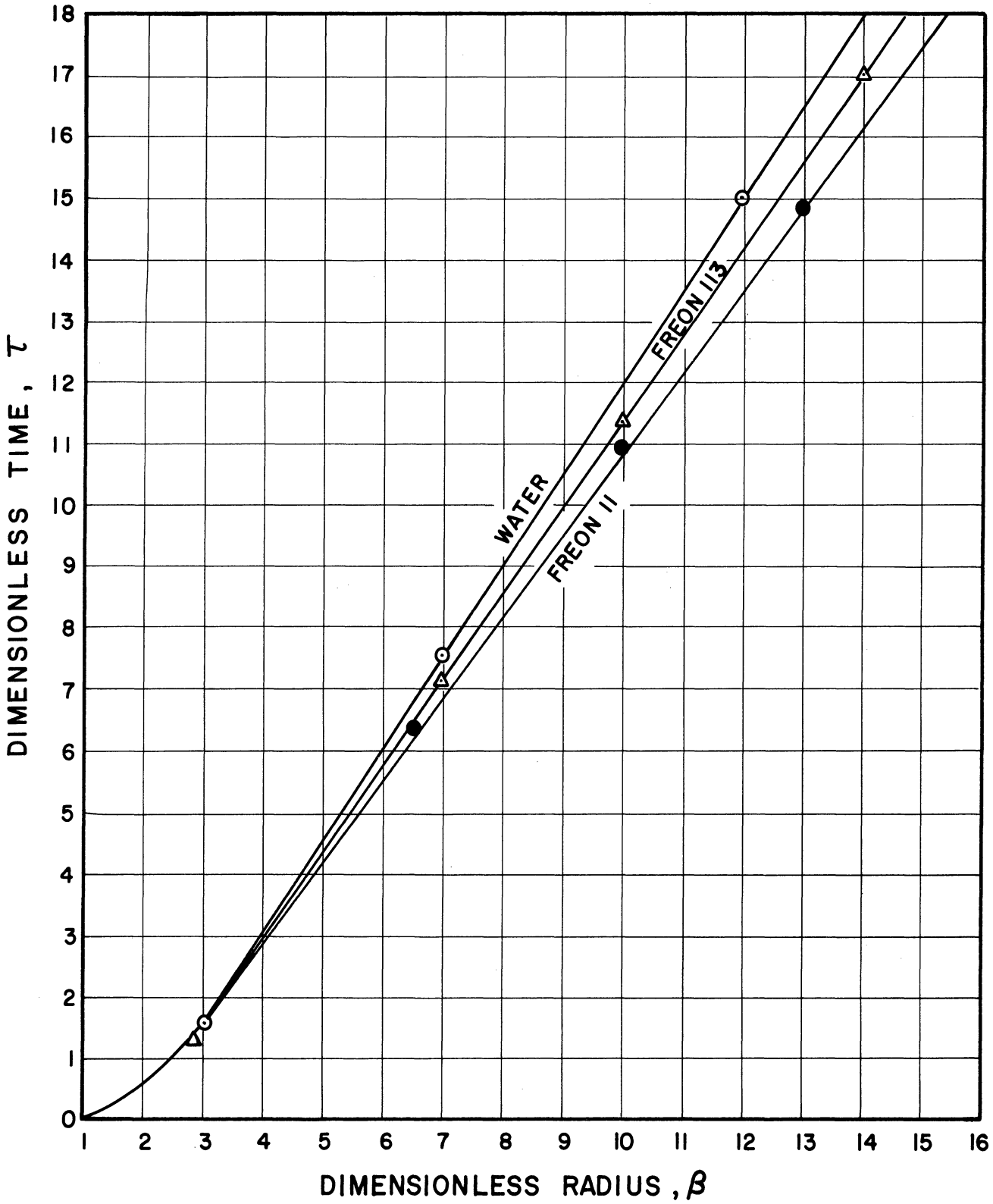

Figure 10. Plot of Dimensionless Time versus Dimensionless Radius for Water, Freon 11 and Freon 113.

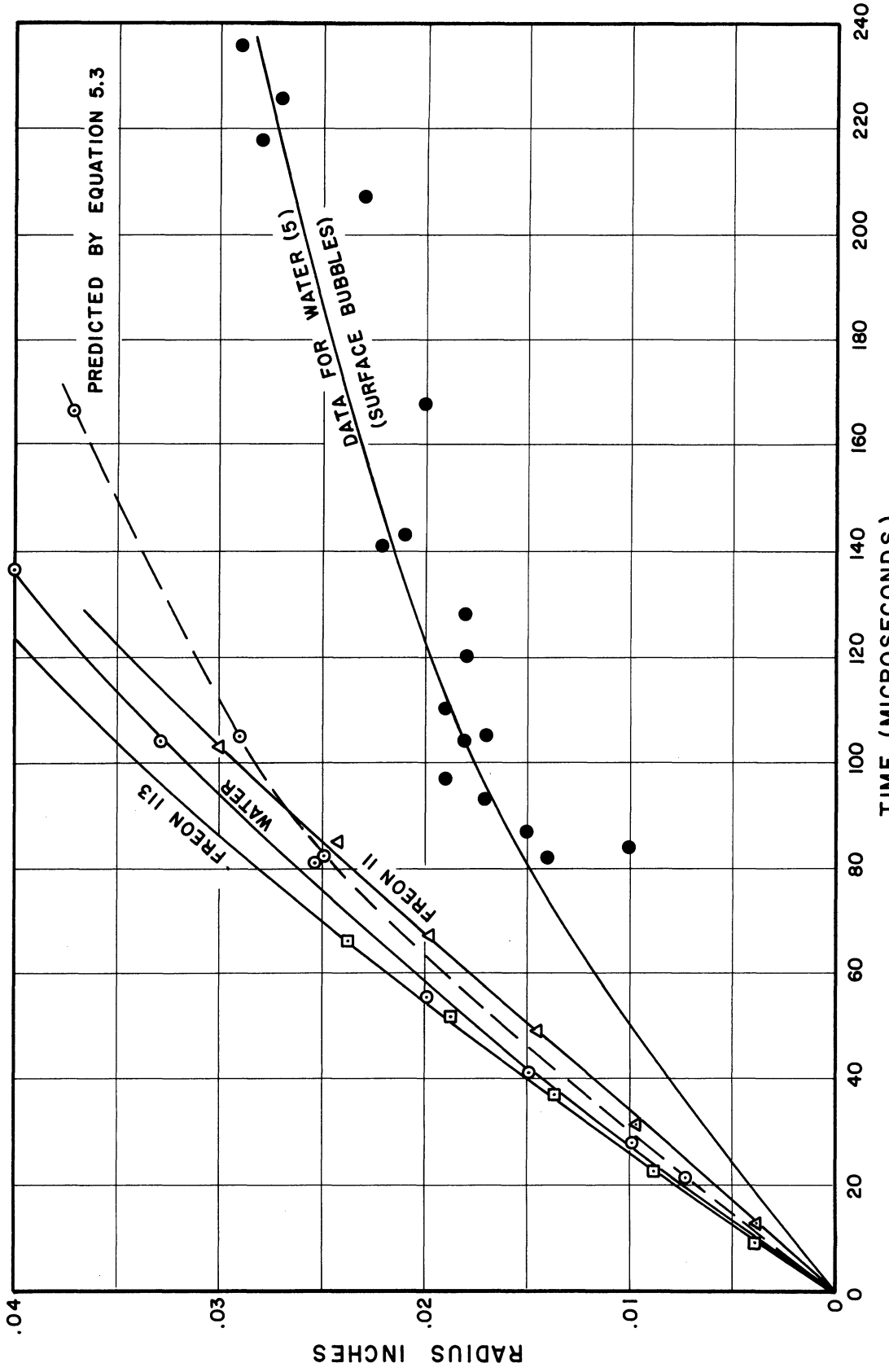

Figure 11. Growth Rate Curves for Water, Freon 11 and Freon 113.

curves which show this effect. The effect of the fluid properties may be summarized as follows:

(1) An increase in viscosity will cause a marked decrease in the bubble growth rate.

(2) An increase in fluid density will cause a slight increase in the bubble growth rate.

(3) An increase in surface tension will cause a slight decrease in the growth rate but at large bubble diameters (say .05 or more inches), this effect will not be very noticeable.

(4) An increase in the vapor pressure difference term will result in an increase in the growth rate. This effect will be partially offset by a decrease in the minimum bubble radius.

It is interesting to determine the agreement between Equations (5.8) and (5.3) and between Equation (5.8) and the experimental data of Brown[5] for the growth of vapor bubbles on the surface of a superheated liquid jet. This comparison is shown in Figure 11 and it will be seen that the deviation is not too large considering the assumptions involved in determining the initial radius.

3. Effect of Physical Variables on the Breakup Mechanism

The term physical variable is used here to represent any variable which may be changed by experiment, e.g., pressure drop, diameter of the nozzle etc., as opposed to the other variables such as surface tension which were called fluid properties. These latter, of course, may not be altered at will.

As would be expected from the introductory material of Chapter II, the physical variables must also play a role in the shatter of the jet, albeit a sometimes passive role. This is clearly demonstrated from the data of Table IV. Consider for example runs number 5, 6 and 7. These three runs are all at the same nozzle diameter and using Freon 11. The only variable present is the pressure drop across the orifice. A decrease in the pressure in all cases causes an increase in the shatter temperature. The magnitude of the change of temperature is dependent upon the fluid and upon the jet diameter, but in general a lowering of the pressure by 60 psi results in an increase in shatter temperature of from five to ten degrees. To phrase it in a different manner, at the same bubble growth rate one liquid jet will be disintegrated while the same jet, but at a lower pressure, will not be broken. From the data of the same table it will also be seen that at any given pressure level the shatter temperature decreases rapidly with increasing nozzle diameter. Both of these effects can be predicted in a semiquantitative way, using jet stability theory. Consider for example Figure 1. At one given diameter as the pressure drop decreases the Reynolds number also decreases, tending to move the location of a point horizontally to the left. Also as diameter increases for any given value of the pressure level, the Reynolds number increases directly, tending to move a point on Figure 1 downward and to the right.

We may think of any action which causes a point to move towards the boundary between regions II and III as reducing the jet stability and bringing it nearer to immediate disintegration. Such a movement should require less energy to be imparted to the jet by vapor

evolution in order to disintegrate it. Since this latter energy may be characterized by the shatter temperature, the effects described above are precisely what would be expected.

Attention should also be drawn to runs 3 and 24, of Table IV. These two runs are for the same nozzle diameter and at essentially the same injection pressure, but the two fluids are different. The shatter temperature for Freon 11 is 108°F and for Freon 113 is 125°F. These two temperatures represent superheats of 36 and 8°F, respectively, and a weight per cent flashing of 14.5 and 3.75 per cent. Also the temperature required to shatter the smallest jet represents much less superheat for Freon 113 than it does for Freon 11. This occurs in spite of the fact that the important fluid properties of surface tension, liquid and vapor density, latent heat of vaporization, thermal conductivity and viscosity are not too much different from each other. This large difference in the weight per cent flashing is attributable to the fact that the vapor bubbles grow more rapidly in Freon 113 than in Freon 11 at the shattering conditions, as is illustrated by Figure 11, and to the effect of temperature on the liquid viscosity. This further serves to point out the interplay between all of the fluid properties in affecting the disintegration of the jet by flashing.

One might well ask at this point what effect if any does the level of turbulence have upon the shatter temperature (or upon the bubble growth rate since the two are interrelated)? It will be recalled that the solution to the bubble growth rate problem assumes a laminar flow field immediately surrounding the expanding bubble wall. If this

assumption is not valid then turbulence should be accounted for in some manner; i.e., the exclusive consideration of the heat conduction problem is invalid. It can be shown that the characteristic diffusion length is about 5 to 10 per cent of the film thickness for heat transfer and thus the thickness of the layer surrounding the bubble in which the major temperature drop occurs is much less than the thickness of the laminar boundary layer. As a consequence the effect of turbulence upon the bubble growth rate should be negligible for the cases studied.

4. Shatter Temperature Correlation

A correlation of the shatter temperatures was developed, using the approach of dimensional analysis. Assuming that the shatter termperature, designated by T, is a definitive characteristic of the jet breakup, a relationship may be sought of the form:

$$f(T, D, V, \Delta P, \rho, \mu, k, H_{fg}, \sigma) = 0 \qquad (5.9)$$

where

H_{fg} is the latent heat, and

$f(T,D,V,\Delta P,\rho,\mu,\sigma,k,H_{fg})$ represents an unknown function to be determined.

Examination of Bernoulli's equation for flow through a nozzle shows that V and ΔP are not independent and only one of them need be considered. Eliminating the variable V and applying the standard method of dimensional analysis and assuming a power relationship yields the equation

$$\frac{Tk}{\mu H_{fg}} = a(N_{we})^b (Z)^c \qquad (5.10)$$

The constants a,b,c were determined by regression for the three fluids individually and for the three fluids combined. For the individual cases Equation (5.10) becomes, for water,

$$\frac{Tk}{\mu H_{fg}} = 0.705 \left(N_{we}\right)^{-0.560} \left(Z\right)^{-0.134} \qquad (5.11)$$

for Freon 11,

$$\frac{Tk}{\mu H_{fg}} = 26.3 \left(N_{we}\right)^{-0.021} \left(Z\right)^{-0.608} \qquad (5.12)$$

and for Freon 113

$$\frac{Tk}{\mu H_{fg}} = 0.914 \left(N_{we}\right)^{-0.875} \left(Z\right)^{0.0899} \qquad (5.13)$$

The over-all correlation coefficients for the three equations are 0.89, 0.84 and 0.98, respectively. The values of the dimensionless groups are given in Table VII.

The exponent on the Weber number in the above equations is negative for all three fluids which is to be expected from the remarks previously made about the stability theory of liquid jets. The exponent for the Ohnesorge number is also negative, except for Freon 113 and for this latter case the value is very near to zero.

As a part of the computer program used to determine the best equations (in a statistical sense), the correlation coefficients between the Weber and Ohnesorge numbers were calculated. These are 0.21, 0.73

TABLE VII

CALCULATED VALUES OF DIMENSIONLESS GROUPS FOR BREAKUP DATA

Run	Fluid	$\frac{Tk}{\mu H_{fg}}$	N_{We}	Z (x 10-3)	Bubble Growth Rate Constant ($Ft/Hr^{1/2}$)	$\frac{Tk}{\mu H_{fg}}$ Calculated Eq. (5.11, 12 or 13)	$\frac{\rho_V}{\rho_L}$ x 10-3
1	F-11	.648	5.49	2.96	6.35	.674	15.8
2	F-11	.637	8.16	2.99	5.95	.659	14.75
3	F-11	.483	17.95	2.18	2.75	.514	7.23
4	F-11	.503	10.42	2.15	2.90	.530	7.47
5	F-11	.633	8.43	2.42	5.90	.578	14.62
6	F-11	.621	12.3	2.45	5.55	.567	13.5
7	F-11	.643	5.54	2.40	6.10	.593	15.2
8	F-11	.429	16.8	1.89	1.10	.473	4.93
9	F-11	.451	13.85	1.95	1.70	.489	5.53
10	F-11	.601	13.81	2.23	5.10	.531	12.37
11	F-11	.577	20.6	2.27	4.60	.521	11.05
12	F-11	.637	13.3	2.41	5.90	.558	14.6
13	F-11	.443	27.6	1.971	1.50	.468	5.25
14	F-11	.656	5.23	3.48	7.15	.746	17.38
15	F-11	.449	19.0	1.985	1.60	.484	5.44
16	F-11	.487	10.85	1.855	2.50	.483	6.86
17	F-113	.496	4.07	4.95	2.50	.501	8.60
18	F-113	.480	5.51	5.15	2.17	.490	7.65
19	F-113	.456	11.55	3.78	1.70	.447	7.02
20	F-113	.477	6.77	3.65	2.10	.466	7.77
21	F-113	.442	11.02	3.39	1.38	.444	6.46
22	F-113	.456	7.23	3.32	1.70	.460	7.02
23	F-113	.448	13.91	3.35	1.50	.435	6.68
24	F-113	.415	19.91	3.08	1.30	.418	5.60
25	F-113	.434	14.95	2.96	1.60	.427	6.32
26	F-113	.408	18.50	2.65	0.65	.415	5.40
27	F-113	.398	26.7	2.74	0.42	.403	5.11
28	F-113	.411	23.4	2.68	0.58	.407	5.31
29	F-113	.398	22.5	2.53	0.42	.406	5.11
30	F-113	.396	30.9	2.54	0.30	.395	5.03
31	W	.736	5.63	0.903	16.3	.638	2.06
32	W	.729	6.14	0.915	15.9	.649	1.995
33	W	.665	4.78	0.931	14.0	.746	1.760
34	W	.641	7.17	0.899	13.1	.596	1.655
35	W	.627	7.75	0.915	12.6	.569	1.60
36	W	.483	9.71	0.793	5.8	.511	0.983
37	W	.404	14.4	0.925	0.7	.401	0.684
38	W	.673	6.94	0.877	14.3	.609	1.792
39	W	.667	5.38	0.883	14.0	.703	1.76
40	W	.654	7.75	0.899	13.6	.571	1.705
41	W	.642	5.47	0.860	13.1	.698	1.655
42	W	.483	8.25	1.08	5.8	.537	0.940
43	W	.654	5.92	0.687	13.6	.688	1.705
44	W	.579	7.85	0.760	10.8	.579	1.402
45	W	.473	9.34	0.899	5.4	.514	0.949
46	W	.427	11.6	0.973	2.5	.449	0.767

and 0.91 for water, Freon 11 and Freon 113, respectively. These values indicate that almost as good a correlation could be obtained for Freon 113 using either group alone, but for water and Freon 11 no single group correlation will exist. For the particular case of water this has been demonstrated by Brown(5) who has shown that no linear correlation exists using the Weber number alone.

When Equation (5.10) was tested using all of the experimental data, the over-all correlation coefficient fell to 0.65, indicating that the relationship does not adequately describe all of the data together. This implies that a variable necessary to interrelate the fluids was not present in Equation (5.10). An interesting fact which arose while trying to correlate all of the data using the two-group model was that the equation would not accurately describe any two of the data sets taken together except for the Freon pair. Inclusion of a vapor density ratio in Equation (5.10) results in

$$\frac{T k}{\mu H_{fg}} = a \left(N_{we}\right)^{b} \left(Z\right)^{c} \left(\frac{\rho_v}{\rho_L}\right)^{d} \qquad (5.14)$$

The constants a,b,c and d were determined by regression on the IBM 709 computer. Equation (5.14), then becomes

$$\frac{T k}{\mu H_{fg}} = 0.344 \left(N_{we}\right)^{-0.231} \left(Z\right)^{-0.272} \left(\frac{\rho_v}{\rho_L}\right)^{0.139} \qquad (5.15)$$

The over-all correlation coefficient for the above model was 0.86. At

a 95 per cent confidence level the exponents are given by:

$$b = -0.231 \pm 0.03$$

$$c = -0.272 \pm 0.054$$

$$d = 0.139 \pm 0.02$$

The correlation coefficients between the groups were 0.070, 0.26 for 0.079, substantiating the above remarks that a correlation for all of the data of the form of Equation (5.10) does not exist. The results indicated by Equation (5.15) are shown graphically in Figure 12 and in a tabular form in Table VIII.

The signs of the exponents of Equation (5.15) are worthy of some comment. The negative sign on the exponent of the Weber number is entirely consistent with the stability theory of liquid jets since at increasing values of the Weber number, the jet tends to break up under the action of inertial and surface tension forces alone, without the addition of superheat. The negative sign on the exponent of the Ohnesorge number is very interesting, since either its value or magnitude would be very difficult to predict. The Ohnesorge number contains four very important variables, viscosity, diameter and surface tension and density. At a constant level of Weber number and density ratio

$$T \propto \frac{\sqrt{D\rho\sigma}}{\mu}$$

The negative sign then indicates the very strong importance of the diameter as a variable controlling jet breakup, since based on surface tension and density <u>alone</u> the sign would have been positive.

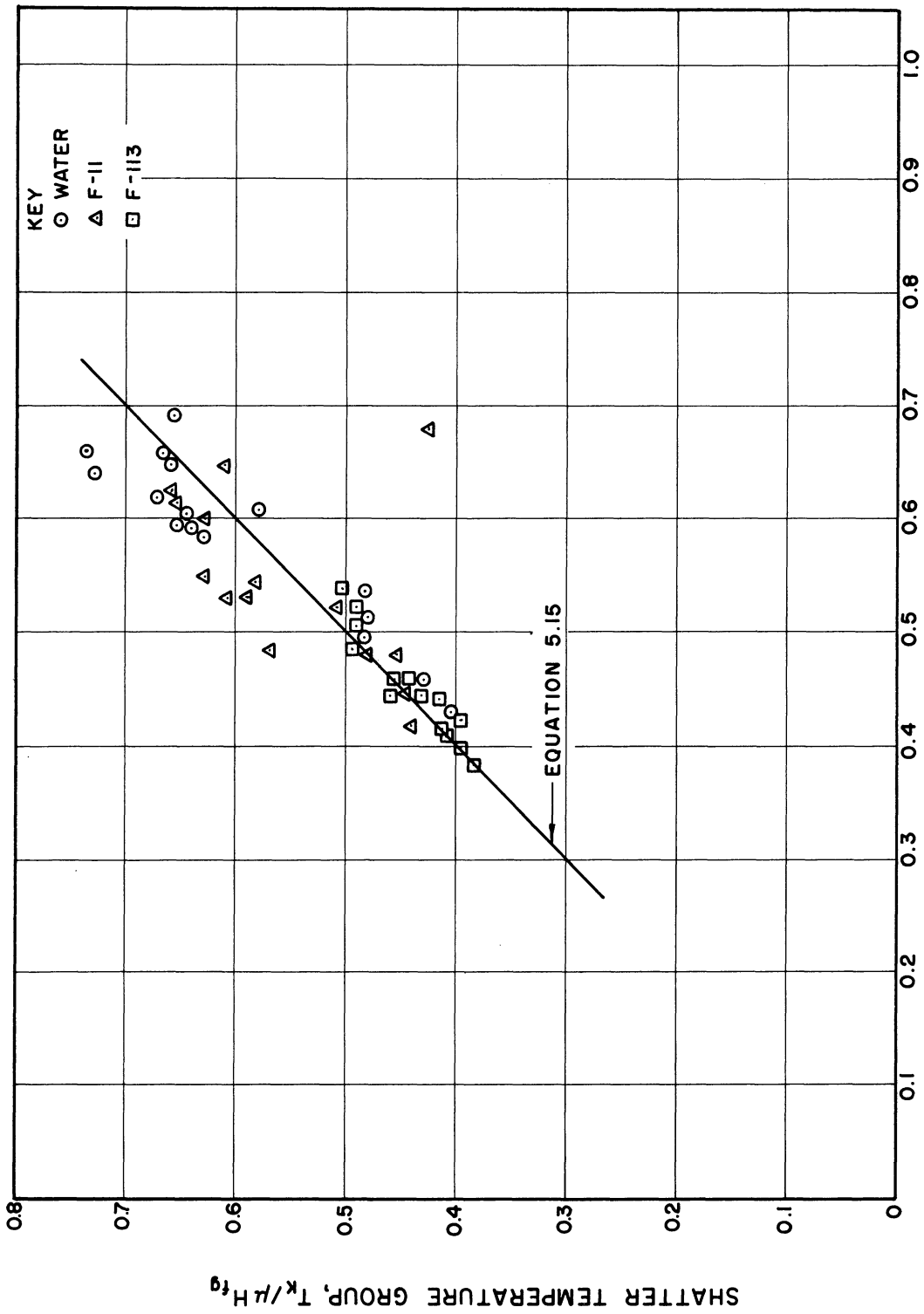

Figure 12. Shatter Temperature Correlation.

TABLE VIII

COMPARISON OF CALCULATED AND EXPERIMENTAL VALUES
OF SHATTER TEMPERATURE GROUP

Run	$\frac{Tk}{\mu H_{fg}}$ Exp.	$\frac{Tk}{\mu H_{fg}}$ Calc. (Eq. 5.15)
1	0.648	0.613
2	0.637	0.551
3	0.483	0.456
4	0.503	0.522
5	0.633	0.589
6	0.621	0.530
7	0.643	0.655
8	0.429	0.616
9	0.451	0.458
10	0.601	0.528
11	0.577	0.470
12	0.637	0.532
13	0.443	0.405
14	0.656	0.594
15	0.449	0.443
16	0.487	0.537
17	0.496	0.541
18	0.480	0.489
19	0.456	0.454
20	0.477	0.528
21	0.442	0.470
22	0.456	0.530
23	0.448	0.450
24	0.415	0.414
25	0.434	0.458
26	0.408	0.442
27	0.398	0.397
28	0.411	0.415
29	0.398	0.424
30	0.396	0.394
31	0.736	0.660
32	0.729	0.640
33	0.665	0.660
34	0.641	0.602
35	0.627	0.584
36	0.483	0.537
37	0.404	0.436
38	0.673	0.620
39	0.667	0.654
40	0.654	0.594
41	0.642	0.651
42	0.483	0.495
43	0.654	0.696
44	0.579	0.608
45	0.473	0.515
46	0.427	0.459

5. Summary

From the discussion of the previous sections of this chapter we may conclude that the shatter temperature is definitive of the breakup of a superheated liquid jet and that this shatter temperature is unique for any given set of physical and fluid variables. The relationship expressed by Equation (5.15), which relates the shatter temperature to the variables of the system can be used to calculate the breakup temperature of other superheated liquid jets. This relationship would perhaps not be completely accurate at very high liquid viscosities or in cases where the receiving pressure is very far removed from atmospheric. High liquid viscosities could occur if liquids containing impurities (slurries) or artificial thickeners were injected. High viscosities can not result from the use of other liquids and hence Equation (5.15) may be considered to apply to all pure liquids.

CHAPTER VI

SPRAY EVAPORATION

1. Theory

The problem of calculating or predicting the evaporation rate of liquid droplets contained in sprays has received fairly wide attention in recent years. To gain an appreciation of the factors involved in the problem, let us first consider the simplest possible case--a spherical drop of a pure liquid of diameter D and temperature T in still air. For this case the total diffusion is given by

$$N = 2\pi D D_t \frac{\Delta P}{RT} \tag{6.1}$$

where

N is the total diffusion rate

D is the drop diameter

D_t is the diffusivity

T is the drop temperature

R is the gas constant

ΔP is the vapor pressure at T minus the pressure of the diffusing liquid at an infinite distance.

Froessling[16] has studied this problem theoretically and has obtained some interesting and useful results, particularly in the limiting case of zero Reynolds number; i.e., no relative velocity. This case is of practical use in representing a finely dispersed spray system.

He was able to predict the relationship:

$$\frac{h_c D}{k_f} = \frac{k_g M D P_f}{D_t \rho} = 2.0 \qquad (6.2)$$

where

h_c is the convection heat transfer coefficient

k_f is the thermal conductivity of the gas film surrounding the evaporating drop

k_g is the mass transfer coefficient

M is the mean molecular weight of the gas vapor mixture in the boundary layer surrounding the drop

P_f is the average value of the vapor pressure of the non diffusing gaseous component surrounding the drop

ρ is the density of the liquid

For the more general case of forced convection, many investigators have validated the semi-empirical expressions:

$$\frac{h_c D}{k_f} = 2.0 + 0.60 (N_{Pr})^{1/3} (N_{Re})^{1/2} \qquad (6.3)$$

$$\frac{k_g M D P_f}{D_t \rho} = 2.0 + 0.60 (N_{Sc})^{1/3} (N_{Re})^{1/2} \qquad (6.4)$$

where

N_{Pr} is the Prandtl number

N_{Sc} is the Schmidt number

N_{Re} is the Reynolds number

An expression equivalent to (6.1) is

$$\frac{dW}{d\Theta} = \frac{2\pi D D_t \rho}{P_f} (P_s - P_o) \qquad (6.5)$$

in which ρ/P_f has been substituted for RT in (6.1). In the use of the above equation Ranz and Marshall[45] have shown experimentally that the drop temperature is essentially that of the temperature of the surface of the drop and that this surface temperature is the wet bulb temperature for the humidity conditions involved. They also developed and discussed the significance of Equations (6.3) and (6.4). They argued as follows: In still air the drop evaporates uniformly from all portions of its surface. When the drop is in a moving gas stream, this symmetry must be destroyed except at very low relative air velocities. The equations account for this loss of symmetry, resulting from the changed pattern of air flow around the drop, by modifying the coefficients for evaporation in still air.

Although the same theoretical considerations apply to clouds of drops as to a single drop, the problem is complicated by additional factors. One of these is that the drops may be dispersed in a turbulent gas stream. Liu[27] and Soo[54] from a study of this aspect of the problem concluded that the eddy diffusivity of the particles and of the gas are almost equal for small particles and at low intensities of turbulence. This means that small drops, in a turbulent gas stream, should evaporate at a rate corresponding to the rate which occurs at zero relative velocity.

Kessler[23] studied a similar problem and showed experimentally that for alcohol drops in the 14 to 30 micron size range that the

evaporation rate was that predicted for stagnant conditions. Mirsky[35] in a recent study arrived at essentially the same conclusion--viz. that small drops evaporate as though stagnant conditions prevail.

A factor which must be considered in this study is that nearly all of the data were taken in a region in which the great majority of the liquid drops were decelerating. A few studies have been carried out in which the effects of acceleration or deceleration on the rate of evaporation were studied. Manning and Gauvin[31] in a series of interesting experiments demonstrated that the correlations of Ranz and Marshall accurately describe their measured heat transfer (or mass transfer) coefficients, in the zone of deceleration. The drop sizes, velocities and deceleration rates correspond roughly to those encountered in this investigation. Crowe[7] in his recent Ph.D. thesis was able to show on a theoretical basis that deceleration will affect the evaporation rates only at magnitudes of deceleration much above those encountered here. On the basis of this theoretical and experimental evidence Equations (6.3) or (6.4) may be assumed to give a reasonable description of the evaporative process of the spray droplets.

Rewriting Equation (6.5) in a different form leads to:

$$\frac{dW}{d\Theta} = \frac{h_c A(\Delta t)}{\lambda_s} \qquad (6.6)$$

where

A is the area for heat transfer

$\Delta t = t_a - t_s$ where t_a and t_s are the air and surface temperatures respectively

λ_s is the latent heat of vaporization corresponding to t_s

Θ is the time

If the two relations for h_c at either zero or finite relative velocity are substituted into (6.6), there results:

$$\frac{dw}{d\theta} = \frac{2k_f}{D} \frac{A(\Delta t)}{\lambda_s} \tag{6.7}$$

for zero relative velocity, and

$$\frac{dw}{d\theta} = \frac{A(\Delta t) k_f}{\lambda_s D} \left(2.0 + 0.60 \left(N_{Re}\right)^{1/2} \left(N_{Pr}\right)^{1/3} \right) \tag{6.8}$$

for finite relative velocity.

Equation (6.7) may be integrated directly to give

$$\theta = \frac{\rho \lambda_s}{8 k_f \Delta t_m} \left(D_o^2 - D^2 \right) \tag{6.9}$$

where

D_0 is the initial drop diameter at some arbitrary time zero

D is the drop diameter at any other time θ

Rearranging Equation (6.9)

$$D^2 = D_o^2 - K\theta \tag{6.10}$$

where

$$K = \frac{8 k_f \Delta t_m}{\rho \lambda_s}$$

For the case of finite relative velocity, substitution and subsequent integration yields

$$\theta = \frac{\rho \lambda_s}{4 k_f \Delta t} \int_D^{D_o} \frac{D\,dD}{\left(1 + 0.3 \left(N_{Re}\right)^{1/2} \left(N_{Pr}\right)^{1/3}\right.} \tag{6.11}$$

Integration of Equation (6.11) can be carried out by a stepwise process having a knowledge of a relationship between the drop diameter and drop velocity. However it has been demonstrated[32] that for drops below 100 microns in diameter the effect of air velocity on the rate of evaporation is negligible and the use of Equation (6.10) is justified. For drops larger than this size, Equation (6.11) should be utilized. For the particular case under investigation all of the drops of 100 microns and above are traveling at velocities of the order of 50 to 100 feet per second. As a result they require a time of about 10^{-3} seconds to traverse the distance from four to seven inches away from the nozzle. Consequently, their contribution to the rate of evaporation is small enough so that Equation (6.10) can be used for all drop sizes, without introducing a serious error.

2. Prediction of Drop Size Using a Measured Initial Size Distribution

The experimental data afford an excellent opportunity to study evaporation rates of sprays formed by the flashing process. The evaporation of the spray is reflected in the variation of the average drop diameter as a function of location in the spray and distance from the nozzle. This variation is tabulated in Table XVII, Chapter VIII and is shown graphically in Figures 15 through 22. It will be observed that there is no simple relationship between average diameter and distance from the nozzle.

In estimating the evaporation times and/or rates, it is necessary to be able to specify or estimate the droplet temperature in order to evaluate the term Δt_m. One manner in which to do this is to measure

the humidity and temperature of the air in the spray and from this information determine the wet bulb temperature. This requires fairly elaborate experimental equipment which was not available. An estimated value of Δt_m of 20°F was used in these calculations for the evaporation of the water sprays. This value was arrived at from two considerations:

(1) An ordinary mercury thermometer was placed in the spray and the temperature difference between it and the air temperature was very near 20°F. This is admittedly not an extremely accurate determination, but it will give a very good estimate.

(2) The air temperature is of the order of 80°F and the droplet temperature cannot be below about 40°F, as an extreme; this gives the maximum attainable Δt_m as about 40°F.

Fortunately, it was discovered from the calculations that the choice of either 20 or 40°F for Δt_m made very little difference to the final answer.

Having estimated Δt_m as 20°F then

$$K = \frac{8 k_f \Delta t_m}{\rho \lambda_s}$$

becomes equal to 1000 microns^2/sec. for water. The calculations were then carried out in the manner described below. To illustrate these calculations, location 1 (center line) has been chosen as a specific example. The drop size distribution at a distance of four inches from the nozzle was assumed to be correct and using this as a starting point,

the drop number distributions at distances of five, six and seven inches were calculated. Time zero was assigned to the distance of four inches and the times for the drops to reach a distance of five, six and seven inches were calculated using the known velocity data. Figures 13 and 14 depict the drop velocity profiles for this location. The size ranges referred to are those tabulated in Table XXI of Appendix B. Table IX summarizes the results of these calculations, both for this particular example and for all of the other spray locations. It now is a fairly easy matter to utilize Equation (6.10) to determine the new mean diameters at distances of five, six and seven inches. In carrying out the calculation it was assumed that the average diameter of any size range was representative of all the drops in the size interval. This, or some similar assumption, is necessary, because of the method used in taking the raw data. When the drops were counted no indication was made as to where they fit into the size interval; i.e., whether they are near to one extreme or the other or near the average diameter. On this basis the data given in Table X was calculated. Examination of Table X illustrates vividly the well known fact that smaller diameter drops evaporate much more rapidly than larger diameter drops. Using the information in Table X and the known number distribution at a distance of four inches, the drop size distributions were then calculated at the three other distances from the nozzle. From this the new average drop diameters were calculated. Figure 15 shows a comparison between these "calculated" average diameters and the experimentally observed values. Figures 16, 17 and 18 show similar comparisons for the other three spray locations

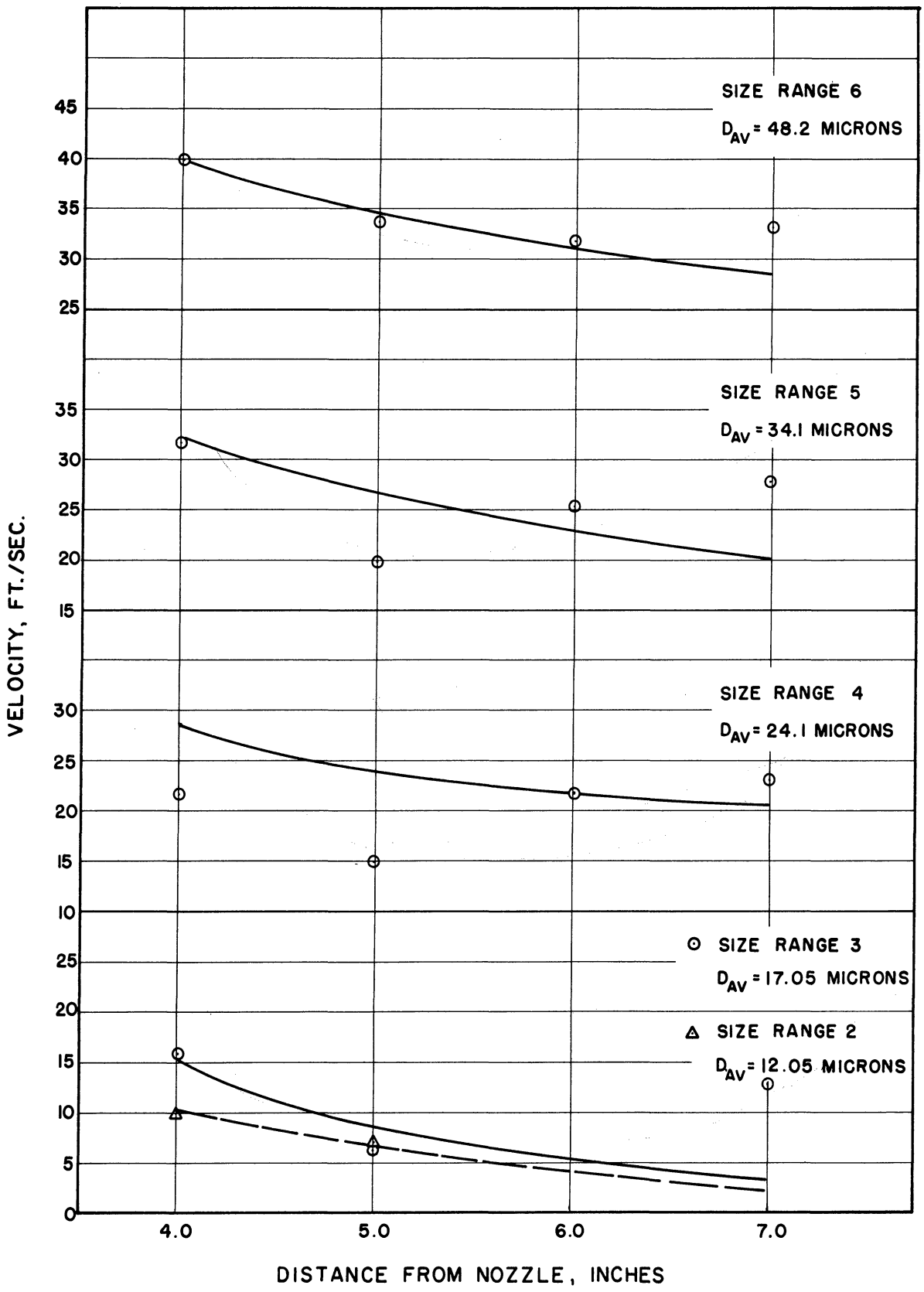

Figure 13. Velocity Profiles for Water System Location 1, Injection Temperature 287°F, 120 Psig.

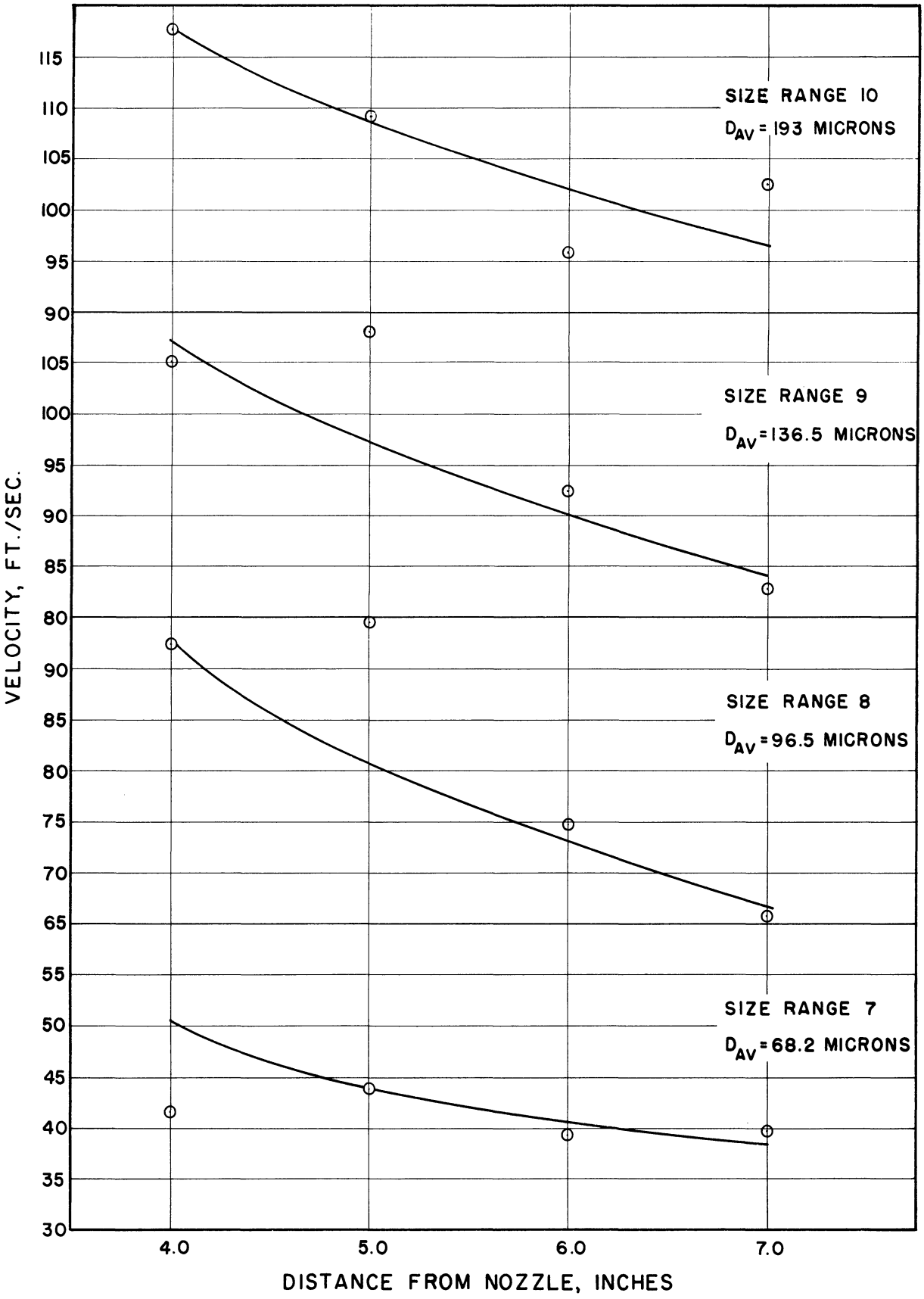

Figure 14. Velocity Profiles for Water System, Location 1, Injection Temperature 287°F, 120 Psig.

TABLE IX

TRAVEL TIMES FOR SPRAY DROPLETS
(Times Seconds x 10^{-3})

Run	Loc.	Size Range								
		2	3	4	5	6	7	8	9	10
2	1	0.000	0.000	0.000	0.000	0.000	0.000	0.000	0.000	0.000
3	1	12.20	8.450	3.990	3.550	2.800	2.210	1.190	1.020	0.920
4	1	2.73	17.07	8.52	7.74	5.95	4.67	2.54	2.12	1.90
5	1	52.2	41.26	13.4	12.6	9.40	8.29	4.02	3.31	2.94
2	2	0.00	0.00	0.00	0.00	0.00	0.00	0.00	0.00	0.00
3	2	-	10.2	6.18	3.64	2.91	2.30			
4	2	-	27.6	13.8	9.23	6.42	5.00			
5	2	-	48.7	22.1	14.7	10.7	8.00			
2	3	0.00	0.00	0.00	0.00	0.00	0.00			
3	3	-	17.01	7.28	4.67	4.29	-			
4	3	-	42.6	17.47	10.8	9.53	-			
5	3	-	81.8	29.47	17.7	15.6	-			
2	4	0.00	0.00	0.00	0.00	0.00	0.00			
3	4	-	11.54	9.70	9.17	7.41	4.67			
4	4	-	23.1	20.4	20.4	16.7	11.2			
5	4	-	28.8	31.6	33.0	27.3	19.6			
7	1	0.00	0.00	0.00	0.00	0.00	0.00			
8	1	6.40	4.14	1.96	1.51	1.00	1.48			
9	1	-	-	2.16	1.73	1.05	1.63			
10	1	-	-	2.18	1.81	1.08	1.74			
7	2	0.00	0.00	0.00	0.00	0.00	0.00			
8	2	-	4.00	2.31	1.87	1.12	0.944			
9	2	-	-	2.56	2.02	1.22	1.04			
10	2	-	-	2.74	2.20	1.30	1.11			
7	3	0.00	0.00	0.00	0.00	0.00	0.00			
8	3	-	4.57	2.73	2.12	1.54	1.11			
9	3	-	-	3.33	2.37	1.70	1.28			
10	3	-	-	4.16	2.60	1.81	1.49			

Note: Times are not given past the point of evaporation for the drop.

TABLE X

SUMMARY OF NEW AVERAGE DIAMETERS
(Diameters in Microns)

Size Range	Initial Diameter	WATER Location 1			2			3			4		
		Distance From Nozzle, Inches											
		5	6	7	5	6	7	5	6	7	5	6	7
2	12.05												
3	17.05	16.7	16.4	15.8	16.7	16.2	15.6	16.6	15.7	14.4	16.0	11.1	-
4	24.1	24.0	23.9	23.8	23.9	23.8	23.6	23.9	23.8	23.5	23.5	22.7	21.5
5	34.1	34.0	33.9	33.9	34.0	33.9	33.8	34.1	34.0	33.9	33.8	33.5	33.0
6	48.2	48.1	48.0	48.0	48.2	48.2	48.1	48.2	48.1	48.0	48.1	47.8	47.6
7	68.2	68.2	68.2	68.2	68.2	68.2	68.1	68.2	68.2	68.2	68.2	68.1	67.9
8	96.5	96.5	96.5	96.5	96.5	96.5	96.5	96.5	96.5	96.5	96.5	96.5	96.4
		FREON-11											
3	17.05	12.1	-	-	11.6	-	-	11.0	7.40				
4	24.1	22.5	20.4	18.1	22.2	19.7	16.7	21.9	18.4	13.1			
5	34.1	33.2	32.2	31.2	33.1	31.8	30.4	32.9	31.4	29.7			
6	48.2	47.7	47.2	46.7	47.7	47.2	46.6	47.5	46.7	46.0			
7	68.2	68.0	67.7	67.5	68.0	67.6	67.3	67.8	67.5	67.1			

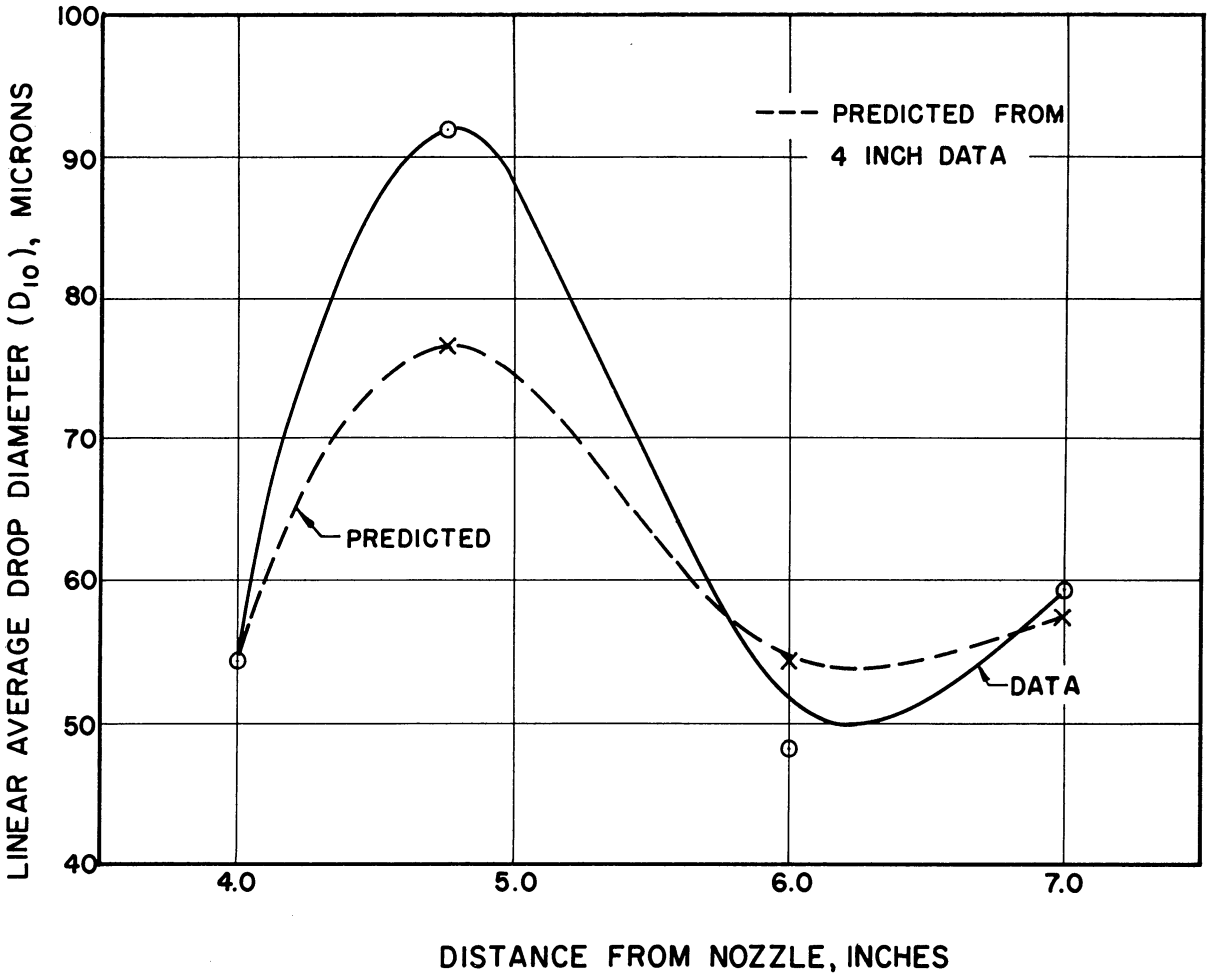

Figure 15. Comparison of Measured and Predicted Average Drop Diameters for Water, Location 1.

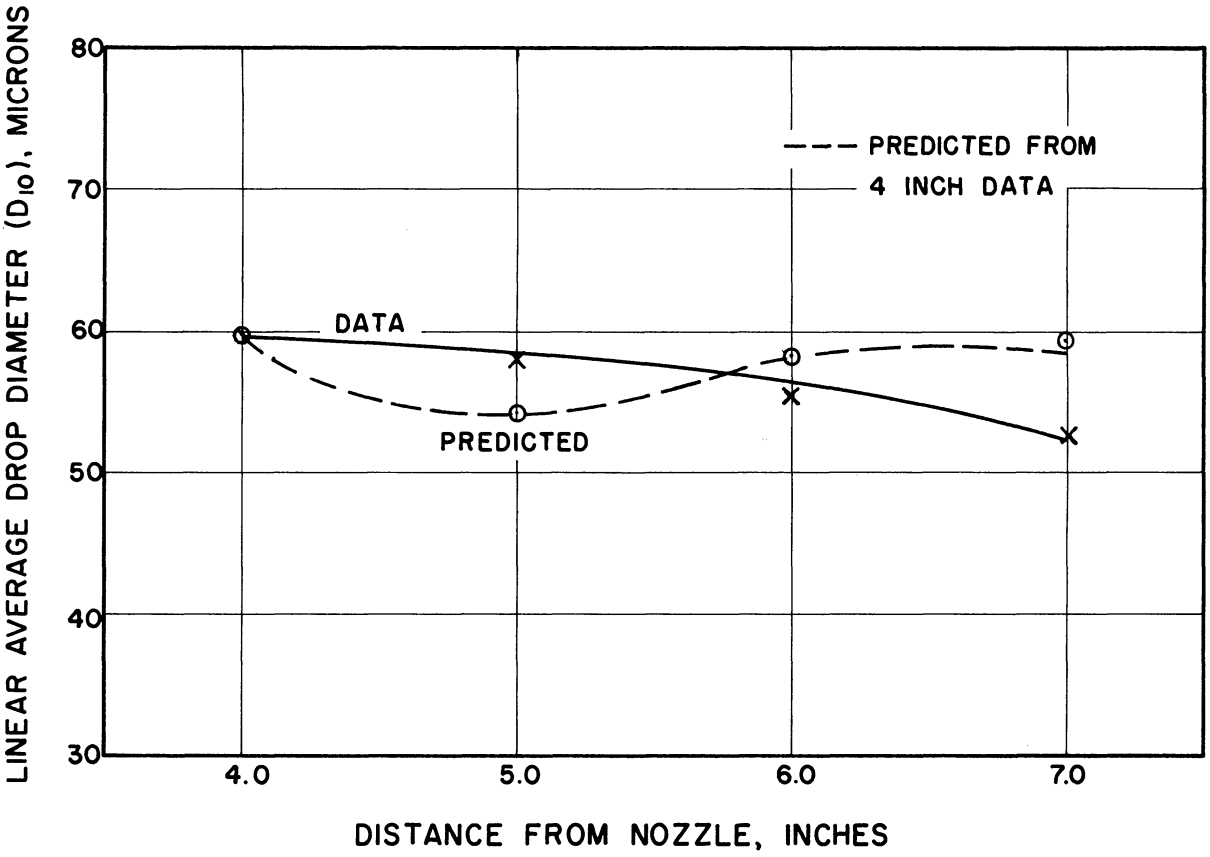

Figure 16. Comparison of Measured and Predicted Average Drop Diameters for Water, Location 2.

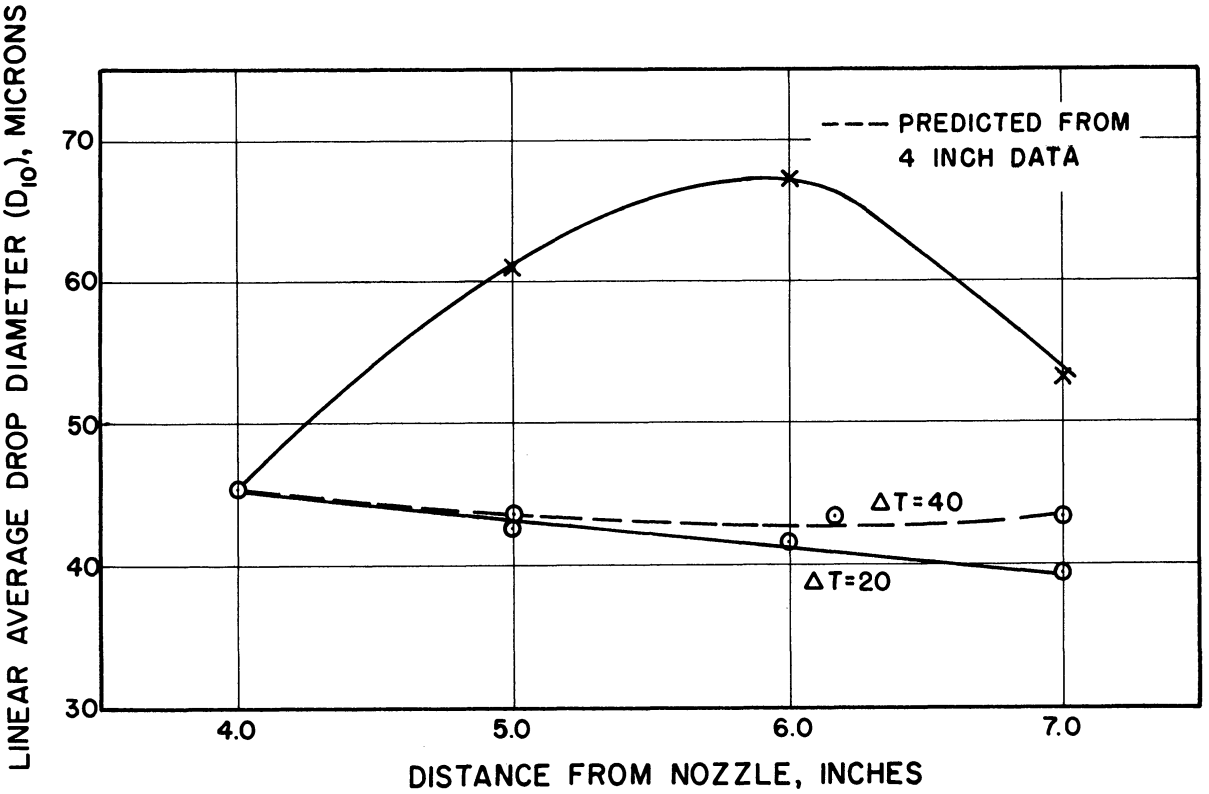

Figure 17. Comparison of Measured and Predicted Average Drop Diameters for Water, Location 3.

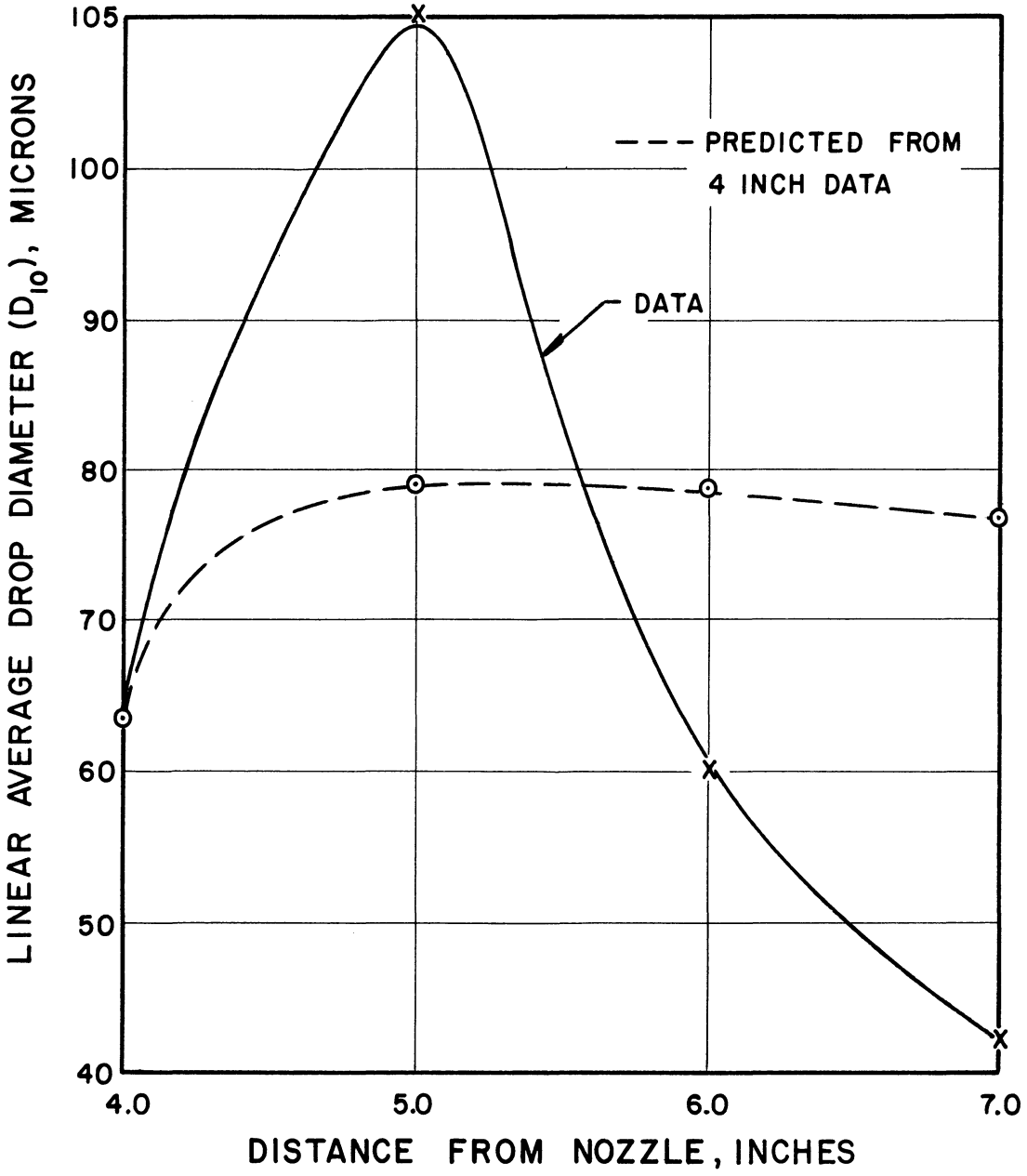

Figure 18. Comparison of Measured and Predicted Average Drop Diameters for Water, Location 4.

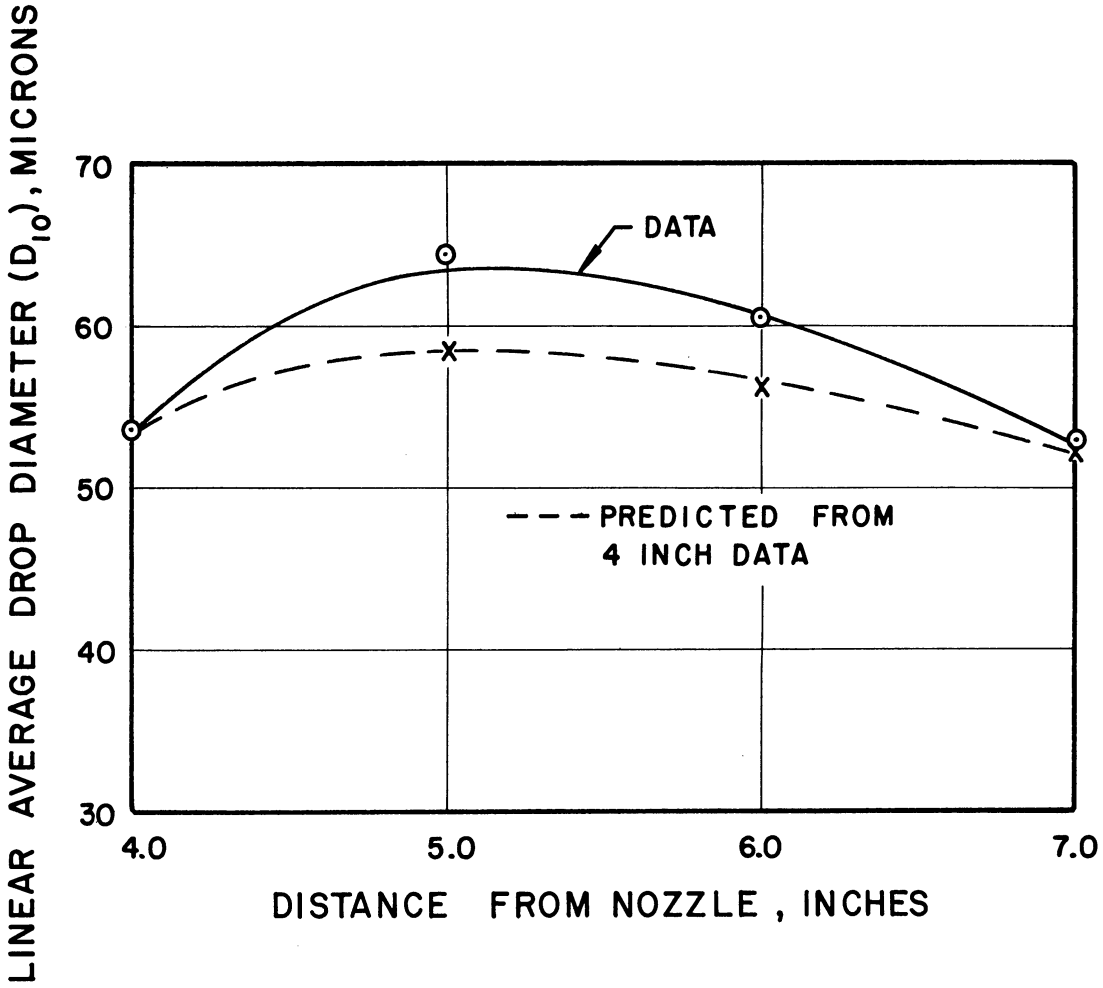

Figure 19. Comparison of Measured and Predicted Average Drop Diameters for Water, Total Spray.

and Figure 19 depicts the comparison for the linear average diameter for the total spray.

Similar calculations were carried out for the Freon 11 spray using a value of Δt_m of 80°F. This value was determined in a manner similar to the Δt_m for water. The value of the evaporation coefficient K for Freon 11 is 40600 microns^2/sec. This is much larger than the value of the coefficient for water, in part because of the larger Δt_m, but primarily because the latent heat of vaporization is an order of magnitude less (78.5 Btu/lb as compared to 970.3 Btu/lb). The results of the calculations are shown in Figures 20 through 22.

Attention should be directed in particular to Figure 17 which shows the worst agreement between experiment and calculations. This afforded an excellent chance to investigate the effect of a variation in Δt_m and hence in the value of the evaporation coefficient K. (Remember that only a small range of Δt_m is permissible, because of the physical limitations imposed by the system.) Reference to Figure 17 demonstrates that changing the value of Δt_m from 20°F to 40°F has a relatively small effect on the calculated drop distribution. In fact any error in the choice of Δt_m is far outweighed by any error in the experimental data which is used as a starting point in the calculations. This observation is further borne out by the data given in Figure 21, where once again a change in the value of Δt_m does not significantly alter the predicted drop distributions.

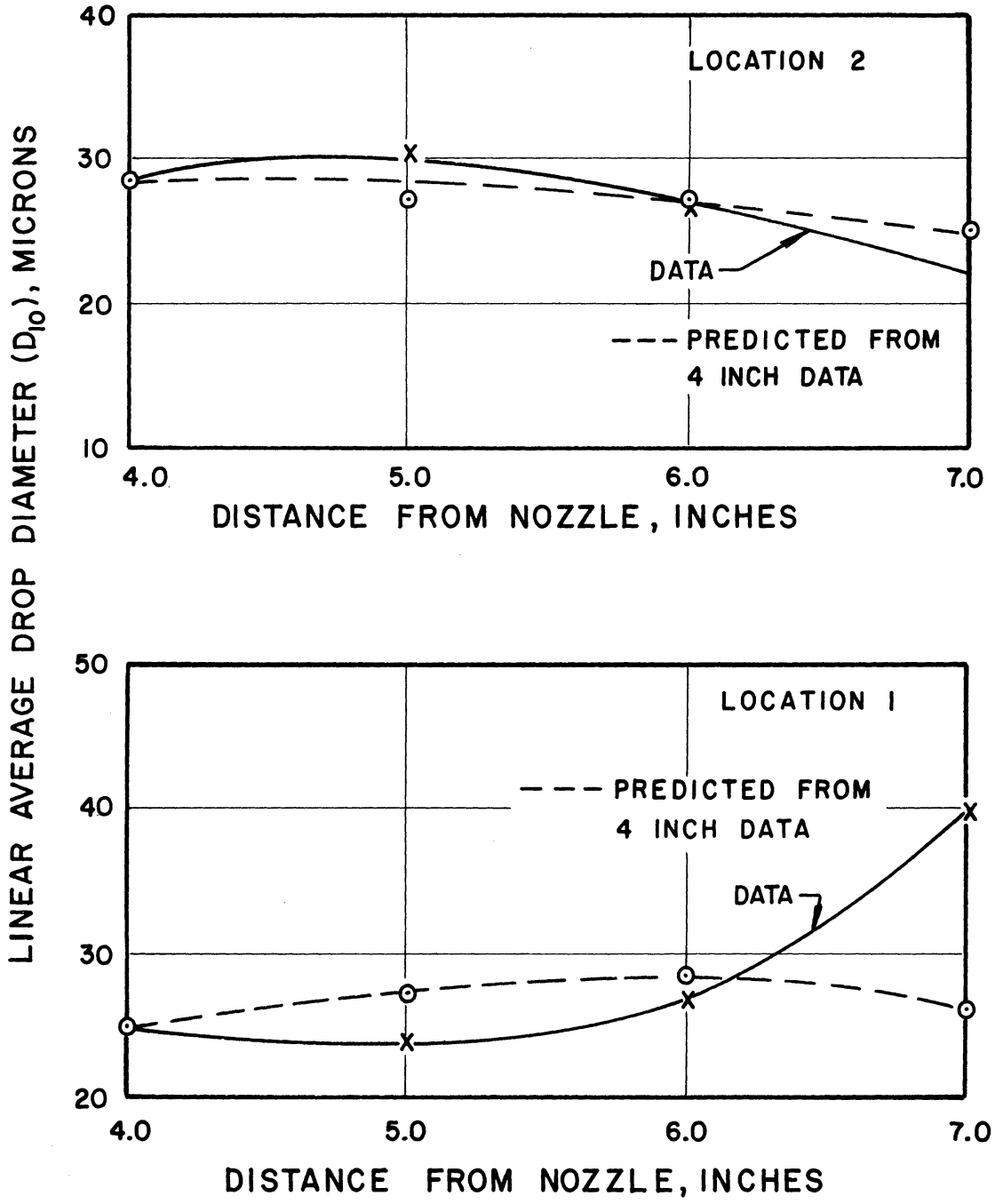

Figure 20. Comparison of Measured and Predicted Average Drop Diameters for Freon 11, Locations 1 and 2.

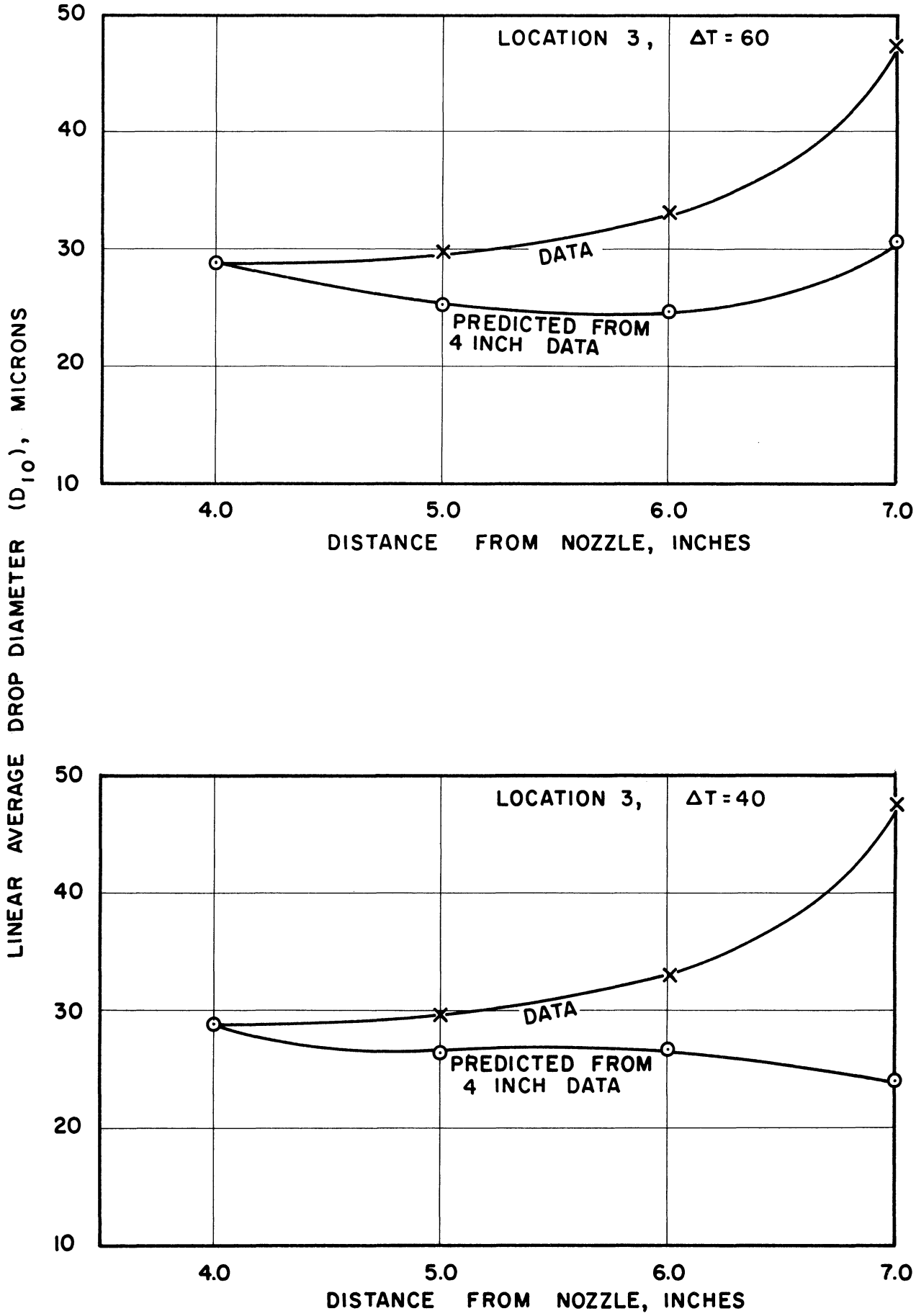

Figure 21. Comparison of Measured and Predicted Average Drop Diameters for Freon 11, Location 3.

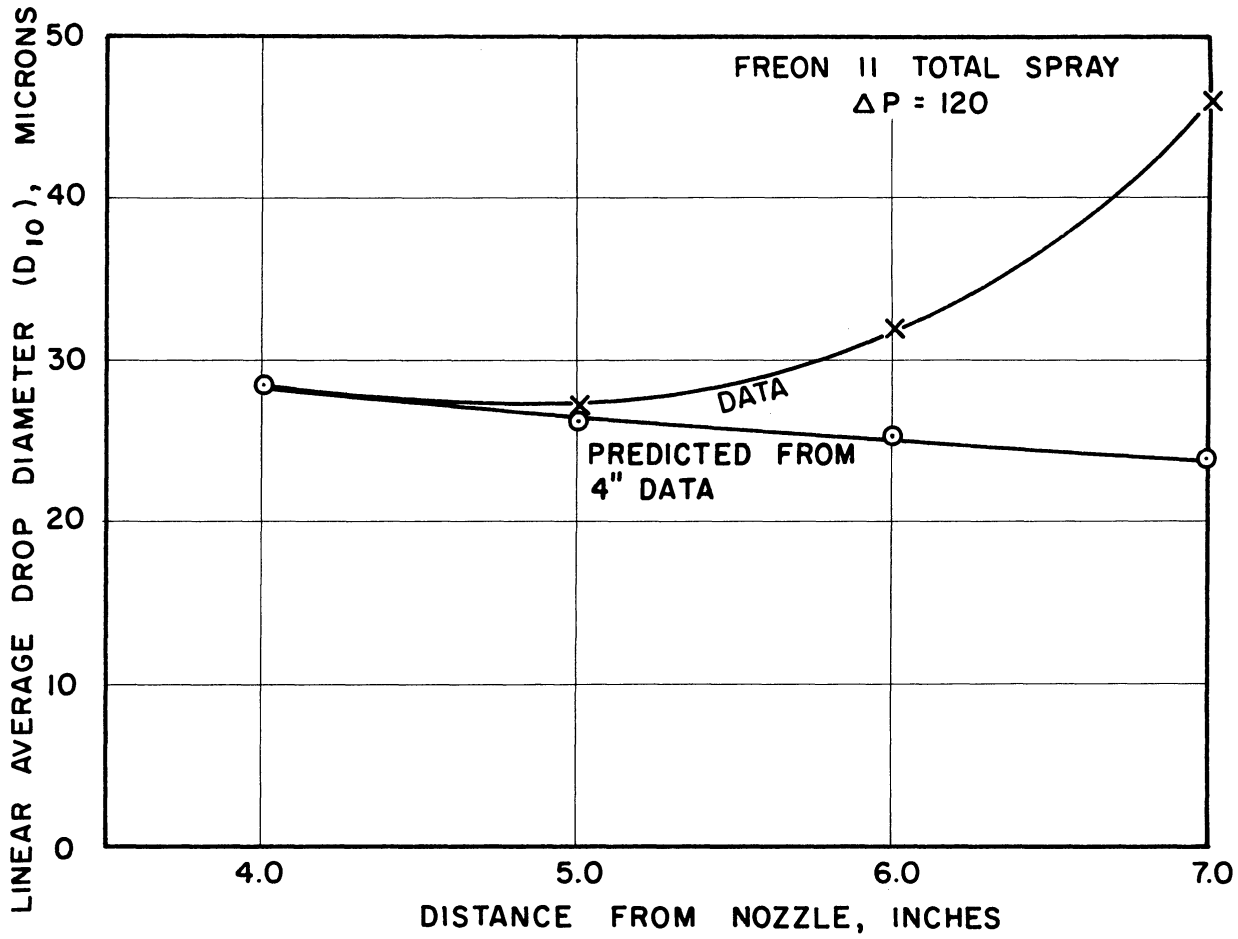

Figure 22. Comparison of Measured and Predicted Average Drop Diameters for Freon 11, Total Spray.

3. Flow Rate Checks Based Upon Evaporation

One manner in which the over-all accuracy of the spray analyses may be measured is by comparing the computed flow rate of the spray from the drop size analyses and their velocities, and the flow rate of the injected liquid jet. This procedure immediately poses a problem--how much of any given spray will evaporate between the nozzle and the point at which the experimental data were taken? Evaporation, in this case, will result from two things. Firstly, evaporation due to loss of sensible heat in the liquid drops which must cool from their boiling point down to the wet bulb temperature and, secondly, the type of evaporation discussed in the previous section.

3.1 Evaporation Due to Sensible Heat Loss

When the droplets are formed at the nozzle their temperature will be very close to the saturation temperature. There is considerable evidence in the literature to indicate that once dynamic equilibrium conditions have been attained, evaporating spray drops remain at the wet bulb temperature to the drying air.(32)

Near the nozzle an unsteady state period can be expected to occur before the drops reach a constant temperature. The time required to reach this steady state condition is very strongly dependent upon the drop sizes present at atomization. Coarser droplets will require a longer distance than finer droplets. From theoretical calculations El Wakil, Uyehara and Myers(13) estimated that a 50 micron drop of octane issuing from a pressure nozzle with an initial velocity of 100 ft/sec. would require 0.23 seconds to reach a steady temperature.

Lyons[30] in 1951 supplied some very useful experimental information. Using a copper constantan-thermocouple probe located 1/8 inch away from the nozzle, he reported the following observations:

(1) With a feed water temperature of 81°F the wet bulb temperature of the air (61°F) was reached in 1/8 inch.

(2) With increasing feed water temperature and fine atomization the wet bulb temperature was again reached if the feed water temperature did not exceed 102°F. The spray temperature at a distance of 1/8 inch was 2°F higher than the wet bulb for a feed water of 114°F and 12°F higher for a feed water of 164°F.

An estimate of the time required for a droplet to reach a steady temperature, for the conditions of interest here, can be estimated by solution of an equation developed by Froesling:

$$-\frac{dm}{dt} = \frac{2\pi D_m P_v D}{RT}\left(1 + 0.276\,(N_{Re})^{1/2}(N_{Sc})^{1/3}\right) \qquad (6.12)$$

where

D_m is the molecular diffusivity of water or Freon through air

D is the drop diameter

P_v is the vapor pressure of the vaporizing liquid at the drop surface temperature.

Equation (6.12) may be integrated to give an estimate of the time required for this process. It can be shown that Equation (6.12) for the case of water becomes

$$-\frac{dm}{dt} = \frac{0.5\,\pi D_m P_v D}{RT} \qquad (6.13)$$

The results of integrating this equation predicted that the drops considered would lose their sensible heat and reach the wet bulb temperature in a distance of about one inch. This prediction was verified qualitatively by means of a thermocouple placed in the spray at this point. It was found that the spray temperature at this distance did approximate the wet bulb temperature. In a similar manner it was estimated that Freon 11 drops would reach a steady temperature in about the same distance. On the basis of this evidence it was deemed safe to assume that by the time the droplets were four inches away from the nozzle they were at their wet bulb temperature.

3.2 Convective Evaporation

There are three techniques reported in the literature for the estimation of the evaporation rate of sprays. These were developed by Sjenitzer,[53] Fledderman and Hanson[14] and Probert.[42] Marshall in his recent symposium recommends the use of Proberts method, which will be used here. The details of his development of the analytical technique are given in Appendix C. In it there are assumptions made which are worthy of discussion at this point.

(1) Probert found it necessary to assume zero relative velocity between the droplet and the air stream. The justification for this same assumption for the particular case under study has already been discussed.

(2) Probert further assumed a constant value of the evaporation coefficient K. Recalling that the evaporation coefficient K is, $K = \frac{8k_f \Delta t_m}{\rho \lambda_s}$, this assumption is tantamount to assuming a constant value of Δt_m.

(3) He assumed that the spray drop size distribution could be represented by the Rosin-Rammler equation. As is shown in Chapter VIII, this equation does fit the data as well as the log normal distribution, so any per cent error resulting from its use will be negligible.

Using the numerical integration chart given by Probert (shown in Figure 41) and the values of the constants in the Rosin-Rammler equation found in Chapter VIII, estimates of the evaporation losses from the spray were then prepared. Adding together this loss with the loss due to evaporation from the sensible heat, the flow rates obtained from the drop count were compared with the measured flow rates. The total evaporation is given in Table XI below and the results of the flow rate comparison are shown graphically in Figure 23. The per cent error in most cases is of the same order of magnitude as those reported by Brown.(5) The largest deviation occurred at a distance of 7 inches from the nozzle for Freon 11. Examination of the data revealed that this was caused by two or three large drops present in the sample which were not present at the other three distances. The occurrence of these drops alters the calculated flow rate by a considerable margin.

TABLE XI

CALCULATED PER CENT EVAPORATION OF SPRAYS

Distance from Nozzle (Inches)	Per Cent Evaporated	
	Water	Freon 11
4.0	16	70
5.0	17	72
6.0	18	80
7.0	19	85

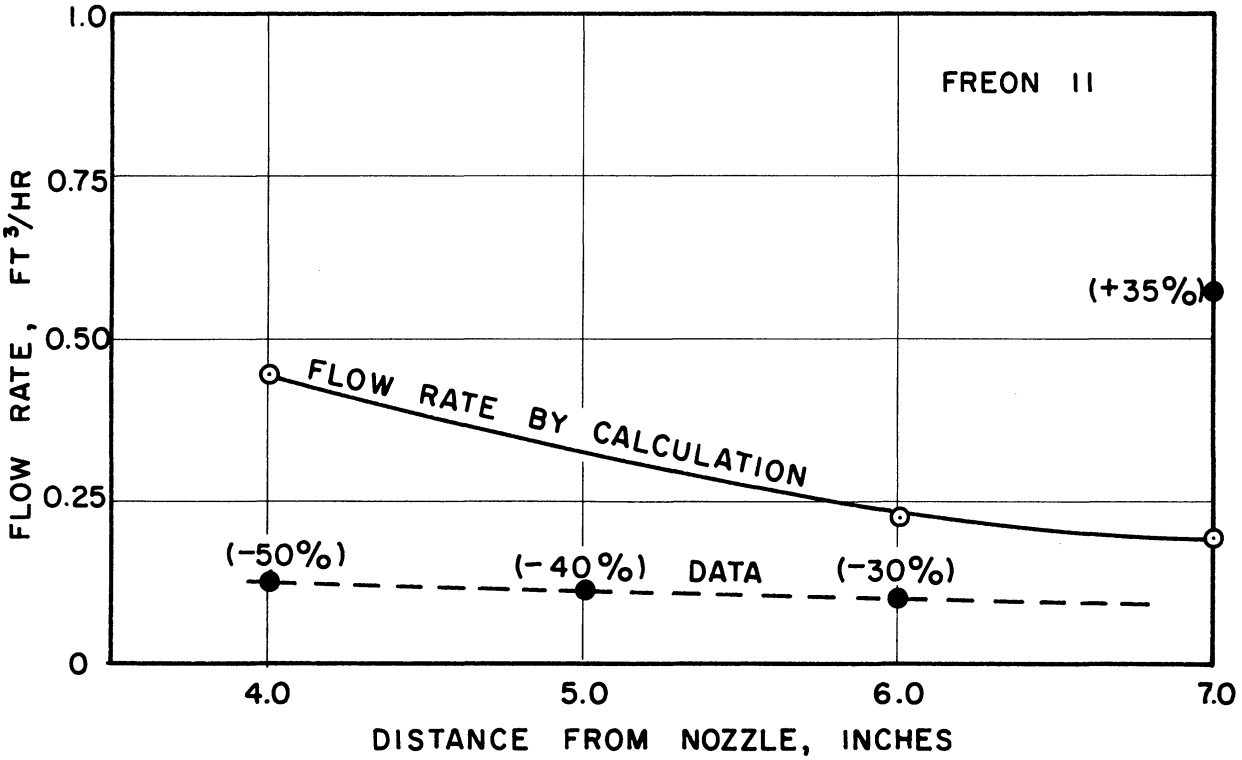

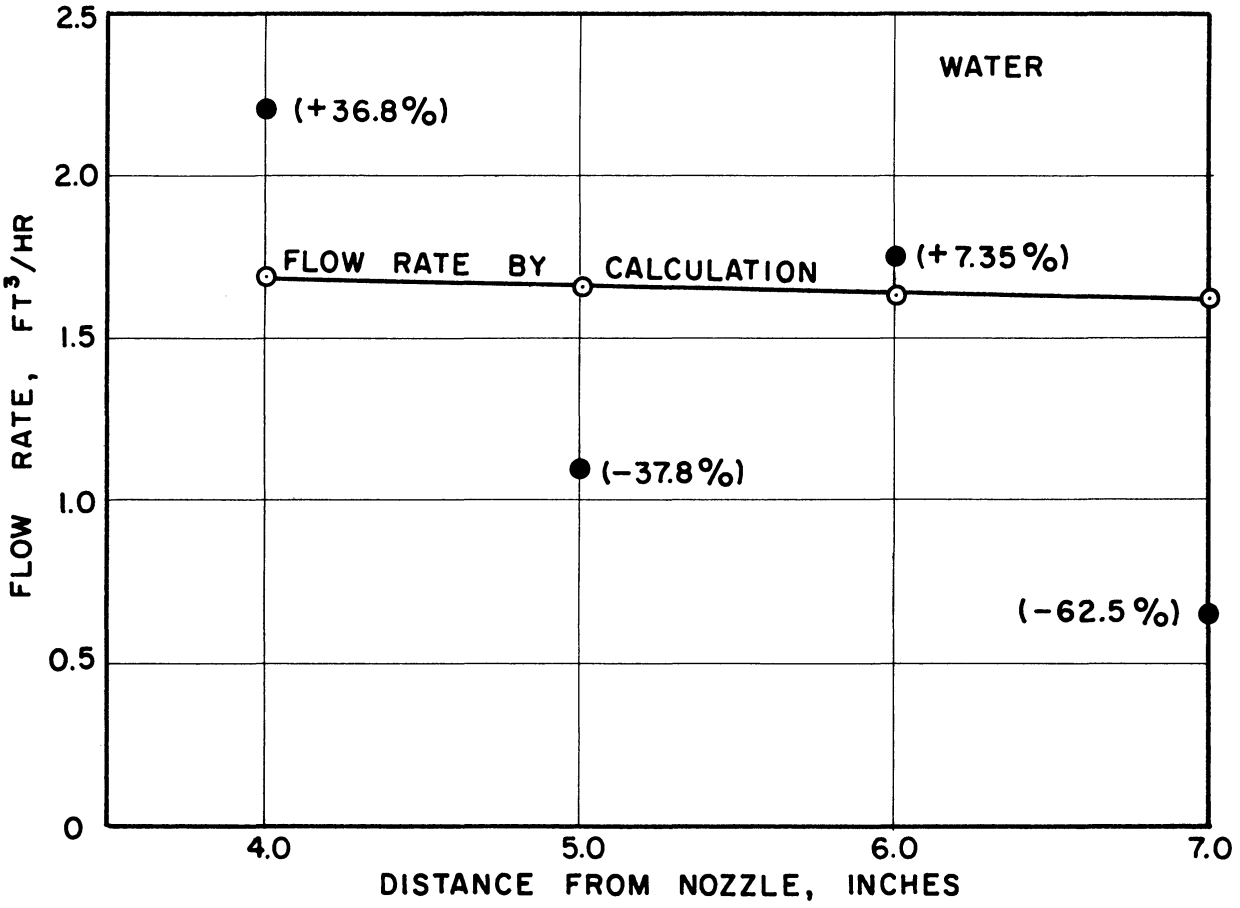

Figure 23. Comparison of Experimental and Measured Flow Rates.

4. Summary

The data presented in this chapter support the conclusion that the evaporation of this type of spray may be calculated using the drop size distribution and the standard rate equations for heat and mass transfer. However, the sensible heat content of the droplets at their injection must be accounted for.

Another important conclusion is that evaporation must be taken into account when attempting to check a measured flow rate (i.e., using the drop count and velocities taken from the photographic negatives) with that given by the orifice equation. This must be done not only because of the high injection temperatures but also because of the large number of small drops present and the small average drop diameters.

CHAPTER VII

DROP VELOCITY PROFILES WITHIN THE SPRAY

As explained in a preceding chapter, drop velocity measurements were taken at each of the spray locations and for both water and Freon 11. This data is tabulated in Appendix B. The drop velocities were measured at distances from the nozzle of four, five, six and seven inches from the nozzle for an injection pressure of 120 psig. Velocities were also determined for a distance of four inches at an injection pressure of 90 psig.

The drop velocity at any point within the spray would be expected to be a function of the initial velocity (injection pressure), the velocity of the gas stream through which it is traveling (induced air velocity) and of the so-called drag coefficient applicable to the drop under question. Before discussing the data, a brief review of the ballistics of droplets will be given.

1. Equation of Motion of a Particle

We can write down the equation of motion for a droplet using Newton's second law and a defining equation for the drag forces acting on a particle. The hydrodynamic drag acting on a body moving in an infinite fluid field may be written as

$$D = C_D \left(\frac{\rho v^2}{2}\right) A \qquad (7.1)$$

where

C_D is a dimensionless drag coefficient

ρ is the density of the fluid

V is the velocity of the particle

A is the projected area of the particle on a plane oriented at right angles to the direction of motion.

With this definition for the drag forces, the equation of motion is

$$M^o \frac{d^2X}{dt^2} = -C_D\left(\frac{\rho}{2}\right)\left(V_x - \frac{dx}{dt}\right)^2 A + E_x \qquad (7.2)$$

$$M^o \frac{d^2y}{dt^2} = -C_D\left(\frac{\rho}{2}\right)\left(V_y - \frac{dy}{dt}\right)^2 A + E_y \qquad (7.2a)$$

where

M^O is the mass

V_x, V_y are the components of the stream velocity in x and y directions, respectively

E_x and E_y are the components of any external forces acting on the droplets.

It is clearly apparent that E_y is zero and it is demonstrated in Appendix E that gravity forces acting on the droplets may be neglected relative to the drag forces. Thus E_x may be set equal to zero.

Let us assume radial symmetry within the spray, or in other words, we shall consider that the spray has ceased to expand in radius and has taken on a cylindrical rather than a conical shape. This situation occurs about four inches from the nozzle for the fluids used. Equation (7.2) then becomes, at low Reynolds numbers

$$M^o \frac{d^2X}{dt^2} = 6\pi N_{Re}\left(V_x - \frac{dx}{dt}\right) \qquad (7.3)$$

where use has been made of the fact that $C_D = \frac{24}{R_e}$ for R_e less than 2.0. In Equation (7.3) the Reynolds number is defined using the relative velocity between the particle and the gas stream. For the sake of convenience, let us correct for any deviations from the relation in (7.3) by writing

$$M^\circ \frac{d^2x}{dt^2} = k(6\pi N_{Re})\left(V_x - \frac{dx}{dt}\right) \tag{7.4}$$

The correction factor k will not be the same for all drop diameters, but over a reasonably small range of Reynolds numbers could be considered to be constant. Defining the dimensionless parameters

$$T = \frac{M}{k(6\pi N_{Re})}$$

$$\mathcal{E} = \frac{x}{T V_x}$$

$$\tau = \frac{t}{T}$$

Equation (7.4) becomes

$$\frac{d^2\mathcal{E}}{d\tau^2} + \frac{d\mathcal{E}}{d\tau} - 1 = 0 \tag{7.5}$$

which has as its solution

$$\mathcal{E}(\tau) = \mathcal{E}(0) + \tau + \mathcal{E}'(0) - \mathcal{E}'(0)e^{-\tau} + e^{-\tau} - 1 \tag{7.6}$$

Equation (7.6) is of the form

$$\varepsilon(\tau) = A + Be^{-\tau} + \tau \qquad (7.7)$$

where the terms A and B have an obvious meaning, and $\epsilon'(0)$ is the value of $\left.\frac{d\epsilon}{d\tau}\right|_{\tau=0}$.

Differentiation of (7.7) then yields an expression for velocity as a function of time:

$$\frac{d\varepsilon}{d\tau} = 1 - Be^{-\tau} \qquad (7.8)$$

Equation (7.8) predicts that velocity decreases exponentially with time and hence will decrease with distance in a manner approximating an exponential decay.

2. Corrections to the Drag Coefficient

In the step between Equation (7.3) and (7.4) a correction term was applied to the so-called Stokes law drag coefficient. The question naturally arises as to what considerations are involved in this correction.

Corrections to the Stokes law relation should be made if any of the following situations arise:

(1) If the fluid is not infinite in extent

(2) If the motion is not dominated entirely by viscous forces; i.e., if vortices and/or separation occur behind the sphere

(3) If the fluid is not continuous--for the case of very small spheres the fluid must be regarded as a discontinuous molecular field

(4) If the sphere undergoes accelerated or decelerated motion in the fluid

(5) If the sphere is evaporating to a significant extent.

Clearly (1) and (3) above do not apply to spray systems such as this. The remaining corrections will be briefly discussed.

2.1 Corrections for Non-Creeping Flow

At values of the Reynolds number above 2.0, inertial forces can no longer be neglected in determining the drag coefficient. This correction is nearly always made by finding a function which will fit the experimentally determined data. A typical function is that of Langmuir:

$$C_D = \left(1 + 0.197 N_{Re}^{0.63} + 2.6 \times 10^{-4} N_{Re}^{1.38}\right) \frac{24}{N_{Re}} \qquad (7.9)$$

This equation describes the experimental data up to a Reynolds number of 2000 within an error of about seven per cent.

2.2 Corrections for Accelerated Motion

The drag coefficient is a function of the Reynolds number alone only when the motion is steady. There is very little experimental data available in the literature concerned with the acceleration effects on the drag relations. Most investigations which have been carried out point to the conclusion that the drag coefficient increases for both low and high Reynolds numbers whenever the density of the body approaches the density of the fluid. Basset[4] and Pearcy and Hill[39] have both

concluded from their studies that the effect of acceleration is small for small spheres and increases with increasing fluid density.

Crowe[7] has conducted a very interesting theoretical analysis of the effect of a constant linear acceleration on the drag coefficient. He was able to show that

$$\frac{\Delta C_D}{C_D} \leq -\frac{\pi}{9} A_c \qquad (7.10)$$

where

$$A_c = \frac{D}{V^2} \frac{dV}{dt}$$

By use of Equation (7.10) it is readily shown that acceleration will have no effect on the drag coefficients in sprays since the value of the acceleration modulus, A_c, is of the order of 10^{-4}.

2.3 Corrections for Evaporation of the Droplet

The most useful work carried out on the effect of evaporation on the drag coefficient was published by Crowe.[7] He began with the momentum equation describing the system and included in it the term for mass flux at the surface of the drop. The resulting integro-differential equation was solved by a perturbation technique to yield the relation:

$$\frac{C_{fo}}{C_f} < \frac{1 + 0.28\Delta C}{Sc^{2/3}(1-C_s)^{2/3}(Ce-1)^{1/3}} \qquad (7.11)$$

where

C_{fo} = skin friction coefficient for the case of no evaporation

C_f = skin friction coefficient for the case of evaporation

S_c = Schmidt number

C_s = concentration of the evaporating component at the surface

C_e = concentration of the evaporating component in the free stream

$\Delta C = C_s - C_e$

Crowe was further able to demonstrate that the effect of evaporation in the wake region is negligibly small compared to the effect predicted by Equation (7.11).

Using Equation (7.11) as a basis an estimate was made of the probable effect which evaporation will have for the specific cases of water and Freon 11 sprays. Assuming that the mass fraction in the free stream is near zero, the mass fraction at the surface may be estimated from

$$C_s = \frac{1}{1 + \frac{P}{P_v}\frac{M_A}{M_B}\left(1 + \frac{P_v}{P}\right)} \tag{7.12}$$

where

M_A, M_B are the molecular weights of air and the evaporating component, respectively

P_V is the partial pressure of the evaporating vapor

A semi quantitative measurement of the drop temperatures indicated that they were about 60°F for water and about -20°F for Freon 11. At these conditions P_V/P is small relative to one and Equation (7.12) becomes

$$C_s \approx \frac{P_v}{P}\frac{M_B}{M_A} \tag{7.13}$$

Using data available for water and Freon 11[11,12] the values of C_s were calculated for both systems. Substitution of these values into Equation (7.11) subject to the assumptions given above yields:

$$\frac{C_{fo}}{C_f} < 1 + 0.12 \tag{7.14}$$

for Freon 11, and

$$\frac{C_{fo}}{C_f} < 1 + 0.005 \tag{7.15}$$

for water.

Equations (7.14) and (7.15) state that the drag coefficient for water should be decreased by less than 0.5 per cent and for Freon 11 by less than 12 per cent.

2.4 Corrections for Interaction of Particles

The previous sections of this chapter have been concerned with the motion of individual droplets. If at some point in the spray the concentration of drops becomes large, they will exert a mutual influence upon the flow patterns around each other. The effect of concentration in streamline flow may be allowed for by an equation of the form

$$D = 3\pi\mu V D k_c \tag{7.16}$$

where k_c is a factor dependent upon particle concentration. Two correlations of k_c have been published. Steinour[55] found in a study of hindered settling that

$$k_c = \varepsilon_v^2 10^{-1.82(1-\varepsilon_v)} \tag{7.17}$$

and Birgers[8] in a theoretical study predicted that for relatively dilute "solutions"

$$k_c = 1 + 6.875(1 - \epsilon_v) \qquad (7.17a)$$

In the above two expressions ϵ_v is the fraction of fluid phase present. An estimation of ϵ_v for the sprays studied and use of Equation (7.17) predicted values of k_c of about 1.01 to 1.001. In other words this correction, based upon Equation (7.17) or (7.17a) may be considered negligible.

3. Induced Air Velocity

In Equations (7.2) and (7.3), which describe the motion of a droplet, one of the important parameters is the velocity of the gas stream. For a spray this velocity results from the phenomenon known as induced air flow. When the spray leaves the nozzle the leading droplets impart their energy to the surrounding air causing its forward motion and thereby reducing the air resistance for the following droplets.

Ranz and Binark[44] have conducted an experimental and theoretical investigation of induced air flows in hollow cone and solid cone sprays. The sprays formed by flashing jets are neither truly hollow cone or solid cone. This can be seen by reference to Table XII which summarizes the per cent of total flow by location in the spray (the locations referred to are those described in Chapter III).

TABLE XII

PER CENT OF TOTAL FLOW BY LOCATION IN SPRAY
(Injection Pressure 120 psig)

Distance from Nozzle	water				Freon 11			
	4	5	6	7	4	5	6	7
Location								
1	9.25	2.8	40.0	1.36	8.15	7.05	0.6	3.4
2	35.4	60.4	40.3	15.35	60.7	59.7	28.1	46.2
3	25.8	23.9	15.4	40.7	31.2	33.3	71.3	50.6
4	29.5	12.7	4.07	42.0				

3.1 Analysis of Induced Air Flow in a Hollow Cone Spray

An analysis of the induced air flow in a hollow cone spray can be based on a momentum balance between the total drag force operating on all of the droplets passing through an area in a given time interval and the component of air momentum in the direction of drop motion. As an approximation it can be assumed that at any given location on the outer periphery of the spray an average drop diameter and an average drop velocity can be specified together with the appropriate number of drops. This information is readily available from the experimental data. If one assumes that the average values are correct then the drag force on all of the droplets is

$$n\left(\frac{\pi D^2}{4}\right)\left(\frac{C_D \rho_A V_D^2}{2}\right) \tag{7.18}$$

where

n is the number of droplets

ρ_A is the air density

V_D is the velocity of the drop of diameter D

D is the drop diameter

C_D is the drag coefficient

Ranz has shown that the air enters the spray sheet at right angles to the motion of the droplets. The component of air momentum in the direction of drop motion is

$$\rho_A V_i^2 \operatorname{ctn}\theta \tag{7.19}$$

where

θ is the cone angle

V_i is the induced velocity of air entering from outside the spray.

A momentum balance then yields the expression

$$\frac{V_i}{V_D} = \left[\eta\left(\frac{\pi D^2}{4}\right)\left(\frac{C_D}{2\operatorname{ctn}\theta}\right)\right]^{1/2} \tag{7.20}$$

Using Equation (7.20) an estimate of V_i can be made and from this the air velocity inside the spray may be calculated, which from continuity considerations must be $(V_i/\sin\theta)$.

There are some limitations to this model which are enumerated below:

(1) In writing the momentum balance it was assumed that the air entered the spray at right angles to the direction of motion of the droplets. This assumption was partially verified by Ranz's experiments, but is certainly questionable.

(2) The model suggests that once a drop has slowed to its terminal velocity corresponding to the induced air velocity, that it will be blown into the center of the spray. The experimental data do not completely substantiate this conclusion. The drops on the outer periphery of the spray are, in general, larger than those in the center, but small droplets do occur at this location.

(3) The model assumes an unidirectional flow for the air in the spray core. Visual observations of the spray showed a tendency for swirling to occur, suggesting the occurrence of air flow in other than a vertically downward direction.

Nevertheless, the model is very useful for estimating the induced air velocity. Using Equation (7.20) the air velocity was calculated at a distance of four and five inches from the nozzle. The velocity at distances of six and seven inches were not calculated because at this point the spray was no longer conical but was cylindrical in shape. The results of these calculations are summarized in Table XIII.

TABLE XIII

CALCULATED INDUCED AIR VELOCITIES

Distance from Nozzle Inches	Fluid	Velocity Ft/Sec (Eq. 7.20)	Velocity Ft/Sec (Eq. 7.21)
4	Water	5.4	~40
5	Water	2.6	~40
4	Freon 11	4.9	~30
5	Freon 11	2.8	~30

We may summarize this by quoting from Ranz and Binark: "The air velocity outside the spray cone decreases with increasing distance

from the orifice and increasing distance from the spray sheet. Velocities inside the spray sheet are higher than the corresponding velocities outside the spray sheet and decrease with increasing distance from the nozzle orifice. In a radial traverse the air velocity shows a maximum on the spray cone axis."

Based on this, inside the spray sheet the following qualitative profile should occur:

(1) The air velocity is radially distributed about the center line and the velocity of the small drops should decrease from the center line outwards, since these drops should be carried along with the air stream.

(2) On the outer periphery of the spray sheet the drops should behave approximately according to the well known drag relationships if the induced air enters at right angles. The departure from this relationship could perhaps be construed as a measure of whether or not the induced air does actually enter at right angles.

(3) The drops in the central core should decelerate more or less uniformly and approach either their "terminal" velocity or the induced air velocity, whichever is larger. (The terminal velocity is in a moving air stream and is not to be confused with the more commonly used notion of terminal velocity in a still air stream.) The rate of approach to this terminal velocity will be different for different drop sizes.

3.2 Solid Cone Sprays

Ranz found that for solid cone sprays the air flow was also induced at right angles to the edge of the spray, but on entering the spray turned in the direction of the nozzle axis. He assumed that "average air velocity, drop velocity and liquid flux inside the spray have a normal radial distribution with the same dispersion, and that average drop and air velocities are approximately equal throughout the spray zone." Based on this assumption he showed that

$$\frac{V_A}{V_L} = \exp\left(-\frac{r^2}{s^2}\right)\frac{\left[1 + 32\left(\frac{\rho_A}{\rho_L}\right)\left(\frac{s^2}{D_o^2}\right)\right]^{1/2} - 1}{8\left(\frac{\rho_A}{\rho_L}\right)\left(\frac{s^2}{D_o^2}\right)} \qquad (7.21)$$

where

s is the r distance at which the spray liquid flux equals 1/e times the maximum value

D_o is the orifice diameter.

Using Equation (7.21) for the case of $r = 0$ (center line) and $s = 0.8$ for water and 0.4 for Freon 11 air velocities were once again estimated. They are also given in Table XIII. It is readily seen that this particular model does not describe the induced air flow in the spray very accurately, since the velocities are too high by an order of magnitude.

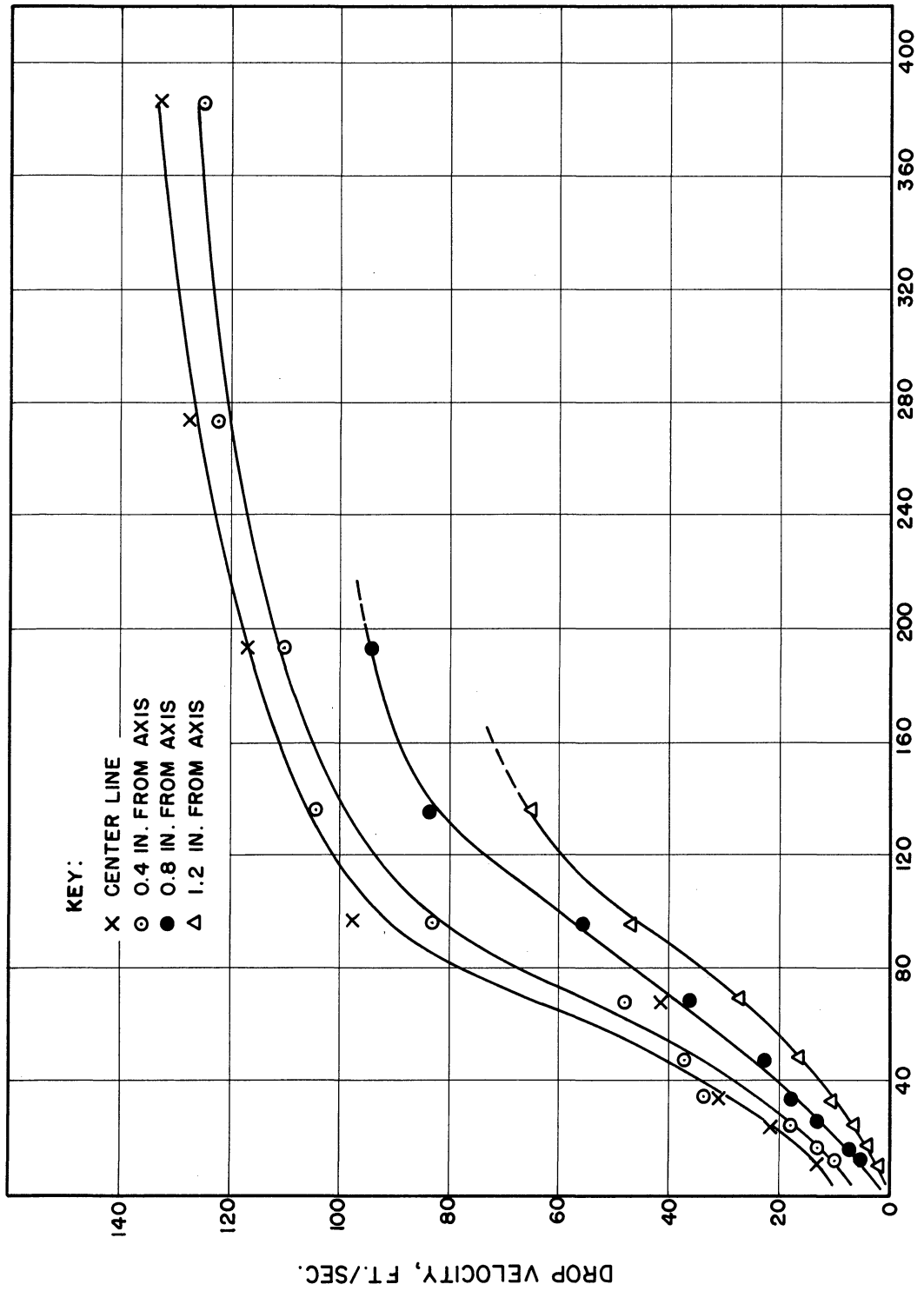

Figure 24. Typical Velocity Profiles -- Water at a Distance of Four Inches from the Nozzle.

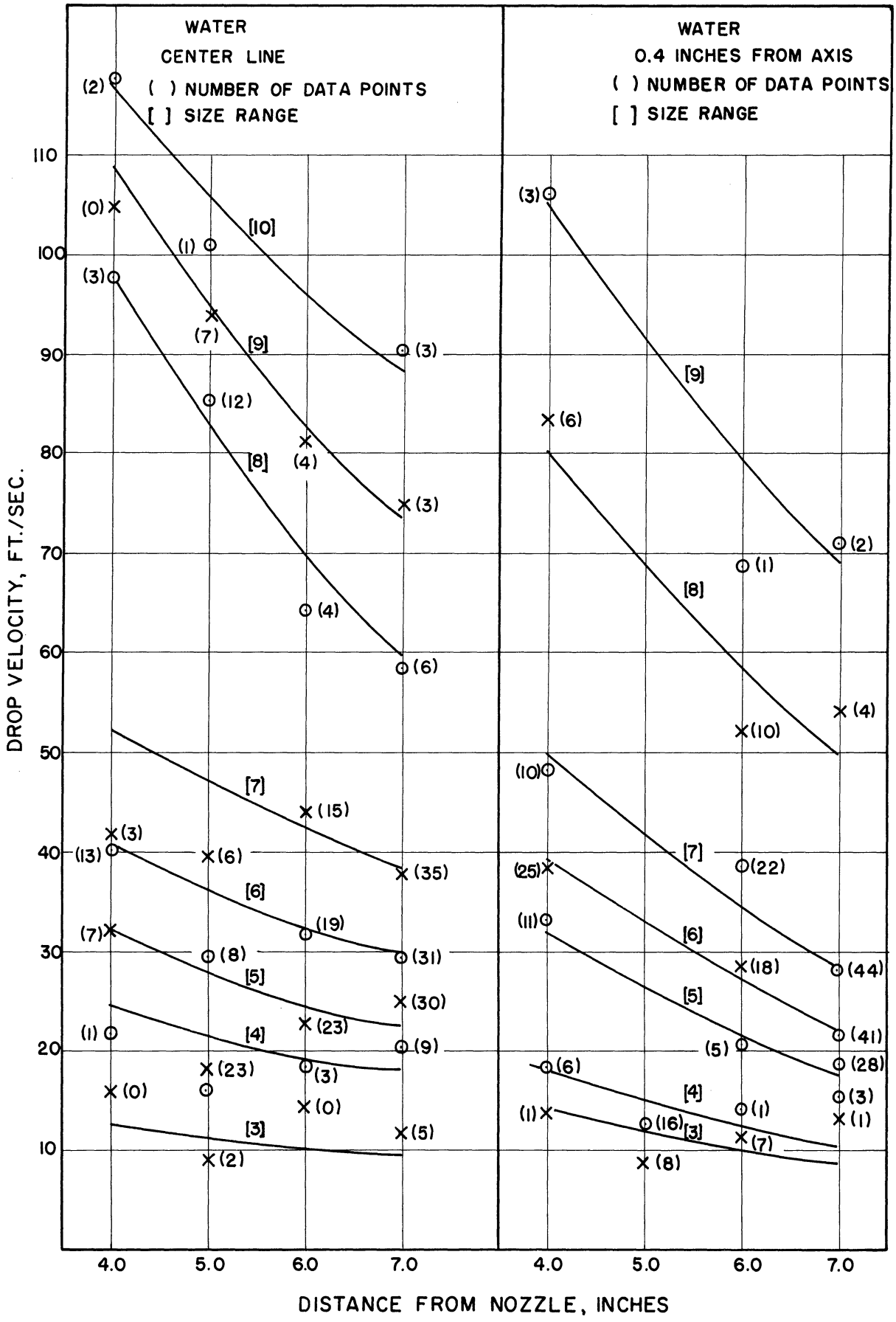

Figure 25. Velocity Profiles for Water, Locations 1 and 2.

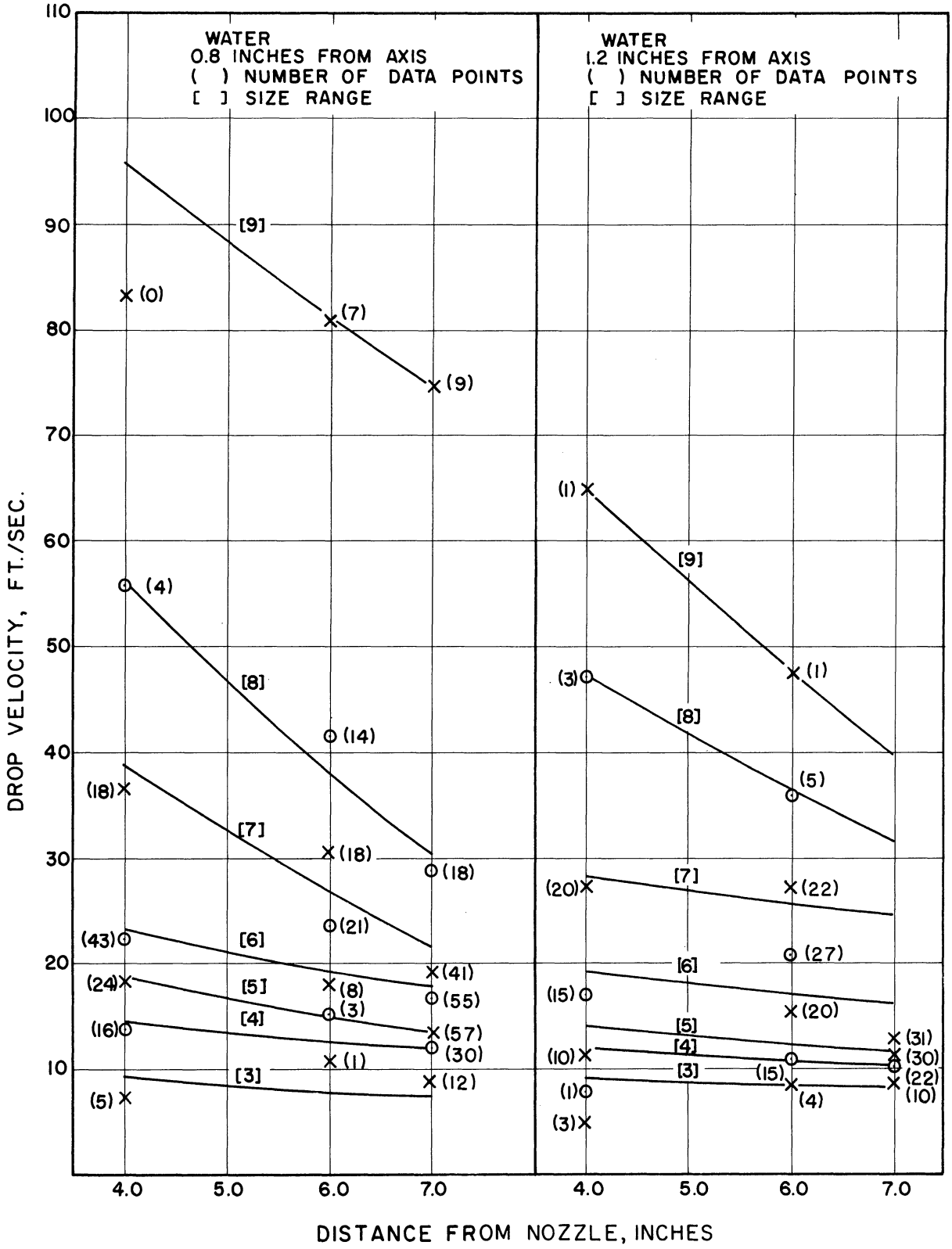

Figure 26. Velocity Profiles for Water, Locations 3 and 4.

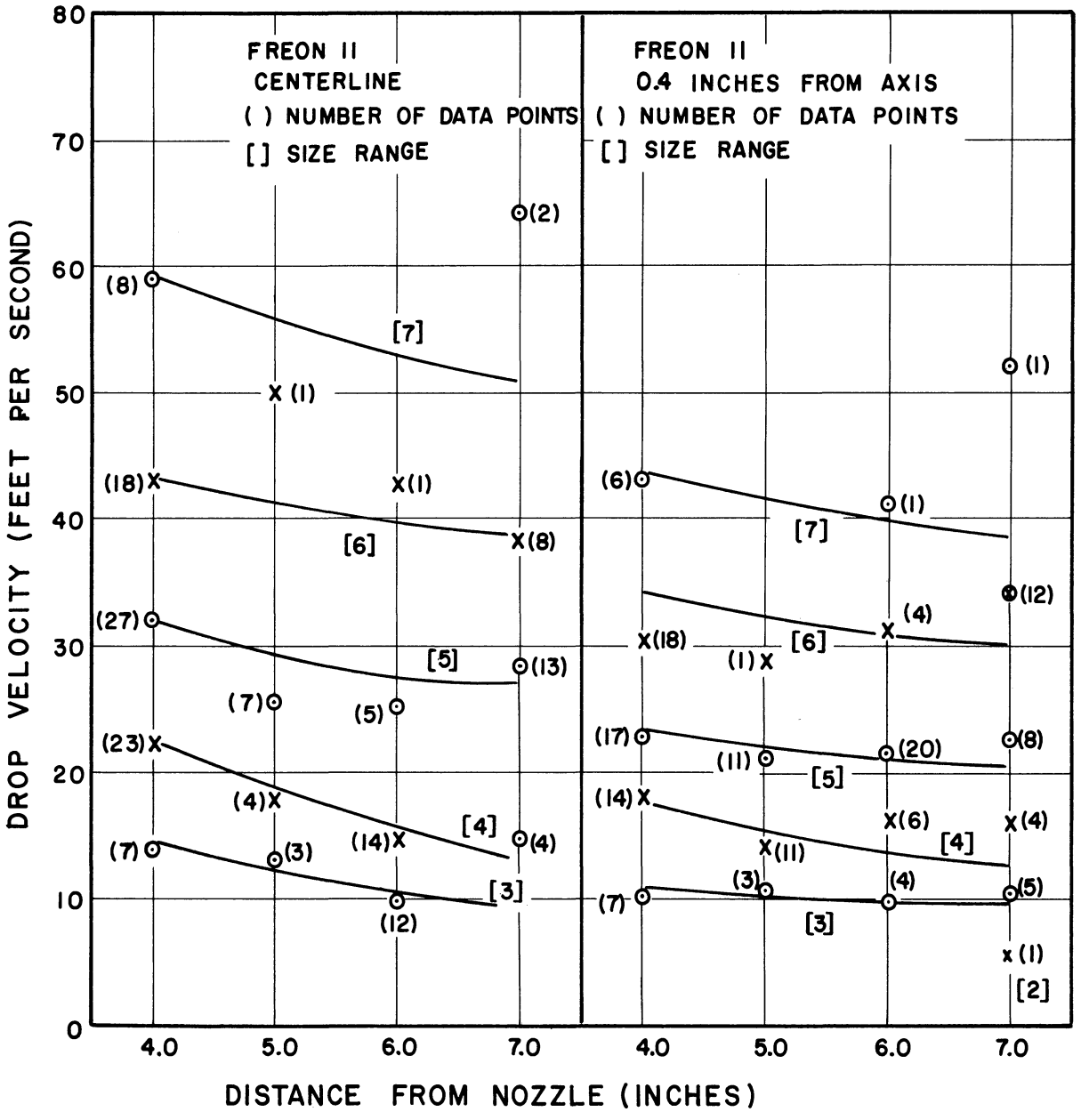

Figure 27. Velocity Profiles for Freon 11, Locations 1 and 2.

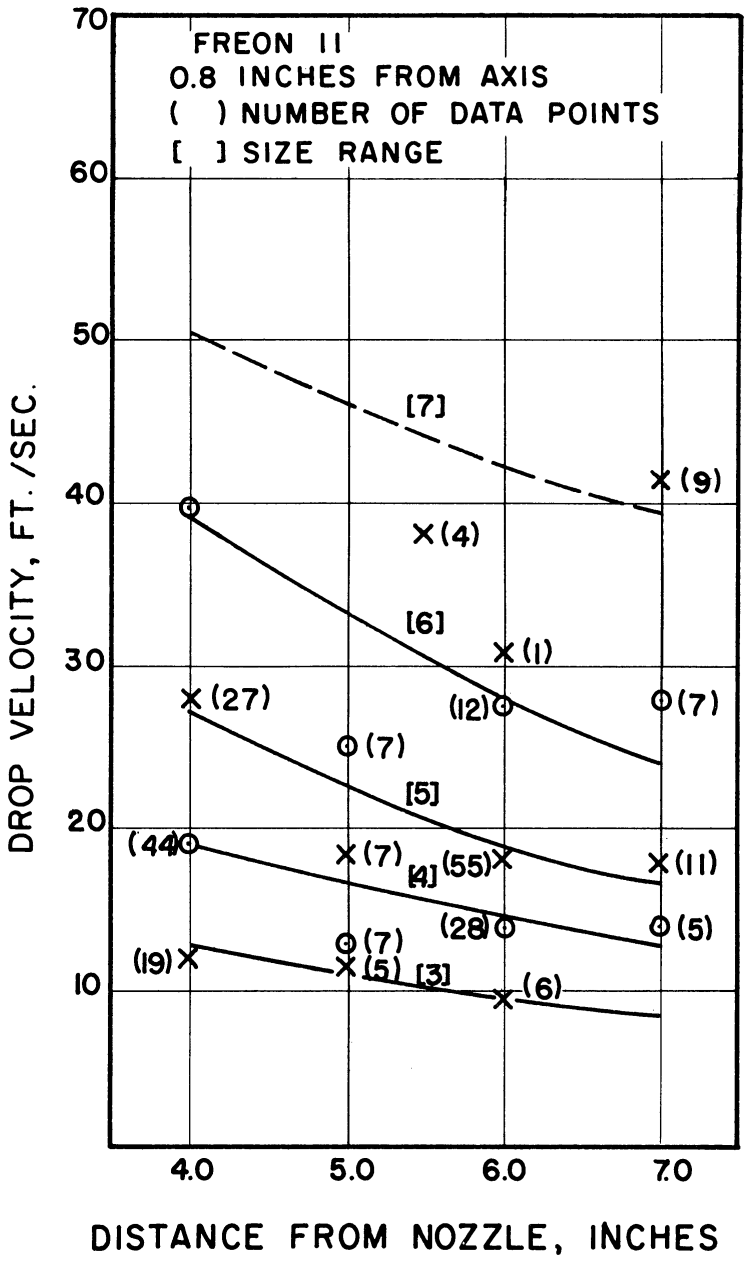

Figure 28. Velocity Profiles for Freon 11, Location 3.

4. Discussion of Data

The velocity profiles at all injection pressures and at all locations are essentially of the same form. Figure 24 is a typical set of velocity curves. It depicts the drop velocities for water at a distance of four inches from the nozzle and at an injection pressure of 120 psig. The curves are seen to be "S" shaped and the drop velocity for any given size range usually decreases as one moves away from the spray axis. Also at a given position relative to the center line larger drops are traveling at a higher velocity than smaller drops. Similar plots for all the other spray locations and for both fluids exhibited these same general characteristics.

A more useful manner of presentation of the velocity data is to construct at each location a plot of drop velocity as a function of distance from the nozzle, with size range as a parameter. Figures 25 through 28 are such plots for water and Freon 11. In all cases the drop velocity showed a tendency to decrease with increasing distance from the nozzle. The rate of decrease of the velocity is seen to be largest for larger drops and less for the smaller drops. In fact drops of about 10 to 15 microns do not appear to change velocity at all in traveling from four to seven inches away from the nozzle. This occurs because the drops are traveling at about the same speed as the induced air velocity, as is shown by Table XIII.

Figure 29 is a comparison of the drop velocities of water and Freon 11 for two injection pressures of 120 and 90 psig, at a distance of four inches from the nozzle. This figure illustrates the effect of pressure on the drop velocity and the effect of the fluid sprayed on the drop velocity.

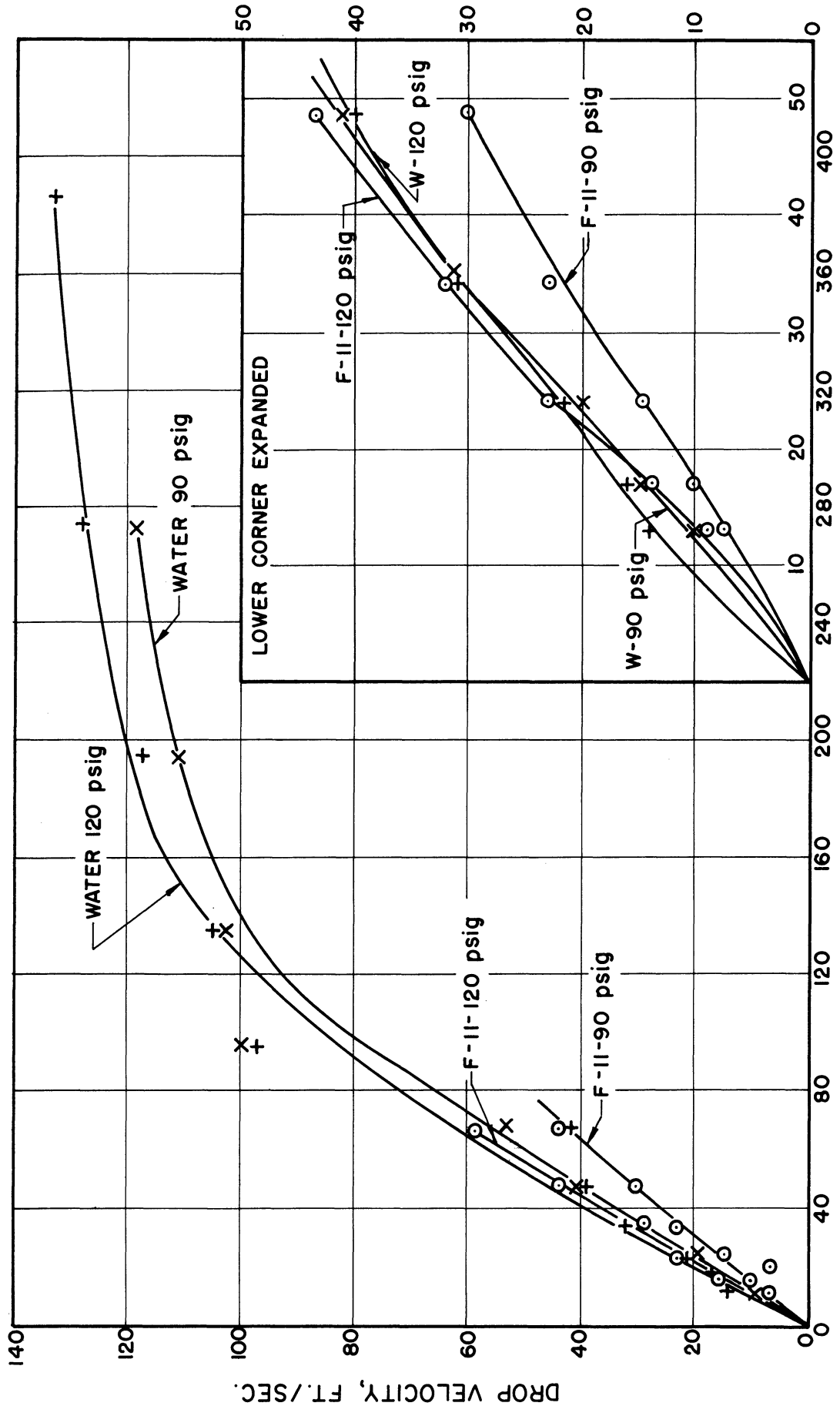

Figure 29. Comparison of Water and Freon 11 Drop Velocities.

A lowering of the injection velocity is found to decrease the drop velocity as would be expected, since the initial velocity corresponding to the injection pressure is lower (for example in the case of water from 110 ft/sec to 90.5 ft/sec). However, this 25 per cent reduction in initial velocity does not result in a 25 per cent decrease in drop velocity at any location. The reason for this is that a lowering of the injection pressure decreases the cone angle and hence tends to increase the induced air velocity, for the same flow rate. Or in other words the drag coefficient tends to be moved towards a lower value because of the increased gas stream velocity.

We may also compare the drop velocities of water and Freon 11 at the same distance from the nozzle and the same injection pressure. The initial velocities are 110 ft/sec for water and 90.5 ft/sec for Freon 11. The cone angles are about 44° and 22°, respectively. On this basis and considering the flow rates we would expect that for any given location and the same injection pressure that Freon drops will be traveling faster than water drops of the same size. We would further expect this because of the effect of evaporation on the drag coefficient. As was discussed in the previous section the drag coefficient for Freon 11 will be about 10 per cent lower than that for water at the same Reynolds number. Reference to Figure 29 and Figures 25, 26, 27 and 28 shows that this is indeed the case. For smaller droplets this tendency is less pronounced and the data do not support this line of argument too well. At least part of the difficulty in this respect arises from the extreme difficulty of accurately measuring drop velocities for drops of a size

below 20 microns, particulary in a very dense spray where it is difficult to separate drop images on a negative.

It will also be noted that the velocity profiles plotted as a function of distance from the nozzle do indeed exhibit an exponential type of decay, as was to be expected from Equation (7.8).

5. Summary

The preceding information may be summarized as follows:

(1) The drag relationships for single droplets may be applied qualitatively to the droplets contained in these sprays after taking into account any correction for the effect of evaporation on the drag coefficient and knowing the pattern of the induced air flow profiles. This same procedure could be applied analytically after an extensive study of these air profiles has been carried out since this is one of the most critical factors which determines the drop velocity profiles.

(2) All of the drops tend towards a common terminal velocity, which is the induced air velocity corresponding to the particular location of the drop. Many drops will have evaporated before they reach this terminal velocity.

(3) The sprays are more nearly hollow cone than solid cone, although they do not strictly belong to either classification.

CHAPTER VIII

SPRAY CHARACTERISTICS

1. Drop Size Distribution Functions

The droplet size distribution is certainly one of the most important characteristics of any spray but it is also the spray property most difficult to predict theoretically. The drop size distribution of any spray is usually represented by two parameters--a mean diameter and a parameter which measures the deviation of the drops from this mean.

1.1 Distribution Function

A probability density function $f(x)$ is said to exist when these criteria are met:

if

$$f(x) \geq 0 \tag{8.1}$$

$$\int_{-\infty}^{\infty} f(x)\,dx = 1 \tag{8.2}$$

and if in addition

$$P(X \leq x) = \int_{-\infty}^{x} f(x)\,dx \tag{8.3}$$

then the $f(x)$ is defined as the probability density function. The probability distribution function is defined in terms of the probability density function as

$$F(x) = \int_{-\infty}^{x} f(x)\,dx \tag{8.4}$$

In Equations (8.1) to (8.4), x is considered to be any random variable. For drop size analyses it is associated with the drop diameter. The methods of expressing distribution functions are usually associated with a number distribution dn/dx or with a volume distribution dv/dx. The term dn/dx may be thought of as representing the number of drops dn in the size interval x to x + dx. Similarly, dv/dx represents the volume of drops in the same size interval. The two distributions are easily related for the case of spherical particles.

Statisticians define the k-th moment about the origin of the frequency curve f(x) by

$$m_k = \int_a^b x^k f(x)\,dx \tag{8.5}$$

Mugele and Evans[36] developed the expression below which may be used to calculate any mean diameter

$$\bar{X}_{pq} = \left[\frac{\int_{x_o}^{x_m} X^p f(x)\,dx}{\int_{x_o}^{x_m} X^q f(x)\,dx} \right]^{\frac{1}{p-q}} \tag{8.6}$$

The most commonly used mean diameters are given in Table XIV.

TABLE XIV

COMMONLY USED MEAN DIAMETERS

p	q	Name of Mean Diameter	Diameters Application
1	0	Linear	Comparisons, Evaporation
2	0	Surface	Surface Area Controlling (Absorption)
3	0	Volume	Volume Controlling (Hydrology)
2	1	Surface Diameter	Adsorption
3	1	Volume Diameter	Evaporation, Molecular Diffusion
3	2	Sauter Mean	Efficiency Studies, Mass Transfer
4	3	De Brouckere	Combustion Equilibrium

There are three commonly used distribution functions in spray analyses--The Rosin-Rammler Equation, the Nukiyama-Tanasawa Equation and the log normal distribution. The first two of these are completely empirical in nature, while the log normal distribution can be derived theoretically[24] by assuming that the droplet size is the result of a large number of small, independent impulses, the effects of which are proportional to the size of the drop. It has been pointed out[43] that all of these distributions are special cases of the equation

$$f(x) = \alpha x^{\beta} e^{-\gamma x^{\delta}} \tag{8.7}$$

The distributions are summarized in the following equations:

(1) Rosin-Rammler Distribution

$$f(x) = bnx^{n-1} e^{-bx^{n}} \tag{8.8}$$

or as it is often written

$$R = e^{-bx^{n}} \tag{8.8a}$$

where R is the volume fraction of drops of size greater than x.

(2) Nukiyama-Tanasawa Distribution

$$f(x) = ax^2 e^{-bx^n} \tag{8.9}$$

where a, b, n are constants.

(3) Log Normal Distribution

$$f(x) = \frac{1}{\sqrt{2\pi}} e^{-\frac{\log x - \log \bar{x}g}{\log \sigma g}} \tag{8.10}$$

where

$\bar{x}g$ is the geometric mean

σg is the geometric standard deviation.

Another commonly used form of Equation (8.10) is

$$\frac{dn}{dy} = \frac{\delta}{\sqrt{\pi}} e^{-\left(\delta y - \frac{2\delta}{3}\right)^2} \tag{8.10a}$$

where

$y = \ln x/\bar{x}$, and

δ is a dispersion parameter.

The three distributions are integrable as special cases of the incomplete gamma function

$$\Gamma_\alpha(\ell) = \int_0^\infty e^{-t} t^{\ell-1} dt \tag{8.11}$$

which is tabulated in most statistics books. The transformations for the integrations are also readily available and are summarized in Table XV.

TABLE XV

TRANSFORMATIONS AND INTEGRALS FOR DENSITY FUNCTIONS

	Transformation	Distribution Function
log normal	$\ell = 1/2$ $t = x^2/2$	$F(x) = \frac{1}{2\sqrt{\pi}} \Gamma_{x^2/2}(1/2)$
Rosin-Rammler	$\ell = 1$ $t = bx^n$	$F(x) = \Gamma_{bx^n}(1)$ $= (1 - e^{-bx^n})$
Nukiyama-Tanasawa	$\ell = 3/n$ $t = bx^n$	$F(x) = \frac{a}{nb^{3/n}} \Gamma_{bx^n}(3/n)$

1.2 Test of Distribution Functions to Fit Experimental Data

The distribution functions may be tested for their fit of the experimental data in the following ways. The Rosin-Rammler distribution shown is applicable to volumes and R is then associated with the volume fraction, larger than some diameter x. Taking logarithms twice of Equation (8.8a) gives

$$\log\log(R) = -\log b - n\log x - \log\log e \qquad (8.12)$$

which is a linear relationship between log log R and log X. The constants b and n may be evaluated either analytically or graphically. Table XXV of Appendix F summarizes the values of these two constants for the sprays studied. The numerical calculations were carried out on the IBM 709 computer using standard statistical techniques.

With the Nukiyama-Tanasawa distribution we are interested in the number distribution expressed as a per cent. Equation (8.9) may

be expressed in the form

$$\log\left[\frac{1}{x^2} f(x)\right] = \log a - b x^n \log e \qquad (8.13)$$

which is a linear relationship in a and b for a predetermined value of n. Nukiyama and Tanasawa have found that values of n between 1/4 and 1/2 give the best fit of drop size data. Three values of the parameter were used--n equal 1/4, 1/3 and 1/2 and in all cases it was found that n equal 1/4 give the best fit, although the difference between any of the three values was small. (Typical correlation coefficients were 0.963, 0.958 and 0.938 for n equal 1/4, 1/3 and 1/2, respectively.) Values of the constants a and b in Equation (8.13) for n equal 1/4 are given in Appendix F. These were determined using the same type of computer program as was used to find the constants in the Rosin-Rammler equation.

The log normal distribution function is most easily tested by plotting on log probability paper the cumulative number per cent versus the drop diameter. (The drop diameter used is the upper limit of the size range.) This plot should yield a straight line if a fit to the log normal distribution is obtained. A typical run is shown in Figure 30 and Table XVI. Similar plots for all of the experimental data may be found in Appendix B. In testing this distribution the end points should likely be truncated since it is obviously impossible to fit any finite range of drop sizes with an infinite range distribution function.

Values of the uniformity parameter [Equation (8.10a)] are readily obtained from the same plots by making use of the relationship

$$\delta = \frac{0.394}{\log_{10}\left(\frac{D_{90}}{D_{50}}\right)} \qquad (8.14)$$

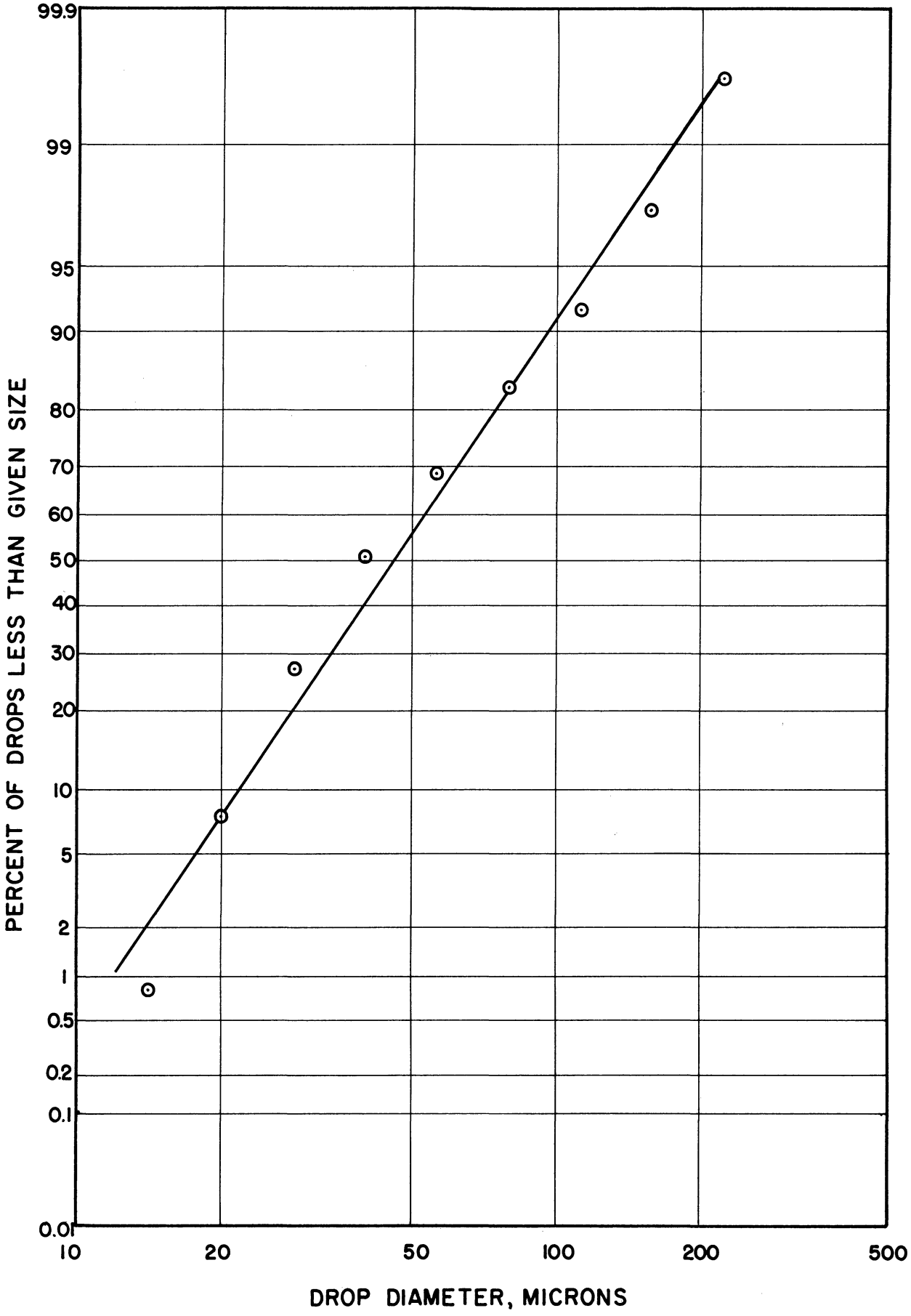

Figure 30. Typical Fit of Log Normal Distribution -- Run No. 2.

where D_{90}, D_{50} are the diameters at cumulative percentages of 90 and 50, respectively.

The values of this parameter are given in Table XVII.

TABLE XVII

SIZE DISTRIBUTION FOR TOTAL SPRAY

RUN 2

Size Range	Per Cent	Per Cent Per Size Range	Cumulative Per Cent
1	0.000	0.00	0.000
2	0.826	0.201	0.826
3	6.88	1.17	7.70
4	18.87	2.30	26.58
5	23.98	2.03	50.56
6	17.79	1.09	68.35
7	14.80	0.627	83.116
8	8.83	0.268	91.99
9	5.68	0.121	97.67
10	1.98	0.0301	99.65
11	.342	0.0036	100.00

1.3 Discussion of the Utility of the Three Functions

Reference to the over-all correlation coefficients given in Appendix F for the Rosin-Rammler and Nukiyama-Tanasawa distribution functions and to the log probability plots shows that all three functions will adequately describe the experimental data. In fact, for an individual location within the spray the Rosin-Rammler distribution is perhaps best, but for purposes of describing the total spray distribution all three appear of equal accuracy. Since the two more complicated distributions do not, in general, give any better fit of the experimental data than the log normal distribution there would appear to

be no justification for their use unless for some specific purpose. Also the log normal distribution does have some additional basis in theory[24] while the other two do not, even though all three are special cases of the gamma function.

2. Experimental Mean Drop Diameters

The various mean drop diameters were previously defined by Equation (8.6). In order to estimate their value using discrete rather than continuous random variables, the expression

$$\bar{D}_{mn} = \left[\frac{\sum_i D_i^m \Delta N}{\sum_i D_i^n \Delta N} \right]^{\frac{1}{m-n}} \tag{8.15}$$

may be used as being approximately equivalent to (8.6). The mean diameters calculated were the linear mean diameter D_{10}, the surface mean diameter D_{20}, the surface diameter D_{21} and the Sauter mean diameter D_{32}. The values computed from the data are given in Table XVII.

The variation of these mean diameters as a function of distance away from the nozzle is discussed in the chapter on spray evaporation. At any fixed distance away from the nozzle the mean diameter tends to increase with increasing distance from the center line. In most instances for water a minimum appears to exist at a distance of 0.4 inches away from the spray axis. For Freon 11 this does not occur and there is no minimum present in the curve. The presence of the minimum can be explained in part by the breakup mechanism. When the vapor bubbles disintegrate the jet the drops will have two components of velocity, one parallel to and one perpendicular to the spray axis. Under these

TABLE XVII

MEAN DROP SIZES

Run	Fluid	P (Psig)	T°F	Location*	Mean Drop Size (Microns) δ	D_{10}	D_{20}	D_{21}	D_{32}
1	W	90	287	1		47.3	54.8	63.4	84.0
1	W	90	287	2		46.7	52.2	58.5	73.2
1	W	90	287	3		65.7	69.5	73.4	82.3
1	W	90	287	4		64.1	68.2	72.6	81.8
1	W	90	287	Total	2.09	54.0	59.7	65.9	78.8
2	W	120	287	1		53.8	64.8	78.0	105.0
2	W	120	287	2		58.9	76.3	98.7	144.0
2	W	120	287	3		44.8	53.9	64.9	89.6
2	W	120	287	4		62.6	68.1	74.2	85.4
2	W	120	287	Total	1.56	52.9	65.3	80.6	115.8
3	W	120	287	1		91.1	127.2	177.6	264.1
3	W	120	287	2		57.6	74.5	96.4	146.4
3	W	120	287	3		60.5	69.2	79.0	93.7
3	W	120	287	4		104.3	108.0	111.9	118.2
3	W	120	287	Total	1.00	63.3	80.6	102.6	159.6
4	W	120	287	1		47.5	55.0	63.7	81.4
4	W	120	287	2		54.8	65.9	79.2	109.4
4	W	120	287	3		66.4	79.6	95.6	131.5
4	W	120	287	4		58.2	68.5	80.6	107.2
4	W	120	287	Total	1.16	59.6	71.0	84.7	115.8
5	W	120	287	1		79.2	120.9	184.7	285.7
5	W	120	287	2		52.0	29.2	67.5	87.9
5	W	120	287	3		52.7	56.7	60.9	69.8
5	W	120	287	4		45.3	48.1	51.2	57.8
5	W	120	287	Total	1.67	52.2	58.8	66.3	97.4
6	F-11	90	158	1		29.4	31.4	33.6	38.3
6	F-11	90	158	2		30.7	33.1	35.7	40.8
6	F-11	90	158	Total	1.90	29.9	32.1	34.4	39.3
7	F-11	120	158	1		26.9	28.1	29.3	31.9
7	F-11	120	158	2		28.0	29.5	31.0	34.6
7	F-11	120	158	3		28.5	29.8	31.2	33.9
7	F-11	120	158	Total	2.36	28.1	29.5	30.9	34.1
8	F-11	120	158	1		23.5	24.5	25.6	27.8
8	F-11	120	158	2		26.2	27.9	29.8	34.4
8	F-11	120	158	3		29.2	30.2	31.3	33.4
8	F-11	120	158	Total	2.43	26.8	28.3	29.8	33.5
9	F-11	120	158	1		26.2	27.5	28.8	32.3
9	F-11	120	158	2		30.0	31.6	33.2	36.7
9	F-11	120	158	3		32.7	34.7	36.9	41.4
9	F-11	120	158	Total	2.03	31.7	33.6	35.6	39.9
10	F-11	120	158	1		39.5	42.1	44.8	50.5
10	F-11	120	158	2		45.3	47.6	50.0	54.8
10	F-11	120	158	3		47.9	50.5	53.2	58.7
10	F-11	120	158	Total	2.10	46.2	48.7	51.3	56.6

* Location refers to those given in Appendix B. "Total" means the mean diameter for the entire spray.

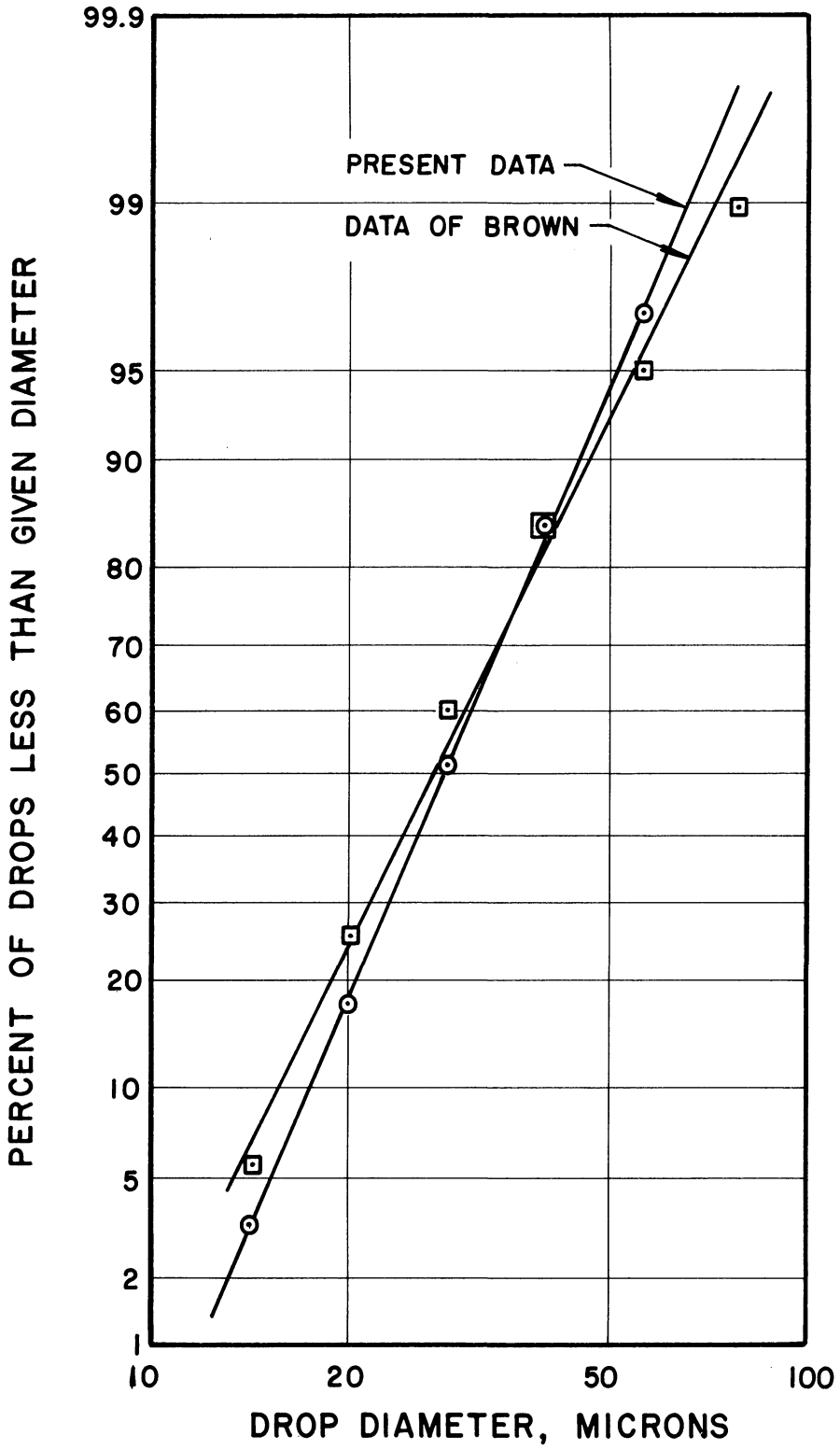

Figure 31. Comparison of Experimental Data with Brown's Data ---Freon 11.

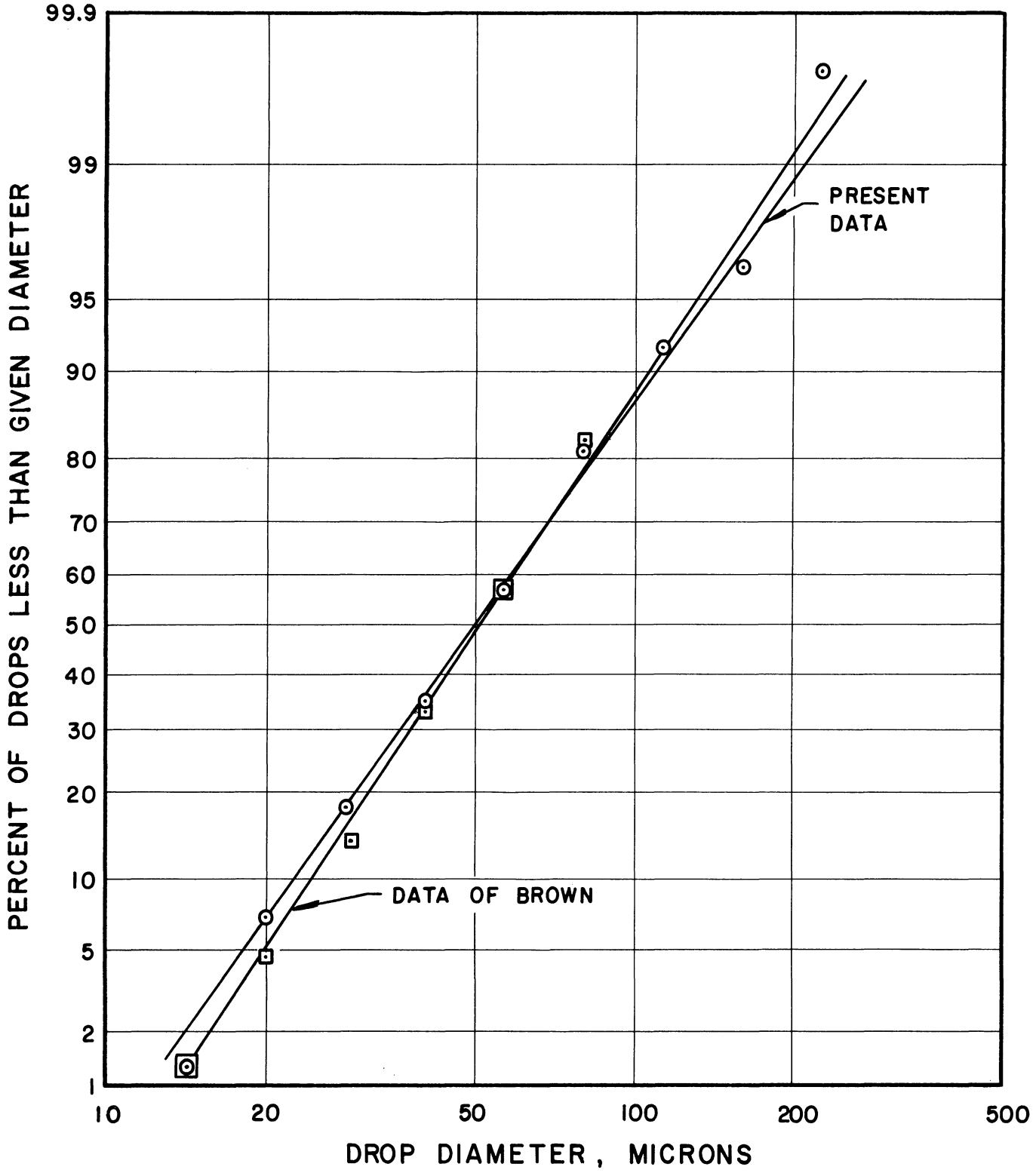

Figure 32. Comparison of Experimental Data with Brown's Data -- Water.

conditions the larger drops will, at any given point, have moved furthest away from the spray axis. The drop diameter might be expected to increase at the spray axis because it is at this point that any drops formed from a portion of the jet not shattered by vapor evolution will likely have only one velocity component. If such drops form they will tend to be slightly larger than those formed from a shattered portion of the jet. A second factor to be considered here is that smaller drops evaporate faster than larger drops and any slight minimum existing in the diameter curve will tend to be accentuated as the distance away from the nozzle (and thus evaporation time) increases.

3. Reproducibility of Experimental Data

Whenever experimental techniques involve a human judgement factor the reproducibility of the experimental data is naturally subject to some question. In Chapter VI it was pointed out that the flow rate as calculated from the drop size distributions is a measure of the accuracy of the data. Another means of judging the experimental accuracy is, in this instance, to simply reproduce data taken by Brown. Figure 31 is a plot of the log normal distribution function for Freon 11 at an injection pressure of 120 psig. The experimental data of Brown for Freon 11 at 120 psig and the same injection temperature is also shown. Similarly, the two sets of data for water at an injection pressure of 120 psig were compared and the results are shown in Figure 32. It will be seen that in both cases the agreement between the two is quite good.

Another valid comparison is between average drop diameters measured by two experiments. The results of this comparison are given

in Table XVIII. Here again the results of the comparison are favorable, particularly for the entire spray. The largest deviations occur either

TABLE XVIII

COMPARISON OF MEAN DIAMETERS WITH BROWN'S DATA
(Diameters in Microns)

	Freon 11		Water	
Location	Brown	Short	Brown	Short
1	46.8	26.2	32.2	47.5
2	21.9	30.0	43.9	54.8
3	22.4	32.7	60.2	66.4
4			74.9	58.2
Total	37.6	31.7	55.5	59.6

at the center line of the spray or at the outer periphery of the spray which could be predicted, because these are the most difficult places in the spray to analyze accurately. However, errors in these two locations do not seriously affect a flow rate calculation for the following reasons:

(1) The major portions of the drops occur in locations two and three.

(2) Even if a high drop density is found at the spray axis, it represents a very small portion of the total volumetric flow, and an error at this point is not magnified to such an extent.

(3) The drop density on the outer edge of the spray is low enough to once again mask any experimental error present when calculating a flow rate.

The results of these comparisons was indeed gratifying and would seem to support the reliability of the data.

CHAPTER IX

CONCLUSIONS

This work has shown that the flashing process is an effective means of producing a fine and uniformly dispersed spray at low values of the Weber number and corresponding low injection pressures.

The shatter temperature is a defining characteristic of a flashing spray and it may be represented by the equation

$$\left(\frac{T_s}{\mu H_{fg}}\right) = 0.344(Z)^{-0.272}(N_{we})^{-0.231}\left(\frac{\rho_v}{\rho_L}\right)^{0.139} \qquad (9.1)$$

The range of variables represented in the above equation would appear to be wide enough to justify its use with fluids other than water, Freon 11 or Freon 113. The use of Equation (9.1) is not likely justified for flashing sprays containing dissolved or suspended materials. Also it may not prove valid at large values of the liquid viscosity since it is an unfortunate fact that all pure liquids at their normal boiling point have about the same viscosity. For this reason the range of viscosities studied was necessarily small. Equation (9.1) may not prove valid if the receiving pressure is too far removed from atmospheric.

The log normal distribution is adequate for the description of drop sizes, particularly if one is interested in the total spray. The other two most commonly used size distributions, the Rosin-Rammler and the Nukiyama-Tanasawa equations, will also give an accurate description of the drop size distributions, but require considerably more expenditure of effort in order to use them, or to evaluate the constants.

The methods of calculating spray evaporation in the literature[32,42] can be applied to sprays formed by this flashing process with a great deal of success. Care must be taken to insure that the spray droplets have cooled from their saturation temperature to their wet bulb temperature before attempting to use any of the methods.

In general, the mean drop diameters increase from the spray axis outwards, at a fixed distance away from the nozzle. No such simple remark may be made about the mean diameter as a function of distance away from the nozzle, at any given location. This functional relationship is strongly dependent upon the drop size distribution and to a lesser extent upon the velocity distribution, both of the air and of the droplets.

The drop velocities within the spray follow the expected patterns. The drops tend to decrease in velocity in an exponential manner as they travel away from the orifice with the smaller drops slowing down more rapidly than the larger drops. The drop velocity (for any given size of drop) decreases as the distance away from the spray axis increases. Drops having a diameter of about 20 microns or less approach a common velocity which is the velocity of the induced air flow.

CHAPTER X

RECOMMENDATIONS

As typically occurs in investigations like this, each problem studied brings forth two or three new and unexpected problems. During the course of the work there were a few questions which arose and seemed worthy of further investigation, at some future date.

1. In discussing the drop velocity profiles, reference was made to the induced air flow. A more accurate knowledge of this air flow would indeed be very valuable to the interpretation of the velocity profiles. It might prove possible to calculate the induced air velocities from the experimental drop velocities given. Such a calculation would be very involved and require a large number of numerical integrations. Other directions of study in this regard should be to formulate the mathematics necessary to compute the air velocities from the experimental data, and to experimentally measure the air velocities, perhaps in a manner similar to Ranz and Binark.
2. A study of the humidity and temperature profiles within the sprays, particularly Freon 11, would enable one to gain much useful information regarding the evaporation rates taking place.
3. A study of the effects of high viscosity upon the flashing mechanism would be very beneficial. This could be done in at least two ways--either by an artificial thickener

such as Methocel or by spraying the liquid into surroundings which are at a pressure below atmospheric. This latter method would effectively change the liquid viscosity by lowering the saturation temperature. Either of these two studies will require extensive modifications to the experimental system. This particular investigation would also have an additional benefit in testing the effect of the surrounding gas density on the shatter temperature correlation, or in other words to see if the Weber number adequately describes this effect.

4. The most laborious and time-consuming job in a study such as this is the counting of drops. It would prove well worthwhile to try to find some easier and less time-consuming means of scanning photographic negatives.

APPENDICES

APPENDIX A

COMPUTER PROGRAM

Shown in the following pages (Tables XIX and XX) is the computer program used to analyze the raw data and the input variables associated with it. The program is written in MAD and with the tables its use is fairly obvious.

Other computer programs were written to carry out the regression analysis of the shatter temperature data and the least squares analysis of the Rosin-Rammler and Nukiyama-Tanasawa distributions. These programs are not included in this dissertation because they use readily available statistical methods [see for example Volk(58)] and are easily programmed.

TABLE XIX

LIST OF INPUT VARIABLES FOR COMPUTER PROGRAM

Height	height of sample size (0.5 inches)
Width	width of sample size (0.4 inches)
Depth	depth of field
Const 1	1.0
Const 2	1.0
Dodia	if equal to 0 will not compute any average diameters
Docum	if equal to 0 will not compute cumulative percentages
Dopin	if equal to 0 will not compute per cent per size interval
Survol	if equal to 0 will not compute surface and volume flow rates
Dogem	if equal to 0 will not use geometric means
M	number of locations
N	number of size intervals
S	highest power on mean diameter (usually 3)
VOLV	if equal to zero will not compute volume distributions
KE	if equal to 0 will not compute kinetic energies
MOMN	if equal to 0 will not compute momentum flux
SUPER	if equal to 0 will not consider the spray as superheated
BAD	0 (controls error check in program)
Dens (I)	fluid density at i-th location
Radius (I)	radial vector from nozzle to center of i-th location
Angle (I)	angle between radius vector and vertical
Photos (I)	number of photographs at i-th location

TABLE XIX (CONT'D)

Endpoint (I)	endpoint of size range (begins at zero)
Cell (I)	size interval of each size range
NUM (I)	numerator in mean diameter calculation
DEN (I)	denominator in mean diameter calculation
	e.g., NUM = 1; DEN = 0 is the linear mean diameter
SPEED (I,J)	velocity of drops in i-th size interval, j-th location
NUMBER (I,J)	number of drops in i-th size interval, j-th location
DM	nozzle diameter
DELP	pressure drop across the nozzle
VISC	fluid viscosity
DG	surrounding gas density
SIGMA	fluid surface tension
H21	enthalpy of superheated liquid
H2F	enthalpy of liquid at saturation point
H1F	enthalpy of vapor at saturation point
RHO2	density of liquid
RHO1	density of vapor
K	fluid thermal conductivity
SPHT	specific heat of liquid

TABLE XX

COMPUTER PROGRAM

```
          DIMENSION SUM(30), SUMN(30)
          DIMENSION RADIUS(20), ANGLE(20), PHOTOS(20), CELL(30),          1 DPK
         0 ENDPT (60), TDIAM (10), W (30), AREA (20), VOLUME (20),        2 DPK
         1 G(30), NUM(10), DEN(10), RATIO(30),RAT2(30),DENS(30)           3 DPK
          DIMENSION SPEED (300,D), NUMBER (300,D), PCT (300,D),           4D--K
         0 CUMPCT (300,D), PCTINT (300,D), DIAM (300,B), F (300,C1),      5 DPK
         1 X(300,D), Y(300,D1),MASS(300,D),MOM(300,D),ENERGY(300,D)       6 MPK
          VECTOR VALUES B = 2,1,0
          VECTOR VALUES C1 = 2,2,0
          VECTOR VALUES D = 2,1,0                                         7 DPK
          VECTOR VALUES D1=2,2,0                                          7ADPK
START     READ FORMAT DCARD1, HEIGTH, WIDTH, DEPTH, CONST1, CONST2,       8 DPK
         1 DODIA,DOCUM,DOPIN,SURVOL,DOGEM,M,N,S,VOLV,KE
          VECTOR VALUES DCARD1 = $5F10.5,10I3*$
          READ FORMAT CARD, MOMN, SUPER, BAD
          VECTOR VALUES CARD =$3I3*$
          INTEGER M,N,S,DODIA,DOCUM,DOPIN,SURVOL,DOGEM,I,J,R              10ADPK
          INTEGER NUM, DEN, PHOTOS, VOLV ,KE, MOMN, BAD
          B(1) = M+1
          B(2) = M
          C1(1) = M+1
          C1(2) = M
          D(2) = N                                                        11 DPK
          D1(2)=N+1                                                       11ADPK
          READ FORMAT DCARD, DENS(1)...DENS(M)
          VECTOR VALUES DCARD=$(8F10.4)*$
          READ FORMAT DCARD2, RADIUS(1)...RADIUS(M)                       12 DPK
          VECTOR VALUES DCARD2 = $(8F10.5)*$                              13 DPK
          READ FORMAT DCARD3, ANGLE(1)...ANGLE(M)                         14 DPK
          VECTOR VALUES DCARD3 = $(8F10.5)*$                              15 DPK
          READ FORMAT DCARD4, PHOTOS(1)...PHOTOS(M)                       16 DPK
          VECTOR VALUES DCARD4 = $16I5*$                                  17 DPK
          READ FORMAT DCARD5, ENDPT(0)...ENDPT(N)                         18 DPK
          VECTOR VALUES DCARD5 = $(8F10.5)*$                              19 DPK
          READ FORMAT DCARD6, CELL(1)...CELL(N)                           20 DPK
          VECTOR VALUES DCARD6 = $(8F10.5)*$                              21 DPK
          READ FORMAT DCARD7, NUM(1)...NUM(S+1)
          VECTOR VALUES DCARD7 = $10I5*$                                  23 DPK
          READ FORMAT DCARD8, DEN(1)...DEN(S+1)
          VECTOR VALUES DCARD8 = $10I5*$                                  25 DPK
          READ FORMAT MAT1, SPEED(1,1)...SPEED(M,N)                       26 DPK
          VECTOR VALUES MAT1 = $(8F10.5)*$                                27 DPK
          READ FORMAT MAT2, NUMBER(1,1)...NUMBER(M,N)                     28 DPK
          VECTOR VALUES MAT2 = $(8F10.5)*$                                29 DPK
          WHENEVER DOGEM.E.0, TRANSFER TO RED
          W(1) = (ENDPT(1)).P.(.5)
          THROUGH DOG, FOR J=2,1,J.G.N
DOG       W(J) = (ENDPT(J)*ENDPT(J-1)).P.(.5)
          TRANSFER TO OUT
RED       THROUGH RET4, FOR J=1,1,J.G.N
          W(J)=(ENDPT(J-1)+ENDPT(J))/2.
OUT       CONTINUE                                                        29FDPK
RET4      CONTINUE                                                        29GDPK
          WHENEVER DOGEM.E.0, TRANSFER TO AMEAN1                          29HDPK
          PRINT FORMAT RES23                                              29IDPK
          VECTOR VALUES RES23=$38H1THIS COMPUTATION USES GEOMETRIC MEAN   29JDPK
         0S*$                                                             29KDPK
          TRANSFER TO OUT1                                                29LDPK
AMEAN1    CONTINUE                                                        29MDPK
          PRINT FORMAT  RES24                                             29NDPK
```

TABLE XX (CONT'D)

```
          VECTOR VALUES RES24=$39H1THIS COMPUTATION USES ARITHMETIC MEA 290DPK
         0NS*$                                                          29PDPK
OUT1      CONTINUE                                                      29QDPK
          THROUGH RET1, FOR I=1,1,I.G.M                                 30 DPK
          ANGLE(I)=ANGLE(I)*3.14159/180.                                30ADPKA
          WHENEVER ANGLE(I).NE.0., TRANSFER TO NOZERO                   30ADPK
          RATIO(I)=1.                                                   30BDPK
          RAT2(1) = 1.0
          TRANSFER TO ZERO                                              30CDPK
NOZERO    RATIO(I)=8.*RADIUS(I)*SIN.(ANGLE(I))/WIDTH                    30DDPK
          RAT2(I) = RADIUS(I)/RADIUS(1)
ZERO      CONTINUE                                                      30EDPK
          Y(I,0) =0.0
          THROUGH RET1, FOR J=1,1,J.G.N                                 32 DPK
          X(I,J)=NUMBER(I,J)*SPEED(I,J)/PHOTOS(I)                       33 DPK
          Y(I,J)=X(I,J)+Y(I,(J-1))                                      34 DPK
RET1      CONTINUE                                                      35 DPK
          THROUGH RET2, FOR I=1,1,I.G.M                                 36 DPK
          THROUGH RET2, FOR J=1,1,J.G.N                                 37 DPK
          PCT(I,J)=X(I,J)*100./Y(I,N)                                   38 DPK
          WHENEVER DOCUM.E.0, TRANSFER TO NOCUM                         39 DPK
          CUMPCT(I,J)=Y(I,J)*100./Y(I,N)                                40 DPK
NOCUM     WHENEVER DOPIN.E.0, TRANSFER TO NOPIN                         41 DPK
          PCTINT(I,J)=PCT(I,J)/CELL(J)                                  42 DPK
NOPIN     CONTINUE                                                      43 DPK
RET2      CONTINUE                                                      44 DPK
          PRINT FORMAT RES1                                             45 DPK
          VECTOR VALUES RES1=$42HOVELOCITY WEIGHTED PERCENTAGES BY LOCA 46 DPK
         0TION*$                                                        46ADPK
          THROUGH RET3 , FOR I=1,1,I.G.M                                47 DPK
          PRINT FORMAT RES2,I                                           48 DPK
          VECTOR VALUES RES2=$10HOLOCATION I3*$                         49 DPK
          PRINT FORMAT RES3                                             50 DPK
          VECTOR VALUES RES3=$11H SIZE RANGE,S24,6HNUMBER,S10,          51 DPK
         0 5HSPEED,S8,7HPERCENT*$                                       52 DPK
          WHENEVER DOCUM.E.0, TRANSFER TO NOCUM1                        53 DPK
          PRINT FORMAT RES4                                             54 DPK
          VECTOR VALUES RES4=$1H+,S73,18HCUMULATIVE PERCENT*$           55 DPK
NOCUM1    WHENEVER DOPIN.E.0, TRANSFER TO NOPIN1                        56 DPK
          PRINT FORMAT RES5                                             57 DPK
          VECTOR VALUES RES5=$1H+,S93,18HPERCENT/SIZE RANGE*$           58 DPK
NOPIN1    CONTINUE                                                      59 DPK
          THROUGH RET3, FOR J=1,1,J.G.N                                 60 DPK
          PRINT FORMAT RES6,ENDPT(J-1),ENDPT(J),NUMBER(I,J),SPEED(I,J), 61 DPK
         0 PCT(I,J)                                                     62 DPK
          VECTOR VALUES RES6=$1H ,F10.5,4H TO ,F10.5,S5,F10.5,S5,       63 DPK
         0 F10.5,S5,F10.5*$                                             64 DPK
          WHENEVER DOCUM.E.0, TRANSFER TO NOCUM2                        65 DPK
          PRINT FORMAT RES7, CUMPCT(I,J)                                66 DPK
          VECTOR VALUES RES7=$1H+,S80,F10.5*$                           67 DPK
NOCUM2    WHENEVER DOPIN.E.0, TRANSFER TO NOPIN2                        68 DPK
          PRINT FORMAT RES8, PCTINT(I,J)                                69 DPK
          VECTOR VALUES RES8=$1H+,S100,F10.5*$                          70 DPK
NOPIN2    CONTINUE                                                      71 DPK
RET3      CONTINUE                                                      72 DPK
          PRINT FORMAT RES30                                            72ADPK
          PRINT FORMAT RES31                                            72BDPK
          VECTOR VALUES RES30=$36H1TOTAL VELOCITY WEIGHTED PERCENTAGES* 72CDPK
         0$                                                             72DDPK
```

TABLE XX (CONT'D)

```
                VECTOR VALUES RES31=$11H SIZE RANGE,S23,7HPERCENT*$                72EDPK
                WHENEVER DOCUM.E.0, TRANSFER TO NOCUM3                             72FDPK
                PRINT FORMAT RES32                                                 72GDPK
                VECTOR VALUES RES32=$1H+,S46,18HCUMULATIVE PERCENT*$               72HDPK
NOCUM3          WHENEVER DOPIN.E.0, TRANSFER TO NOPIN3                             72IDPK
                PRINT FORMAT RES33                                                 72JDPK
                VECTOR VALUES RES33=$1H+,S71,18HPERCENT/SIZE RANGE*$               72KDPK
NOPIN3          CONTINUE                                                           72LDPK
                G(0) = 0.0
                TOTAL = 0.0
                THROUGH RET11, FOR J=1,1,J.G.N                                     72ODPK
                G(J) = 0.0
                THROUGH RET11, FOR I=1,1,I.G.M                                     72QDPK
                X(I,J)=X(I,J)*RATIO(I)*RAT2(I)                                     72RDPK
                G(J)=X(I,J)+G(J)                                                   72SDPK
                TOTAL = TOTAL+X(I,J)                                               72TDPK
RET11           CONTINUE                                                           72UDPK
                CUMPCT(M,N)=0.                                                     72UDPKA
                THROUGH RET12, FOR J=1,1,J.G.N                                     72VDPK
                PCT(M,J)=G(J)*100./TOTAL                                           72WDPK
                CUMPCT(M,N)=PCT(M,J)+CUMPCT(M,N)                                   72XDPK
                PCTINT(M,J)=PCT(M,J)/CELL(J)                                       72YDPK
                PRINT FORMAT RES34, ENDPT(J-1),ENDPT(J),PCT(M,J)                   72ZDPK
                VECTOR VALUES RES34=$1H ,F10.5,4H TO ,F10.5,S5,F10.5*$             A72ADPK
                WHENEVER DOCUM.E.0, TRANSFER TO NOCUM4                             A72BDPK
                PRINT FORMAT RES35, CUMPCT(M,N)                                    A72CDPK
                VECTOR VALUES RES35=$1H+,S54,F10.5*$                               A72DDPK
NOCUM4          WHENEVER DOPIN.E.0, TRANSFER TO NOPIN4                             A72EDPK
                PRINT FORMAT RES36, PCTINT(M,J)                                    A72EDPKA
                VECTOR VALUES RES36=$1H+,S79,F10.5*$                               A72FDPK
NOPIN4          CONTINUE                                                           A72GDPK
RET12           CONTINUE                                                           A72HDPK
                WHENEVER VOLV.E.0, TRANSFER TO CAT
                THROUGH RET20, FOR I=1,1,I.G.M                                     A72LDPK
                Y(I,0)=0                                                           A72MDPK
                THROUGH RET20, FOR J=1,1,J.G.N                                     A72NDPK
                X(I,J)=NUMBER(I,J)*SPEED(I,J)*(W(J).P.3.)/PHOTOS(I)                A72ODPK
                Y(I,J)=X(I,J)+Y(I,(J-1))                                           A72PDPK
RET20           CONTINUE                                                           A72QDPK
                THROUGH RET21, FOR I=1,1,I.G.M                                     A72RDPK
                THROUGH RET21, FOR J=1,1,J.G.N                                     A72SDPK
                PCT(I,J)=X(I,J)*100./Y(I,N)                                        A72TDPK
                WHENEVER DOCUM.E.0, TRANSFER TO NOCUM5                             A72UDPK
                CUMPCT(I,J)=Y(I,J)*100./Y(I,N)                                     A72VDPK
NOCUM5          WHENEVER DOPIN.E.0, TRANSFER TO NOPIN5                             A72WDPK
                PCTINT(I,J)=PCT(I,J)/CELL(J)                                       A72XDPK
NOPIN5          CONTINUE                                                           A72YDPK
RET21           CONTINUE                                                           A72ZDPK
                PRINT FORMAT RES40                                                 B72ADPK
                VECTOR VALUES RES40=$49H1VOLUME-VELOCITY WEIGHTED PERCENTAGESB72BDPK
               0 BY LOCATION*$                                                     B72CDPK
                THROUGH RET22, FOR I=1,1,I.G.M                                     B72DDPK
                PRINT FORMAT RES41,I                                               B72EDPK
                VECTOR VALUES RES41=$10H0LOCATION I3*$                             B72FDPK
                PRINT FORMAT RES42                                                 B72GDPK
                VECTOR VALUES RES42=$11H SIZE RANGE,S24,6HNUMBER,S10,5HSPEED,B72HDPK
               0 S8,7HPERCENT*$                                                    B72IDPK
                WHENEVER DOCUM.E.0, TRANSFER TO NOCUM6                             B72JDPK
                PRINT FORMAT RES43                                                 B72KDPK
```

TABLE XX (CONT'D)

```
                VECTOR VALUES RES43=$1H+,S73,18HCUMULATIVE PERCENT*$                B72LDPK
NOCUM6          WHENEVER DOPIN.E.0, TRANSFER TO NOPIN6                              B72MDPK
                PRINT FORMAT RES44                                                  B72NDPK
                VECTOR VALUES RES44=$1H+,S93,18HPERCENT/SIZE RANGE*$                B72ODPK
NOPIN6          CONTINUE                                                            B72PDPK
                THROUGH RET22, FOR J=1,1,J.G.N                                      B72QDPK
                PRINT FORMAT RES6,ENDPT(J-1),ENDPT(J),NUMBER(I,J),SPEED(I,J),B72RDPK
               0 PCT(I,J)                                                           B72SDPK
                WHENEVER DOCUM.E.0, TRANSFER TO NOCUM7                              B72TDPK
                PRINT FORMAT RES7,CUMPCT(I,J)                                       B72UDPK
NOCUM7          WHENEVER DOPIN.E.0, TRANSFER TO NOPIN7                              B72VDPK
                PRINT FORMAT RES8, PCTINT(I,J)                                      B72WDPK
NOPIN7          CONTINUE                                                            B72XDPK
RET22           CONTINUE                                                            B72YDPK
                PRINT FORMAT RES45                                                  B72ZDPK
                VECTOR VALUES RES45=$43H1TOTAL VOLUME-VELOCITY WEIGHTED PERCE
               ONTAGES*$                                                            C72BDPK
                PRINT FORMAT RES31                                                  C72CDPK
                WHENEVER DOCUM.E.0, TRANSFER TO NOCUM8                              C72DDPK
                PRINT FORMAT RES32                                                  C72EDPK
NOCUM8          WHENEVER DOPIN.E.0, TRANSFER TO NOPIN8                              C72FDPK
                PRINT FORMAT RES33
NOPIN8          CONTINUE
                TOTAL=0.                                                            C72IDPK
                THROUGH RET23, FOR J=1,1,J.G.N                                      C72JDPK
                G(J) = 0.0
                THROUGH RET23, FOR I=1,1,I.G.M                                      C72LDPK
                X(I,J) =X(I,J)*RATIO(I)*RAT2(I)
                G(J)=X(I,J)+G(J)                                                    C72MDPKA
                TOTAL=TOTAL+X(I,J)                                                  C72NDPK
RET23           CONTINUE                                                            C72ODPK
                CUMPCT(M,N)=0.                                                      C72ODPKA
                THROUGH RET24, FOR J=1,1,J.G.N                                      C72PDPK
                PCT(M,J)=G(J)*100./TOTAL                                            C72QDPK
                CUMPCT(M,N)=PCT(M,J)+CUMPCT(M,N)                                    C72RDPK
                PCTINT(M,J)=PCT(M,J)/CELL(J)                                        C72SDPK
                PRINT FORMAT RES34, ENDPT(J-1),ENDPT(J),PCT(M,J)                    C72TDPK
                WHENEVER DOCUM.E.0, TRANSFER TO NOCUM9                              C72UDPK
                PRINT FORMAT RES35, CUMPCT(M,N)                                     C72VDPK
NOCUM9          WHENEVER DOPIN.E.0, TRANSFER TO NOPIN9                              C72WDPK
                PRINT FORMAT RES36, PCTINT(M,J)                                     C72XDPK
NOPIN9          CONTINUE                                                            C72YDPK
RET24           CONTINUE                                                            C72ZDPK
   CAT          WHENEVER DODIA.E.0, TRANSFER TO NODIA
                PRINT FORMAT RES9                                                    81 DPK
                VECTOR VALUES RES9=$33H1DROP DIAMETERS FOR EACH LOCATION*$           82 DPK
                THROUGH RET5, FOR R=0,1,R.G.S                                        89 DPK
                THROUGH RET5, FOR I=1,1,I.G.M                                        90 DPK
                F(R,I)=0.                                                            93 DPK
                THROUGH RET5, FOR J=1,1,J.G.N                                        94 DPK
                F(R,I)=(W(J).P.R)*NUMBER(I,J)*SPEED(I,J)/PHOTOS(I)                   95 DPK
               0 +F(R,I)                                                             96 DPK
        RET5 CONTINUE                                                               97 DPK
                THROUGH RET6, FOR I=1,1, I.G.M                                       98 DPK
                PRINT FORMAT RES14, I                                                99 DPK
                VECTOR VALUES RES14=$10HOLOCATION I3*$                              100 DPK
                PRINT FORMAT RES11                                                  101 DPK
                VECTOR VALUES RES11=$1H ,S11,9HNUMERATOR,S9,11HDENOMINATOR,         102 DPK
               0 S12,8HDIAMETER*$                                                   103 DPK
```

TABLE XX (CONT'D)

```
                PRINT FORMAT RES12                                              104 DPK
                VECTOR VALUES RES12=$1H ,S12, 8HEXPONENT,S12,8HEXPONENT*$       105 DPK
                THROUGH RET6, FOR R=0,1,R.G.S                                   106 DPK
                DIAM(R,I) = (F(NUM(R+1),I)/F(DEN(R+1),I)).P.(1.0/(NUM(R+1)-DE
               1N(R+1)))
                PRINT FORMAT RES13,NUM(R+1),DEN(R+1),DIAM(R,I)
                VECTOR VALUES RES13=$1H ,S17,I3,S17,I3,S10,F10.5*$              109 DPK
           RET6 CONTINUE                                                        110 DPK
                PRINT FORMAT RES15                                              111 DPK
                VECTOR VALUES RES15=$16H1TOTAL DIAMETERS*$                      112 DPK
                PRINT FORMAT RES16                                              113 DPK
                VECTOR VALUES RES16=$1H ,S11,9HNUMERATOR,S9,11HDENOMINATOR,     114 DPK
               0 S15,5HTOTAL*$                                                  115 DPK
                PRINT FORMAT RES17                                              116 DPK
                VECTOR VALUES RES17=$1H ,S12,8HEXPONENT,S12,8HEXPONENT,         117 DPK
               0 S12,8HDIAMETER*$                                               118 DPK
                THROUGH RET7, FOR R=0,1,R.G.S                                   119 DPK
                G(R)=0.                                                         120 DPK
                THROUGH RET7, FOR I=1,1,I.G.M                                   122 DPK
                G(R) = F(R,I)*RATIO(I)*RAT2(I) + G(R)
           RET7 CONTINUE                                                        125 DPK
                THROUGH RET8, FOR R=0,1,R.G.S                                   126 DPK
                TDIAM(R) = (G(NUM(R+1))/G(DEN(R+1))).P.(1.0/(NUM(R+1)-DEN(R+1
               1)))
                PRINT FORMAT RES18,NUM(R+1),DEN(R+1),TDIAM(R)
                VECTOR VALUES RES18=$1H ,S17,I3,S17,I3,S10,F10.5*$              129 DPK
           RET8 CONTINUE                                                        130 DPK
         NODIA CONTINUE                                                         131 DPK
                WHENEVER SURVOL.E.0, TRANSFER TO NOSV                           132 DPK
                PRINT FORMAT RES19                                              133 DPK
                VECTOR VALUES RES19=$57HISURFACE AND VOLUME RATES FOR EACH LO134 DPK
               0CATION PER UNIT AREA*$                                          134ADPK
                THROUGH RET10,FOR I=1,1,I.G.M                                   135 DPK
                PRINT FORMAT RES20,I                                            136 DPK
                VECTOR VALUES RES20=$10HOLOCATION I3*$                          137 DPK
                VOLUME(I)=((3.14159)*F(3,I)*CONST2/(HEIGTH*WIDTH*DEPTH*6.))*(
               1l.765E-15)
                AREA(I)=((3.14159)*F(2,I)*CONST1/(HEIGTH*WIDTH*DEPTH))*(5.41E
               1-11)
                PRINT FORMAT RES21, AREA(I),VOLUME(I)                           143DDPK
                VECTOR VALUES RES21 =$10H SURFACE =E13.5,S10,8HVOLUME =
               1E13.5*$
          RET10 CONTINUE                                                        143GDPK
                PRINT FORMAT RES50                                              143HDPK
                VECTOR VALUES RES50=$51H1TOTAL SURFACE AND VOLUME RATES (NOT 143IDPK
               0PER UNIT AREA)*$                                                143JDPK
                THROUGH RET25, FOR I=1,1,I.G.M
                AREA(I) = (AREA(I)*3.14159*(WIDTH.P.2)/4.0*RATIO(I)*RAT2(I))*
               11728.0
                VOLUME(I) = (VOLUME(I)*3.14159*(WIDTH.P.2)/4.0*RATIO(I)*RAT2(
               1I))*1728.0
                PRINT FORMAT RES20, I
                PRINT FORMAT RES21, AREA(I), VOLUME(I)
                WHENEVER BAD.NE.0.AND.I.E.1
                PRINT RESULTS I, RATIO(I), RAT2(I), F...F(200), AREA...AREA(2
               10), VOLUME...VOLUME(20)
                EXECUTE ERROR.
                END OF CONDITIONAL
          RET25 CONTINUE                                                        143PDPK
```

TABLE XX (CONT'D)

```
            AREA(0) = 0.0
            VOLUME(0) = 0.0
            THROUGH GREEN, FOR I=1,1,I.G.M
            AREA(I) = AREA(I) + AREA(I-1)
            VOLUME(I) = VOLUME(I) + VOLUME(I-1)
   GREEN    CONTINUE
            PRINT FORMAT GONE, AREA(M), VOLUME(M)
            VECTOR VALUES GONE =$27H0 TOTAL SURFACE, SQ FT/HR = E13.5,S10
           1,26H0 TOTAL VOLUME, CU FT/HR = E13.5*$
      NOSV CONTINUE                                                  144 DPK
            THROUGH PINK, FOR I=1,1,I.G.M
            THROUGH PINK, FOR J=1,1,J.G.N
            MASS(I,J) =(((((0.0001*W(J))/(12.0*2.54)).P.3)*3.1415*NUMBER(
           1I,J))*DENS(I)/6.0)*(SPEED(I,J))/PHOTOS(I)
            WHENEVER KE.E.0, TRANSFER TO NOKE
            ENERGY(I,J)= (1728.0*MASS(I,J)*(SPEED(I,J).P.2))/(64.4*HEIGTH
           1*WIDTH*DEPTH)
   NOKE     CONTINUE
            WHENEVER MOMN.E.0, TRANSFER TO NOMOMN
   PINK     MOM(I,J) = (MASS(I,J)*SPEED(I,J)*1728.0)/(HEIGTH*WIDTH*DEPTH)
 NOMOMN     CONTINUE
            THROUGH ALPHA, FOR I=1,1,I.G.M
            PRINT FORMAT ABLE,I
            VECTOR VALUES ABLE=$10HOLOCATION I3*$
            PRINT FORMAT BAKER
            VECTOR VALUES BAKER=$11H SIZE RANGE,S23,8HMOMENTUM,S10,14HKIN
           1ETIC ENERGY*$
            THROUGH ALPHA, FOR J=1,1,J.G.N
            PRINT FORMAT CHARL,ENDPT(J-1),ENDPT(J),MOM(I,J),ENERGY(I,J)
            VECTOR VALUES CHARL=$1H ,F10.5,4H TO ,F10.5,S5,E13.5,S5,E13.5
           1*$
   ALPHA    CONTINUE
            PRINT FORMAT FRED
            VECTOR VALUES FRED =$9HOLOCATION,S8,21HKINETIC ENERGY(FT LB),
           1S22,19HMOMENTUM(FT LB/SEC)*$
            THROUGH BLUE, FOR I=1,1, I.G.M
            SUM(0) = 0.0
            SUMN(0) = 0.0
            THROUGH BLUE, FOR J=1,1, J.G.N
            ENERGY(I,J) =(ENERGY(I,J)*RATIO(I)*RAT2(I))/24.0
            MOM(I,J) =(MOM(I,J)*RATIO(I)*RAT2(I))/24.0
            SUM(J) = ENERGY(I,J) + SUM(J-1)
            SUMN(J) = MOM(I,J) + SUMN(J-1)
            SUMN(J) = MOM(I,J) + SUMN(J)
            WHENEVER J.E.N, PRINT FORMAT EASY, I, SUM(J), SUMN(J)
            VECTOR VALUES EASY =$S5,I3,S8,E13.5,S20,E13.5*$
    BLUE    CONTINUE
            WHENEVER SUPER.E.0, TRANSFER TO NOSR
            READ FORMAT DCARD9, DM, DELP, VISC, DG, SIGMA, DENSTY, H21, H
           12F
            READ FORMAT CARD1, H1F, RHO2, RHO1, K, SPHT
            VECTOR VALUES DCARD9 =$4F10.5, E10.5, 3F10.5*$
            VECTOR VALUES CARD1 =$5F10.5*$
            VEL = (64.4*144.0*DELP*DENSTY).P.(0.5)
            RE = (DM*VEL*DENSTY )/VISC
            NWE = (DG*VEL*VEL*DM)/(64.4*SIGMA)
            FLOW = (3.1416*DM*DM/4.0)*VEL*3600.0*
            PDEV = ((FLOW-VOLUME(M))/VOLUME(M))*100.0
            WTPC = (H21-H2F)/(H1F-H2F)
            GRC = WTPC*(RHO2/RHO1)*(3.1415*K/(RHO2*SPHT))
            PRINT FORMAT HELP, VEL, RE, NWE
            VECTOR VALUES HELP =$18H VELOCITY(FT/SEC)=  E13.4,S8,18H REYN
           1OLDS NUMBER = E13.4,S8, 15H WEBER NUMBER = E13.4*$
            PRINT FORMAT JOHN, FLOW, PDEV, WTPC, GRC
            VECTOR VALUES JOHN = $7H PDEV = F6.2,S8,18H PERCENT FLASHED =
           1F6.2,S8,23H GROWTH RATE CONSTANT = F6.2*$
   NOSR     CONTINUE
            TRANSFER TO START
            END OF PROGRAM                                           145 DPK
```

APPENDIX B

RAW DATA

This appendix contains all of the drop size and velocity distribution data which was taken in the course of the study. The data books and the photographic negatives are located in the Multi-Phase Fluids Laboratory in the Fluids Building at the North Campus of the University of Michigan, Ann Arbor, Michigan.

TABLE XXI

DROP SIZE RANGES

Size Range No.	Size Range (Microns)	Average Diameter (Microns)
1	0 - 10.0	5.0
2	10.0 - 14.1	12.05
3	14.1 - 20.0	17.05
4	20.0 - 28.2	24.1
5	28.2 - 40.0	34.1
6	40.0 - 56.4	48.2
7	56.4 - 80.0	68.2
8	80.0 - 113	96.5
9	113 - 160	136.5
10	160 - 226	193
11	226 - 320	273
12	320 - 453	386.5
13	453 - 640	546.5

TABLE XXII

DROP SIZE DISTRIBUTION AND VELOCITY DATA

Jet Diameter = 0.031 Inches

Run No. 1. Water at 90 psig, 287°F, 4 inches from Nozzle

Location	Photos	Number of Drops in Each Size Range										
		2	3	4	5	6	7	8	9	10	11	12
1	2	9	67	300	301	172	69	26	10	1		
2	3	14	85	239	386	255	93	30	8			
3	4			5	25	123	90	21	4			
4	4		3	19	31	97	88	14	3			
		Average Velocities in Each Size Range (Ft/Sec)										
1	4	10.0	15.0	20.0	31.4	41.3	53.3	100.2	103.1	111.0	119.5	
2	4	10.0	11.6	15.2	23.2	30.4	41.3	66.5	76.1	97.8		
3	4			8.3	12.2	18.9	31.3	48.3	73.5			
4	4		7.5	10.9	10.3	15.2	26.3	48.5	73.2			

Run No. 2. Water at 120 psig, 287°F, 4 inches from Nozzle

Location	Photos	Number of Drops in Each Size Range										
		2	3	4	5	6	7	8	9	10	11	12
1	2	5	32	132	193	92	28	22	14	2		
2	2	12	78	231	256	100	46	24	20	11	2	
3	2	44	238	304	182	135	53	22	7	1		
4	4	5	34	71	79	96	103	22	6			
		Average Velocities in Each Size Range (Ft/Sec)										
1	4	14.0	16.0	21.6	31.8	39.9	41.6	97.3	105.0	117.5	127.0	133.0
2	4	10.0	13.9	18.3	33.4	38.4	48.3	83.2	106.0	110.0	123.0	125.0
3	4	5.0	7.4	13.4	18.3	22.0	36.6	55.8	83.7	93.9		
4	4	3.0	4.4	7.2	11.3	16.9	27.3	47.3	64.8			

Run No. 3. Water at 120 psig, 287°F, 5 inches from Nozzle

Location	Photos	Number of Drops in Each Size Range										
		2	3	4	5	6	7	8	9	10	11	12
1	3	46	171	157	141	126	68	37	15	14	7	9
2	3	43	209	204	147	124	122	41	14	3	3	
3	2	4	32	56	92	37	28	23	5			
4	1						2	1	1			
		Average Velocities in Each Size Range (Ft/Sec)										
1	4	7.4	8.7	12.9	17.1	28.4	38.4	85.1	94.0	101	106	110
2	4	6.7	7.9	12.6	13.6	15.6	20.1	37.2	55.1	73.9	86.1	
3	4	4.2	4.6	5.8	7.9	11.3	16.1	32.6	41.7			
4	4						11.7	25.9	36.7			

TABLE XXII (CONT'D.)

Run No. 4. Water at 120 psig, 287°F, 6 inches from Nozzle

Location	Photos	Number of Drops in Each Size Range										
		2	3	4	5	6	7	8	9	10	11	12
1	3	12	111	179	187	137	67	23	9			
2	3	24	112	138	145	125	84	30	7	6		
3	3	16	39	54	90	99	79	39	9	7	1	
4	3	20	75	123	126	114	115	30	12	5		
		Average Velocities in Each Size Range (Ft/Sec)										
1	4	10.9	14.7	18.4	22.5	31.4	44.3	63.9	81.1			
2	4	10.0	11.7	14.2	20.4	28.4	38.4	52.3	68.5	84.4		
3	4	9.2	10.9	15.2	18.0	23.8	30.9	41.7	54.3	72.7	83.3	
4	4	5.9	8.8	10.9	15.8	21.3	27.2	36.0	47.5	65.1		

Run No. 5. Water at 120 psig, 287°F, 7 inches from Nozzle

Location	Photos	Number of Drops in Each Size Range										
		2	3	4	5	6	7	8	9	10	11	12
1	3	27	72	73	60	44	32	16	6	6	2	5
2	2	4	19	41	101	80	44	15	1	1		
3	2	6	18	45	122	207	116	27	2			
4	2		1	14	44	54	20	4				
		Average Velocities in Each Size Range (Ft/Sec)										
1	4	10.0	12.0	20.5	24.6	29.2	37.6	58.5	75.1	90.2	99.5	110
2	4	10.4	13.4	15.5	18.4	21.7	27.6	54.3	71.0	81.7		
3	4	8.0	8.7	12.1	13.4	16.7	19.2	28.8	45.1			
4	4		9.2	10.0	10.1	10.2	10.3	14.2				

Run No. 6. Freon 11 at 90 psig, 158°F, 4 inches from Nozzle

Location	Photos	Number of Drops in Each Size Range							
		2	3	4	5	6	7	8	9
1	4	72	305	536	314	75	14		
2	4	15	33	51	31	12	2		
		Average Velocity in Each Size Range (Ft/Sec)							
1	4	7.7	10.0	14.5	22.9	30.0	42.0		
2	4	5.0	6.3	10.3	15.9	22.4	28.0		

Run No. 7. Freon 11 at 120 psig, 158°F, 4 inches from Nozzle

Location	Photos	Number of Drops in Each Size Range							
		2	3	4	5	6	7	8	9
1	2	58	374	565	310	35	1		
2	2	62	286	631	325	59	6		
3	4	27	112	258	162	24	1		
		Average Velocities in Each Size Range (Ft/Sec)							
1	4	9.0	13.9	22.6	32.1	43.4	58.9		
2	4	8.5	10.0	17.3	21.7	30.6	42.8		
3	4	5.5	12.0	18.5	27.7	39.0	51.0		

TABLE XXII (CONT'D.)

Run No. 8. Freon 11 at 120 psig, 158°F, 5 inches from Nozzle

Location	Photos	Number of Drops in Each Size Range						
		2	3	4	5	6	7	8
1	1	65	225	263	78	5		
2	1	23	149	200	89	9	3	
3	2	2	39	111	78	11		
		Average Velocities in Each Size Range (Ft/Sec)						
1	3	8.6	13.0	17.8	25.5	38.5		
2	3	8.5	10.3	14.1	20.9	28.7	43.0	
3	3	8.0	8.5	11.8	18.1	24.4	38.2	61.7

Run No. 9. Freon 11 at 120 psig, 158°F, 6 inches from Nozzle

Location	Photos	Number of Drops in Each Size Range						
		2	3	4	5	6	7	8
1	2	8	68	106	44	3	1	
2	3	30	232	573	431	89	8	
3	3	34	179	450	430	137	26	
		Average Velocities in Each Size Range (Ft/Sec)						
1	3	8.5	9.8	20.5	25.0	41.5	49.0	
2	3	9.0	9.8	16.7	21.0	33.0	39.5	
3	3	9.0	9.8	13.0	18.0	25.3	30.3	

Run No.10. Freon 11 at 120 psig, 158°F, 7 inches from Nozzle

Location	Photos	Number of Drops in Each Size Range						
		2	3	4	5	6	7	8
1	3	11	133	359	524	316	68	7
2	2	3	36	189	443	418	117	9
3	3		13	133	324	358	120	17
		Average Velocities in Each Size Range (Ft/Sec)						
1	3	9.0	14.5	21.0	29.2	43.0	63.5	68.0
2	3	6.0	10.0	16.0	22.5	34.0	52.7	57.5
3	1	4.5	7.5	13.0	18.0	27.8	41.7	46.5

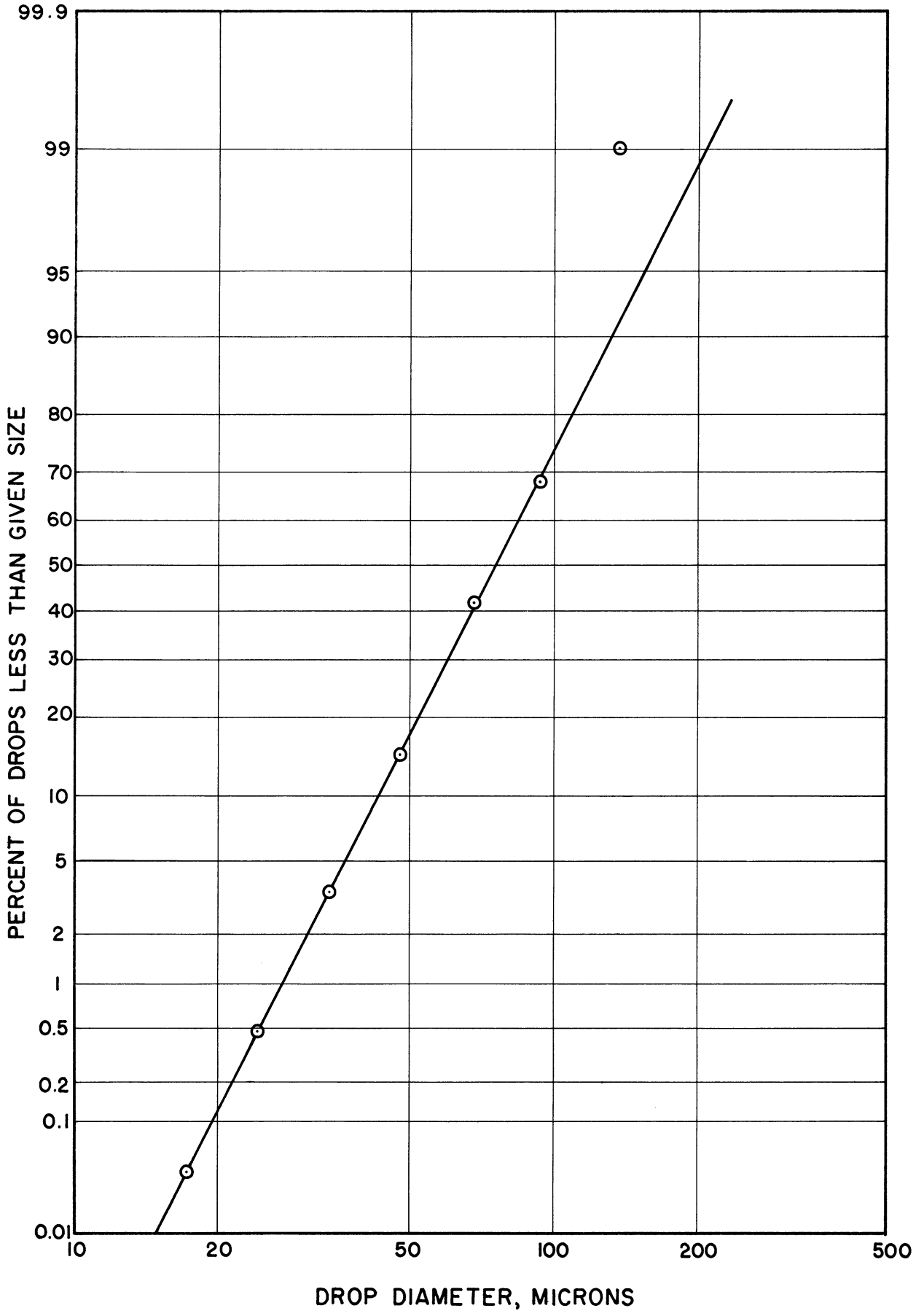

Figure 33. Distribution Plot for Run 1.

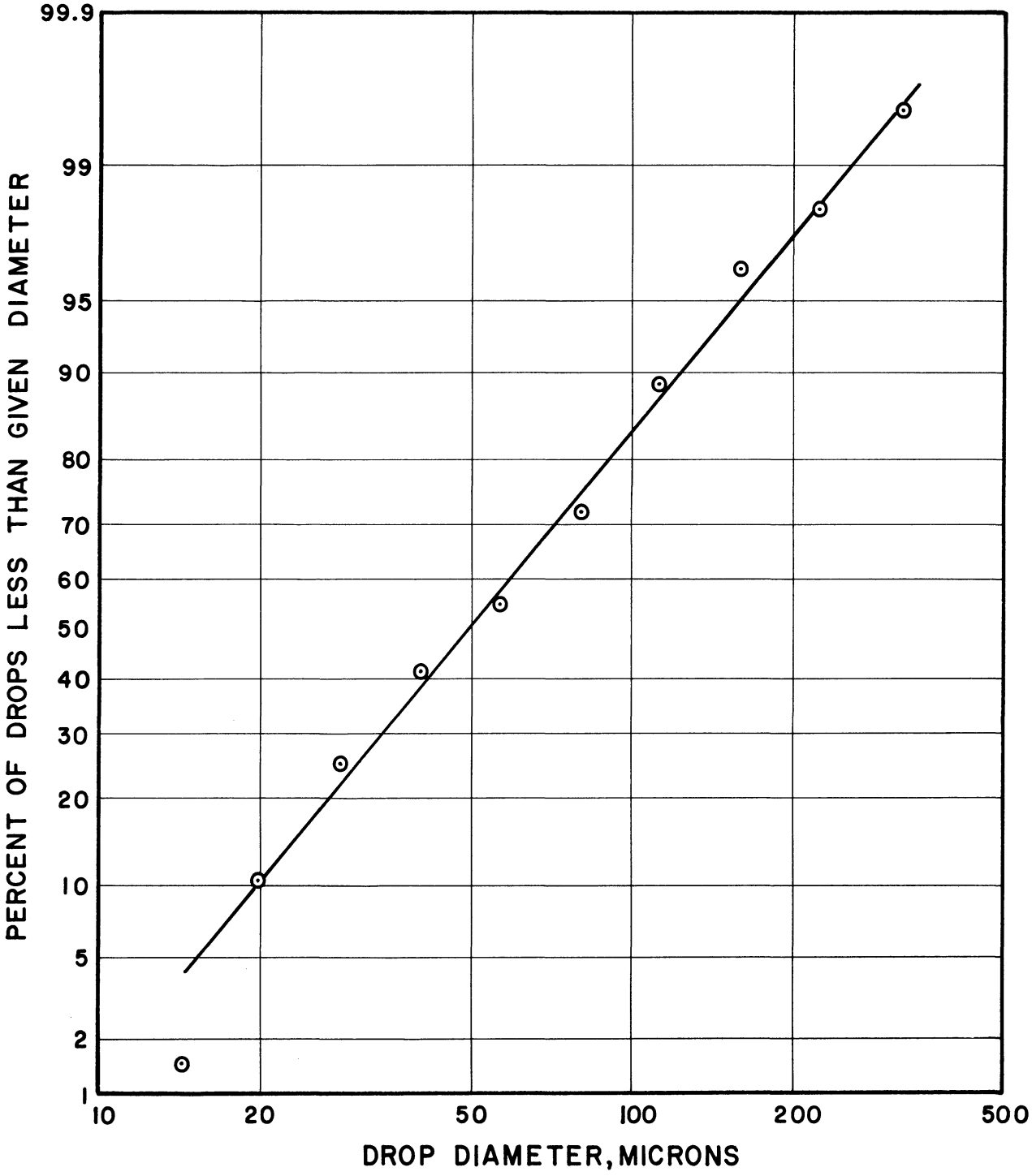

Figure 34. Distribution Plot for Run 3.

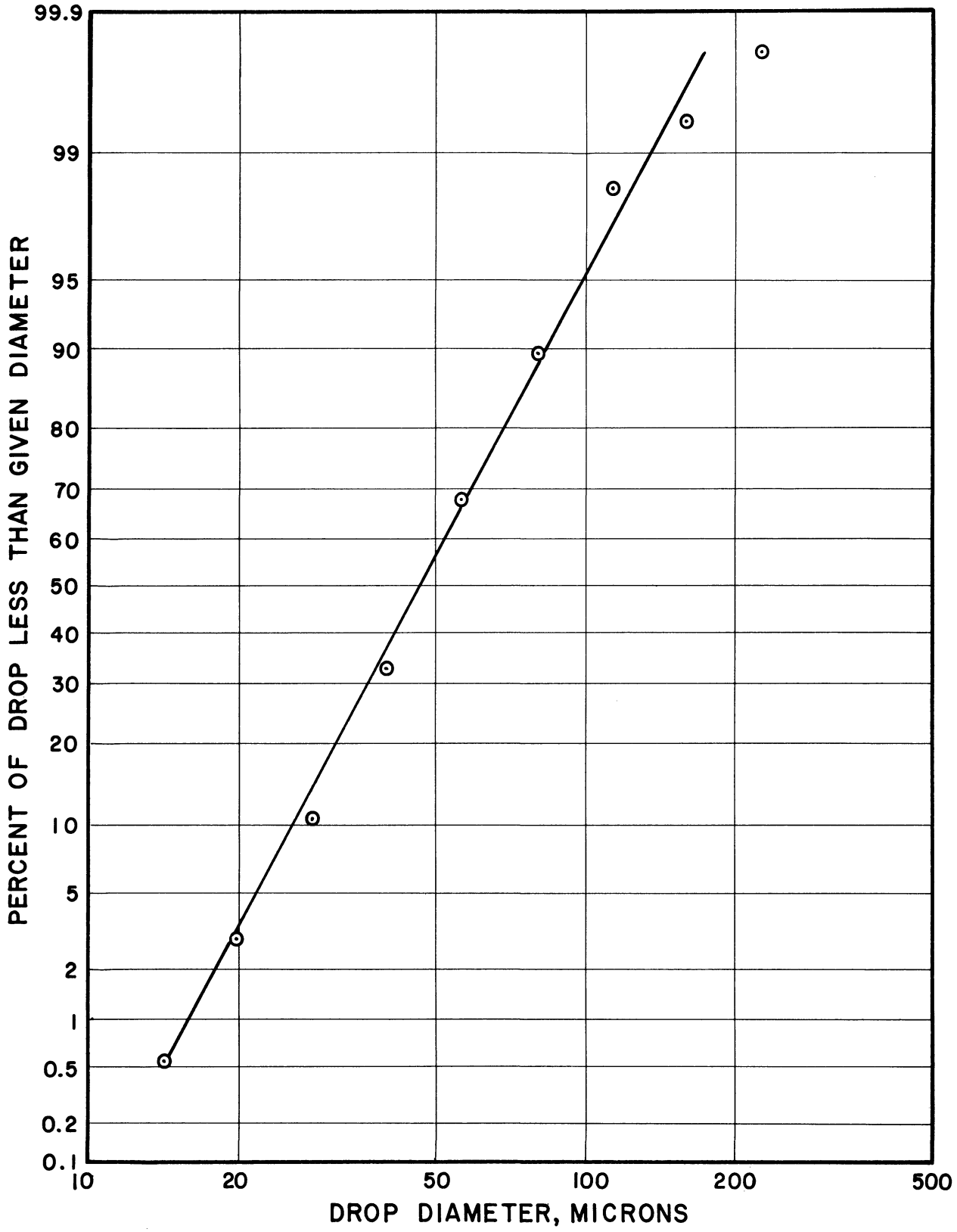

Figure 35. Distribution Plot for Run 5.

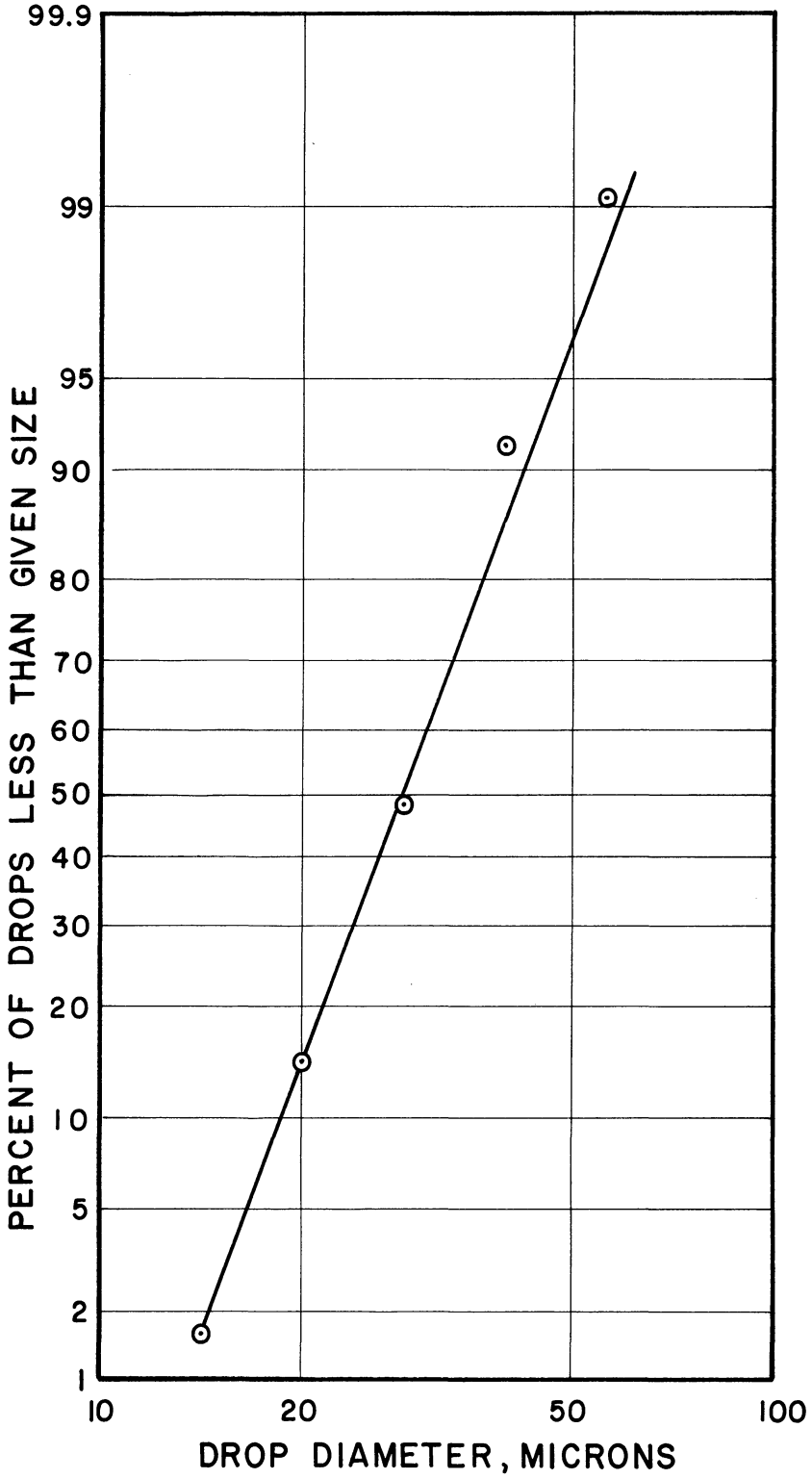

Figure 36. Distribution Plot for Run 7.

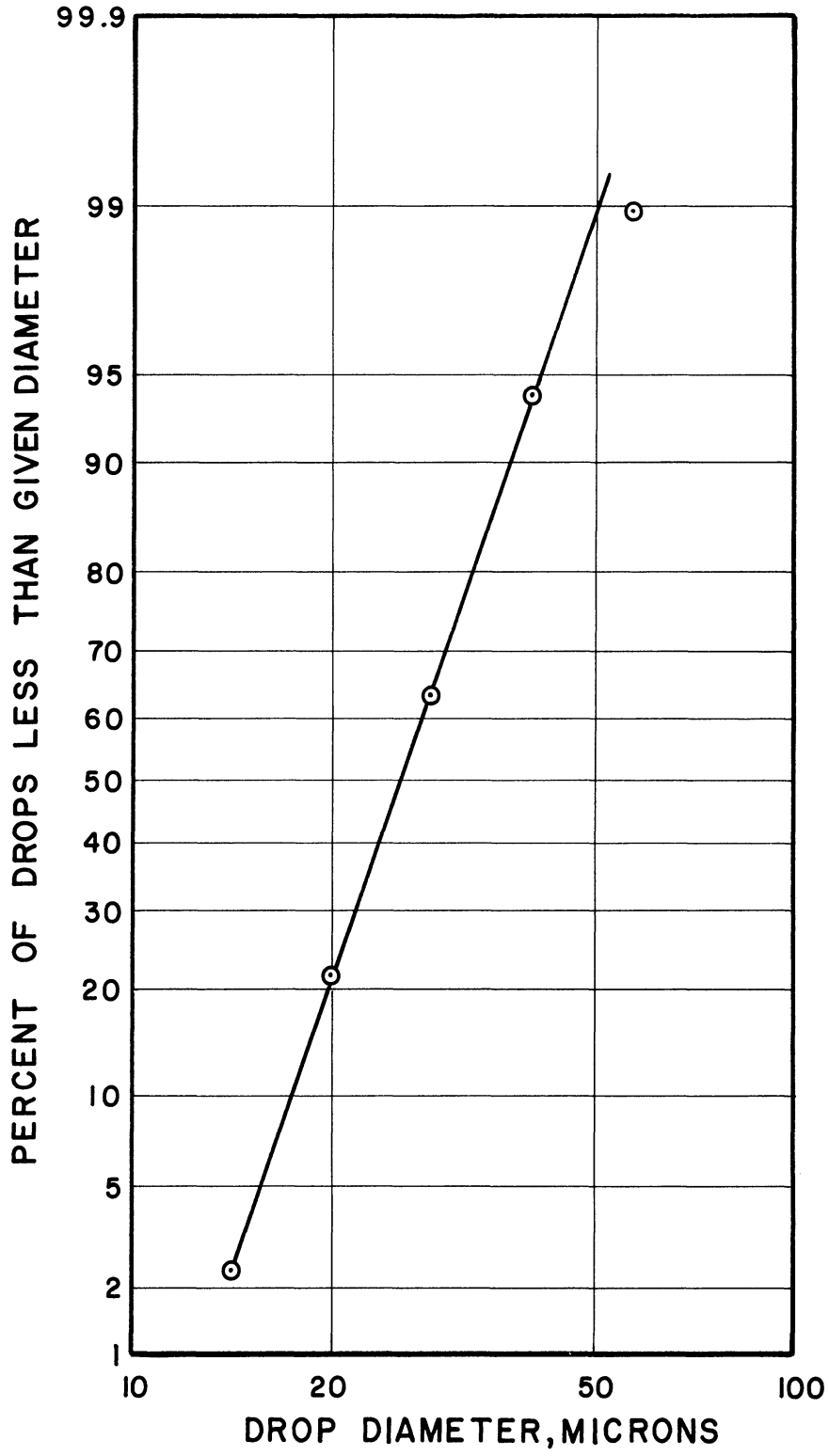

Figure 37. Distribution Plot for Run 8.

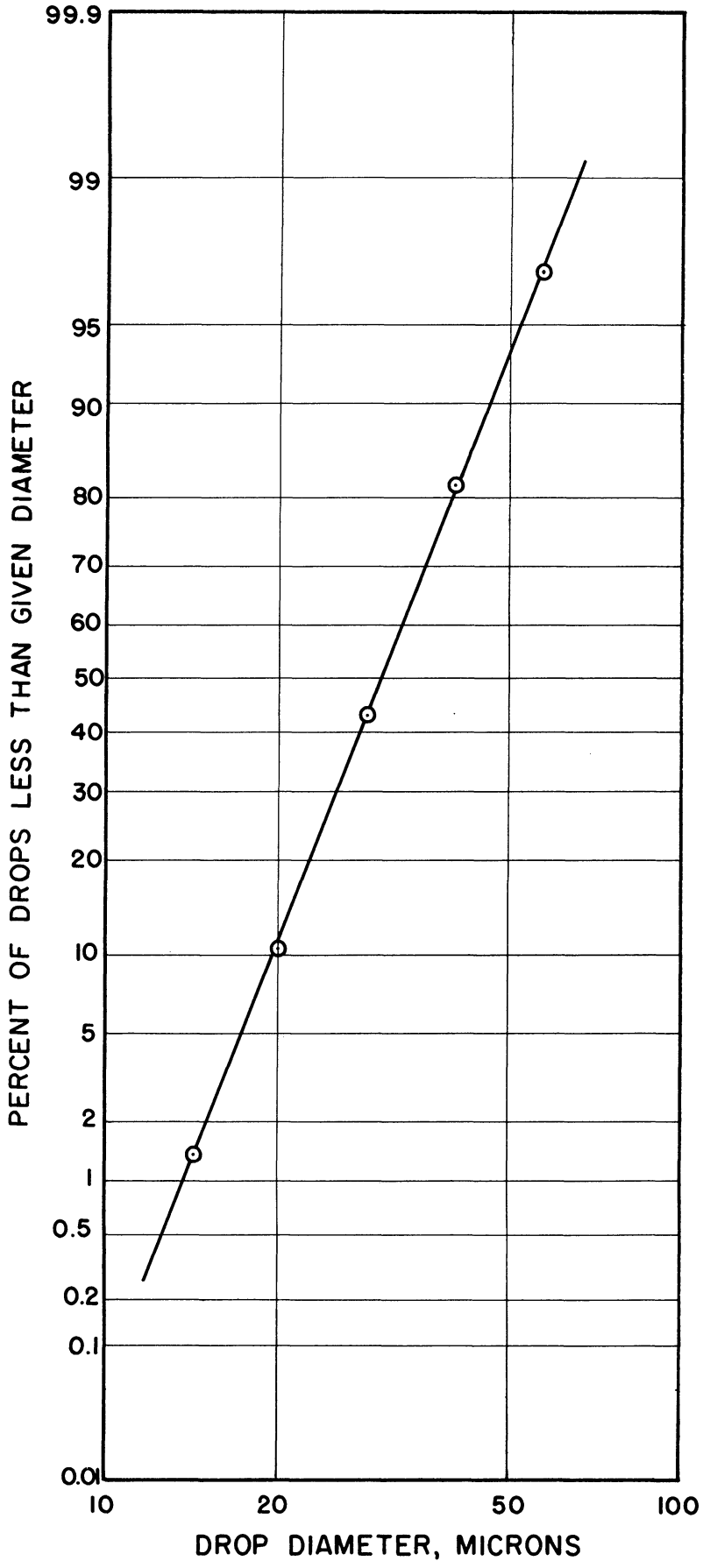

Figure 38. Distribution Plot for Run 9.

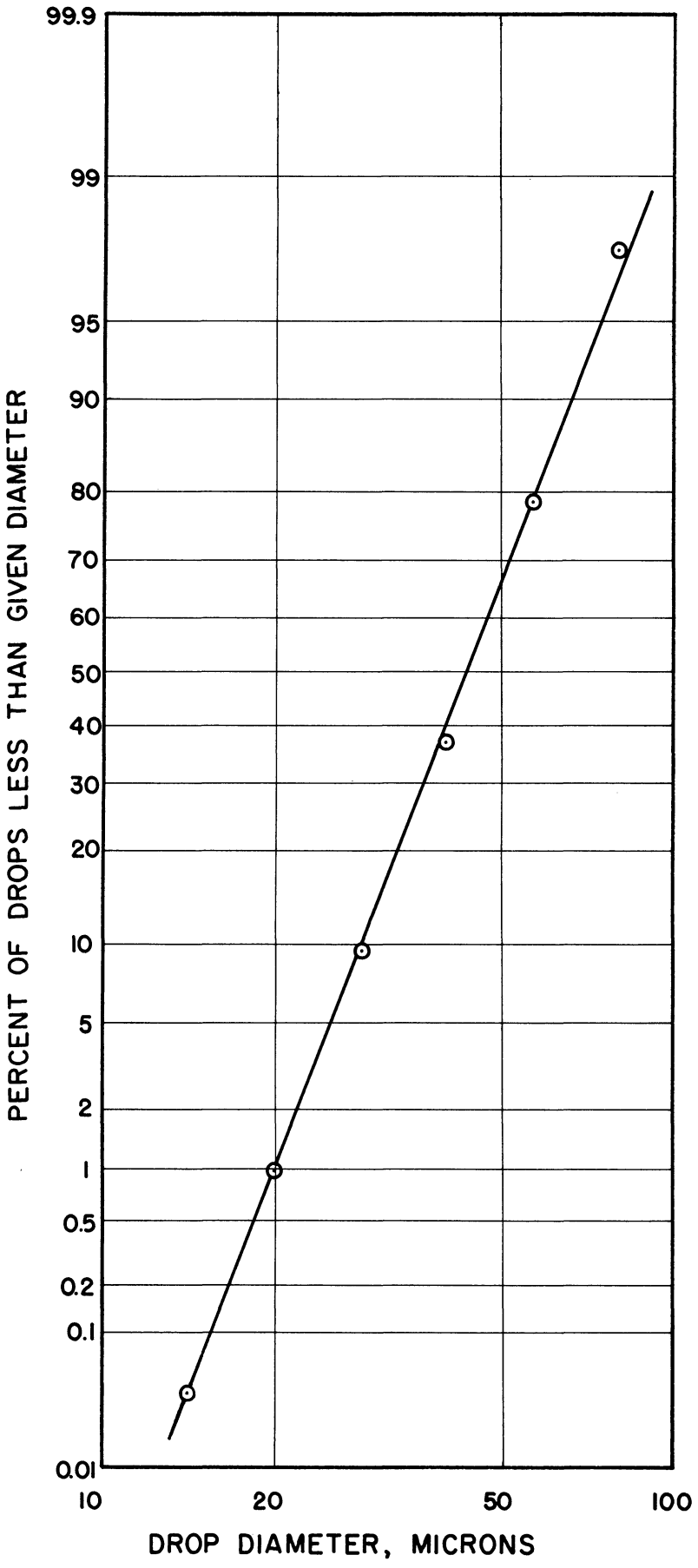

Figure 39. Distribution Plot for Run 10.

APPENDIX C

BUBBLE GROWTH IN A SUPERHEATED VISCOUS LIQUID

The information presented in this appendix is intended to acquaint the reader with the methods used to predict the bubble growth curves shown in Figure 10. The method is due to Poritsky[41] although he did not specifically solve the problem for any of the fluids or conditions given here.

The equations of motion are given by:

$$\rho\vec{a} = -\nabla p + \frac{\mu}{3}\nabla(\nabla\cdot\vec{v}) + \mu\nabla^2\vec{v} \qquad \text{(C-1)}$$

where

$\vec{v}$ is a velocity vector

$\vec{a}$ is the acceleration vector given by

$$\vec{a} = \left(\frac{\partial}{\partial t} + \vec{v}\cdot\nabla\right)\vec{v} \qquad \text{(C-2)}$$

Upon first investigating the problem one is confronted with a paradox: that there is apparently no difference between the equations which govern the growth of a spherical vapor bubble in a perfect (inviscid) liquid and those governing its growth in a viscous liquid. If the fluid is assumed to be incompressible the second term on the right hand side of Equation (C-1) vanishes. It is also true that the Laplacian of the velocity vector v is zero. This arises from the fact that, because of the spherical symmetry of the problem, a potential function may be defined and hence the Laplacian is zero. Thus the paradox presents itself.

Poritsky resolved this disconcerting dilemma by noting "that while it is true that the effect of viscosity vanishes in the equation of motion, so that the resultant of the viscosity stresses per unit of volume at any point internal to the fluid vanishes, this is not necessarily the case with the stresses themselves." Lamb[25] has shown that at any point the three principal stresses P_i and the three principal strains ϵ_i are related by:

$$P_1 = -P - \frac{2}{3}\mu(\epsilon_1 + \epsilon_2 + \epsilon_3) + 2\mu\epsilon_1 \qquad \text{(C-3)}$$

$$P_2 = -P - \frac{2}{3}\mu(\epsilon_1 + \epsilon_2 + \epsilon_3) + 2\mu\epsilon_2 \qquad \text{(C-3a)}$$

$$P_3 = -P - \frac{2}{3}\mu(\epsilon_1 + \epsilon_2 + \epsilon_3) + 2\mu\epsilon_3 \qquad \text{(C-3b)}$$

where the pressure P is the mean of the negative of the three principal stresses P_1, P_2, P_3.

Poritsky applies the above three equations to the free spherical surface of the cavity inside which he supposes that a constant pressure P_0 exists. Note that P_0 is not the value of P in the above equations, existing at the boundary within the fluid, but is calculated from the negative of the proper principal stress, thus arriving at the relation:

$$P_0 = P - 2\mu\epsilon_1 \qquad \text{(C-4)}$$

Applying this equation to the problem of determining the rate of growth of the radius R of the bubble one gets:

$$\frac{P_0 - P_\infty}{\rho} = R\frac{d^2R}{dt^2} + \frac{3}{2}\left(\frac{dR}{dt}\right)^2 + \frac{4\mu}{\rho R}\left(\frac{dR}{dt}\right) \qquad \text{(C-5)}$$

It should be noted that for the case of an inviscid liquid ($\mu = 0$) Equation (C-5) becomes identical to Equation (5.2). Introducing the dimensionless parameters

$$\tau = \frac{t}{R_o}\sqrt{\frac{P_o - P_\infty}{\rho}}$$

$$\beta = \frac{R}{R_o}$$

$$C = \frac{4\mu}{R_o\sqrt{\rho(P_o - P_\infty)}}$$

one obtains the following differential equation:

$$\beta\left(\frac{d^2\beta}{d\tau^2}\right) + \frac{3}{2}\left(\frac{d\beta}{d\tau}\right)^2 + \frac{C}{\beta}\frac{d\beta}{d\tau} - 1 = 0 \qquad \text{(C-6)}$$

If one equates the work per unit solid radian by the pressure P_0 to the kinetic energy acquired by the fluid, starting from rest, the energy relation given below results:

$$\frac{(P_o - P_\infty)(R_o^3 - R^3)}{3} + \frac{\rho R^3}{2}\left(\frac{dR}{dt}\right)^2 + 4\mu\int_0^t R\left(\frac{dR}{dt}\right)^2 dt = 0 \qquad \text{(C-7)}$$

Introducing the same dimensionless variables as before leads to the equation:

$$\frac{1-\beta^3}{3} + \frac{\beta^3}{2}\left(\frac{d\beta}{d\tau}\right)^2 + C\int_0^\tau \beta\left(\frac{d\beta}{d\tau}\right)^2 d\tau = 0 \qquad \text{(C-8)}$$

If the surface tension term, is included, it is readily shown that equation (C-5) and (C-7) become, respectively:

$$\frac{P_o - \frac{2\sigma}{R} - P_\infty}{\rho} = R\frac{d^2R}{dt^2} + \frac{3}{2}\left(\frac{dR}{dt}\right)^2 + \frac{4\mu}{\rho R}\left(\frac{dR}{dt}\right) \qquad \text{(C-9)}$$

$$\frac{(P_o - P_\infty)(R_o^3 - R^3)}{3} - \sigma(R_o^2 - R^4) + \frac{\rho R^3}{2}\left(\frac{dR}{dt}\right)^2$$

$$+ 4\mu\int_o^t R\left(\frac{dR}{dt}\right)^2 dt = 0 \qquad \text{(C-10)}$$

Defining a dimensionless variable

$$D = \frac{\sigma}{R_o(P_o - P_\infty)}$$

and employing the dimensionless variables C, β and τ as before Equation (C-10) becomes

$$\frac{\beta^3 - 1}{3} - D(\beta^2 - 1) - \frac{\beta^2}{2}\left(\frac{d\beta}{d\tau}\right)^2 - C\int_o^\tau \beta\left(\frac{d\beta}{d\tau}\right)^2 d\tau = 0 \qquad \text{(C-11)}$$

The two energy Equations (C-8) and (C-11) lend themselves easily to numerical integration by the method of isoclines. Denoting the integral in Equations (C-8) and (C-11) by I and d/dt by a dot, then

$$I = \int_o^\tau \beta\dot{\beta}^2 d\tau$$

$$\frac{dI}{d\tau} = \beta\dot{\beta}^2 \quad \text{and} \quad \frac{dI}{d\beta} = \beta\dot{\beta}$$

The following first order equations are derivable from the two integral differential equations:

$$M^2 = \left(\frac{dI}{d\beta}\right)^2 = \frac{2(\beta^3-1)}{3\beta} - \frac{2CI}{\beta} \qquad \left(\frac{dI}{d\beta} > 0\right) \tag{C-12}$$

and

$$M^2 = \left(\frac{dI}{d\beta}\right)^2 = \frac{2(\beta^3-1)}{3\beta} - \frac{2CI}{\beta} - D\left(\frac{\beta^3-1}{\beta}\right) \quad \left(\frac{dI}{d\beta} > 0\right) \tag{C-13}$$

The initial condition for the solution to the above equations is $\beta = 1$ when $I = 0$.

In the solution by means of isoclines, curves of constant slope $M = dI/d\beta$ are constructed in the (β, I) plane and then the integral curve is drawn corresponding to the initial values $\beta = 1$, $I = 0$.

After I has been determined as a function of β and the slope $M = dI/d\beta$ determined graphically, the relationship I versus β could be obtained. The dimensionless time τ is found from the following relationships:

$$\dot{\beta} = \frac{d\beta}{d\tau} = \frac{M}{\beta} \tag{C-14}$$

and

$$\tau = \int \frac{\beta\, d\beta}{M} \tag{C-15}$$

Using Equation (C-15) a curve of dimensionless time versus dimensionless radius was constructed.

In order to carry out this solution an estimate of the initial radius R_0 is required. The surface tension of a liquid exerts a pressure on a spherical bubble in a liquid whose magnitude is given by:

$$P = \frac{2\sigma}{R} \qquad \text{(C-16)}$$

where

P = pressure difference between the inside and outside of the bubble

σ = surface tension of the liquid

R = radius of the bubble.

If a bubble is to grow in a superheated liquid, the vapor pressure of the liquid minus the pressure on the liquid must be greater than the pressure given by Equation (C-16).

$$\frac{2\sigma}{R} = P(T_o) - P$$

$$R_m = \frac{2\sigma}{P(T_o) - P}$$

where

R_m = minimum initial radius for bubble growth

$P(T_0)$ = vapor pressure of a liquid at the arbitrary temperature T_0

P = pressure on the liquid.

Table XXIII gives several values of this minimum initial radius for water, Freon 11 and Freon 113. There are two assumptions implicit in the calculation of the minimum initial radius in the above

manner:

(1) That the surface tension is applicable down to such small values of the radius.

(2) That the effect of the small radius of curvature of the drop on the vapor pressure is negligible.

There is no manner in which the validity of the first assumption can be verified. However, an estimate of the order of magnitude error inherent in the second assumption can be made utilizing thermodynamic principles. Such calculations were carried out and the per cent change in the vapor pressure was found to be negligible.

TABLE XXIII

MINIMUM INITIAL RADIUS FOR BUBBLE GROWTH UNDER ONE ATMOSPHERE

Water	R_o (microns)	5.90	1.71	0.605	0.470	0.378	0.300	0.245
	T(°F)	220	240	266	275	284	293	302
Freon-11	R_o (microns)	3.43	.615	.410	.297	.226	.178	.144
	T(°F)	80	100	110	120	130	140	150
Freon-113	R_o (microns)	7.85	2.20	1.45	.947	.765	.573	.491
	T(°F)	120	126	130	136	140	146	150

A detailed summary of the calculations for the growth of a vapor bubble in superheated water is given in the following paragraphs. The calculations for the other two fluids are not shown in any detail, but the results are depicted graphically.

1. Calculation of Dimensionless Parameters

Nozzle diameter = .031 inches, ΔP = 120 psig

Shatter temperature = 268°F

Average temperature above saturation $= \frac{268 + 210}{2} = 239°F$

Liquid viscosity $\mu = 0.25$ cp

Liquid density $\rho = 58.9$ lb/ft^3

$P_0 - P_\infty = 25.825 - 0.36 = 25.46$ lb/in^2

Initial radius $R_0 = 1.71 \times 10^{-4}$ (1.71 microns)

$$C = \frac{4\mu}{R_0 \sqrt{\rho(P_0 - P_\infty)}}$$

$$= \frac{(4)(0.25)(6.72 \times 10^{-4})(2.54)(12)}{(1.71 \times 10^{-4} \quad \sqrt{58.9\ (25.0)(144)(32.2)}}$$

$$= 0.0455$$

$$D = \frac{\sigma}{R_0(P_0 - P_\infty)}$$

Liquid Surface tension = 58.9 dynes/cm.

$$D = \frac{(58.9)(6.85 \times 10^{-5})(12)(2.54)}{(1.71 \times 10^{-4})(25.0)(144)}$$

$$= 0.201$$

2. Conversion of Dimensionless Time to Microseconds

$$\tau = \frac{t}{R_0} \sqrt{\frac{P_0 - P_\infty}{\rho} g_c}$$

$$= \frac{(t)(12)(2.54)}{1.71 \times 10^{-4}} \quad \sqrt{\frac{(25.0)(144)}{58.9} \quad (32.2)}$$

$$= 7.97 \times 10^6 t \quad \text{where} \quad t \quad \text{is measured in seconds}$$

$\tau = 7.97\ t$ where t is measured in microseconds.

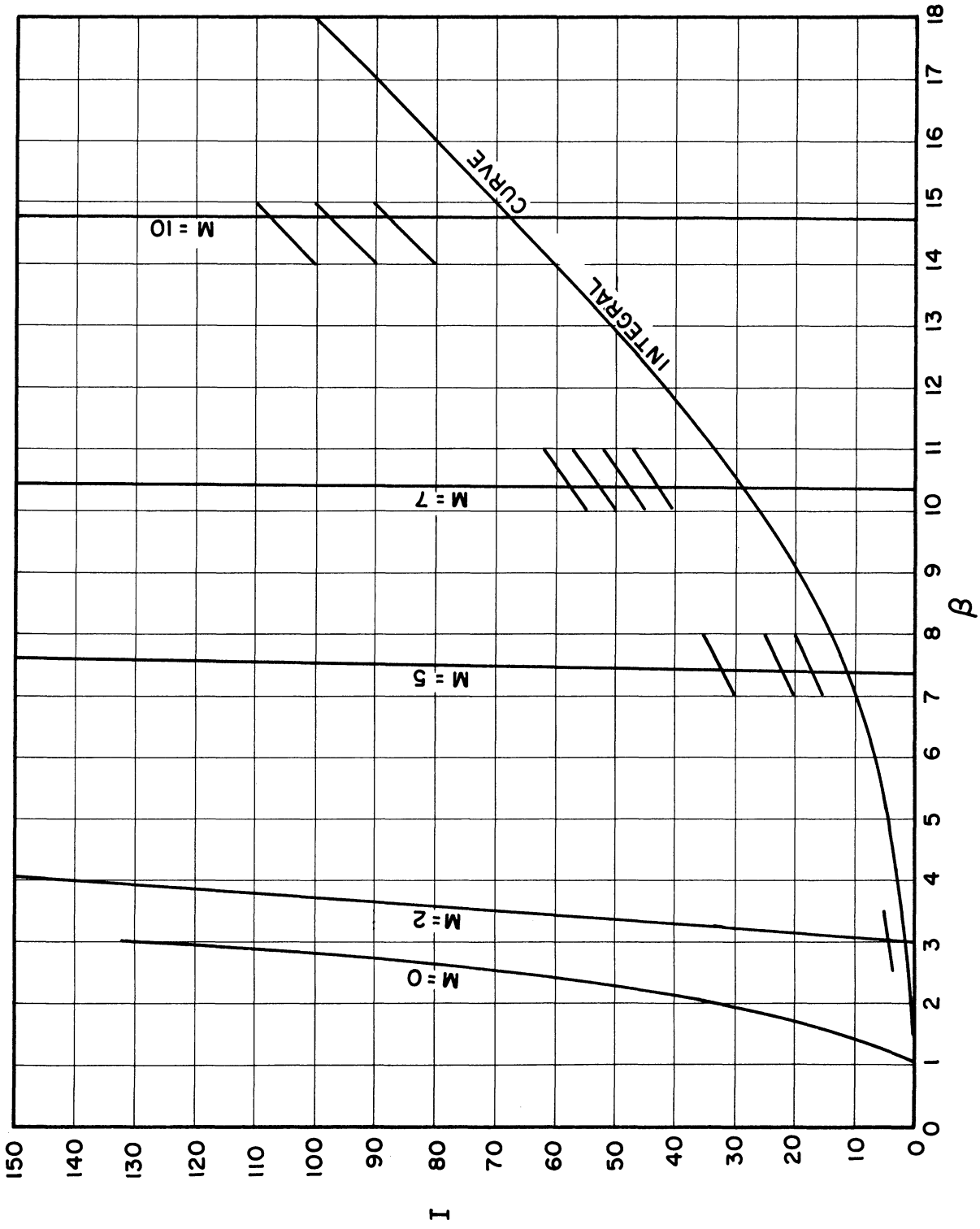

Figure 40. Isoclines for Water.

3. Calculation of Isoclines for D = 0.1695, C = 0.0423

$$M^2 = \frac{2}{3}\left(\frac{\beta^3 - 1}{\beta}\right) - \frac{2CI}{\beta} - D\left(\frac{\beta^3 - 1}{\beta}\right)$$

Substitution of the values for C and D yields the equation below, which may be used to calculate the values of the isoclines required:

$$I = 5.90(\beta^3 - 1) - 11.9\,\beta M^2$$

Figure 40 shows a graph of the isoclines in the (β, I) plane for values of M of 0, 2, 5, 7 and 10. The corresponding integral curve is also shown. In a very similar manner the corresponding curves were obtained for Freon 11 and Freon 113. By integration of Equation (C-15) the curves shown in Figure 10 were drawn. It is then a simple conversion to arrive at Figure 11.

APPENDIX D

PROBERT'S METHOD OF CALCULATING SPRAY EVAPORATION

We assume that the spray has the characteristics such that

$$R = e^{-\left(\frac{x}{\bar{x}}\right)^n} \tag{D-1}$$

R = volume or weight fraction of the spray composed of drops greater than x

$\bar{x}$ = size constant

n = distribution constant

Taking differentials one gets

$$dR = \frac{-nx^{n-1}}{\bar{x}^n} e^{-\left(\frac{x}{\bar{x}}\right)^n} dx \tag{D-2}$$

But this represents the small volume fraction of the injected spray in which drops may be taken as of diameter x. The volume of one drop is

$$\frac{\pi x^3}{6}$$

and therefore the number of drops per unit volume injected of size x is

$$\frac{dR}{\frac{\pi}{6}x^3} = \frac{6}{\pi}(-n)\frac{x^{n-4}}{\bar{x}^{-n}} e^{-\left(\frac{x}{\bar{x}}\right)^n} dx \tag{D-3}$$

Under steady state conditions there will be drops of all sizes present at any point. If at any one instant we consider drops of one size, they can be accounted for in two ways--either as drops injected at that moment and of that size or as drops injected earlier of a larger size which have evaporated down to that size. Let us consider at any instant the drops remaining from the spray injected t seconds earlier. The

drops now of size x were then of size $\sqrt{x^2 + Kt}$, where K is the evaporation coefficient. Therefore the number of drops now of size x per unit volume injected then was

$$\frac{6}{\pi}(-n)\frac{\left(\sqrt{x^2 + Kt}\right)^{n-4}}{\bar{x}^n} e^{-\left(\frac{\sqrt{x^2 + Kt}}{\bar{x}}\right)^n} dx \qquad \text{(D-4)}$$

But the number of drops of a given initial size remains constant as they evaporate. (This of course assumes no secondary atomization or coalescence and also assumes that the drop has not completely evaporated at the time of later examination.) Therefore the total number of drops of size x in the steady state is

$$\sum_{t=0}^{t=\infty} \frac{6}{\pi}(-n)\frac{\left(\sqrt{x^2 + Kt}\right)^{n-4}}{\bar{x}^n} e^{-\left(\frac{\sqrt{x^2 + Kt}}{\bar{x}}\right)^n} dx\,v\,dt \qquad \text{(D-5)}$$

The total volume of drops of size x is

$$x^3 \sum_{t=0}^{t=\infty} \frac{6}{\pi}(-n)\frac{\left(\sqrt{x^2 + Kt}\right)^{n-4}}{\bar{x}^n} e^{-\left(\frac{\sqrt{x^2+Kt}}{\bar{x}}\right)^n} dx\,v\,dt \qquad \text{(D-6)}$$

The total volume of liquid present during evaporation is

$$\sum_{x=0}^{x=\infty} \sum_{t=0}^{t=\infty} (-n)\frac{x^3}{\bar{x}^n}\left(\sqrt{x^2+Kt}\right)^{n-4} e^{-\left(\frac{\sqrt{x^2+Kt}}{\bar{x}}\right)^n} dx\,v\,dt \qquad \text{(D-7)}$$

Considering Equation (D-3), after a time interval of t seconds, these drops have decreased in diameter from x to $\sqrt{x^2 - Kt}$ and the volume of each drop is now $\frac{\pi}{6}(x^2 - Kt)^{3/2}$. Thus the volume of drops initially of size x is now

$$-n\left(\frac{X^{n-4}}{\bar{X}^n}\right) e^{-\left(\frac{X}{\bar{X}}\right)^n} \left(X^2 - Kt\right)^{3/2} dX\, V \qquad \text{(D-8)}$$

If the time allowed for evaporation is T, the drops initially of size $\sqrt{KT}$ are just disappearing and only drops initially greater than $\sqrt{KT}$ are now contributing to the remaining volume. Therefore, the total volume remaining after T seconds is

$$\sum_{X=\sqrt{Kt}}^{X=\infty} -n \frac{X^{n-4}}{\bar{X}^n} \left(X^2 - Kt\right)^{3/2} e^{-\left(\frac{X}{\bar{X}}\right)^n} \delta X\, V \qquad \text{(D-9)}$$

The volume fraction remaining is

$$\sum_{X=\sqrt{Kt}}^{X=\infty} (-n) \frac{X^{n-4}}{\bar{X}^n} \left(X^2 - Kt\right)^{3/2} e^{-\left(\frac{X}{\bar{X}}\right)^n} \delta X \qquad \text{(D-10)}$$

or

$$\int_{\sqrt{Kt}}^{\infty} (-n) \frac{X^{n-4}}{\bar{X}^n} \left(X^2 - Kt\right)^{3/2} e^{-\left(\frac{X}{\bar{X}}\right)^n} dX \qquad \text{(D-11)}$$

This integral was evaluated by Probert to give the values shown on

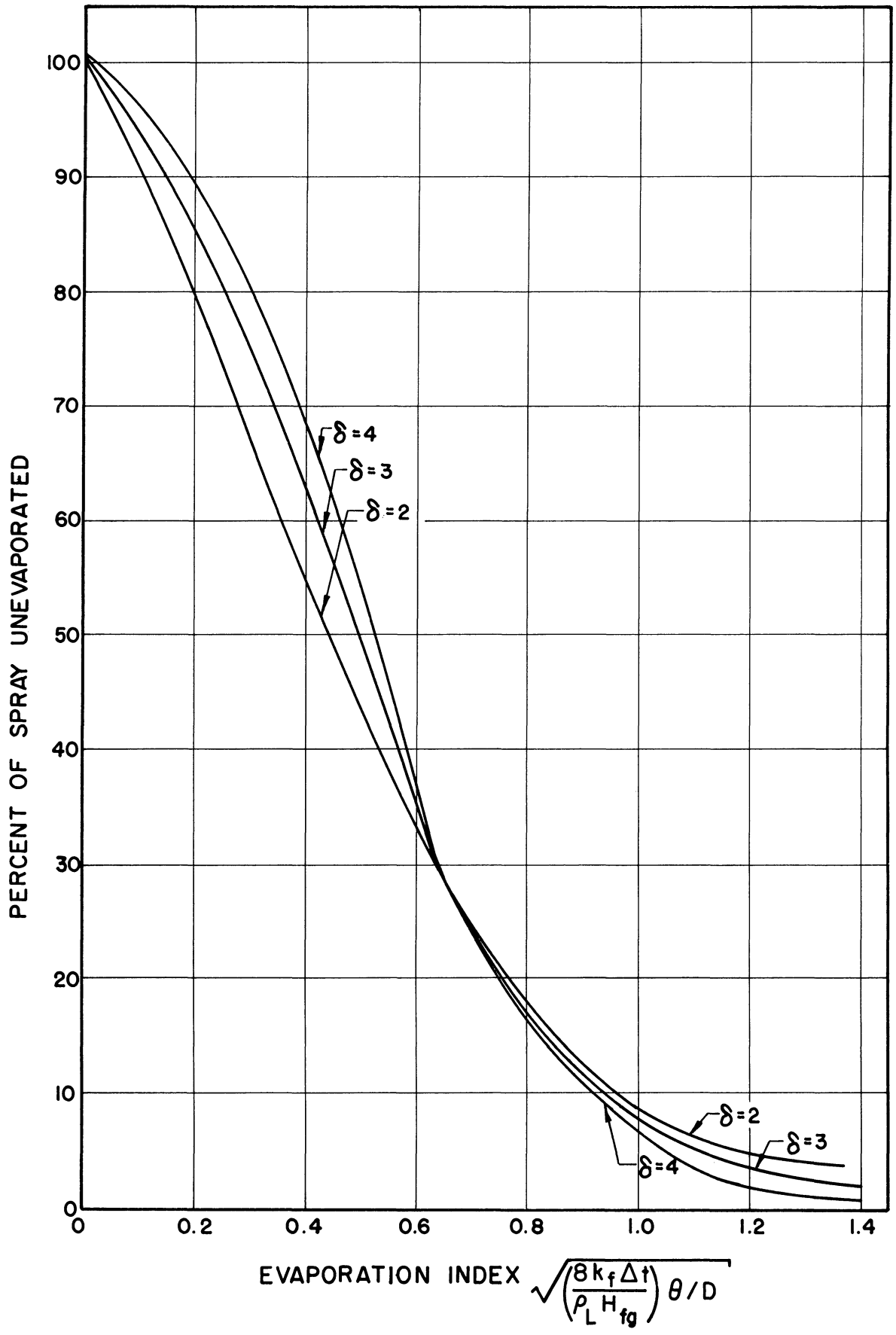

Figure 41. Per Cent of Spray Unevaporated as a Function of Evaporation Index.

Figure 41. This figure is reproduced from his article and was the basis of estimating the evaporation of the sprays studied. It is a plot of the unevaporated spray (per cent) versus $\frac{\sqrt{KT}}{\bar{x}}$ for various values of n, the dispersion parameter of the spray.

APPENDIX E

DETERMINATION OF MAGNITUDE OF GRAVITY EFFECTS

The purpose of this appendix is to calculate the ratio of the drag forces to the gravity forces which act upon the droplets encountered in the sprays studied in this system. Let us assume that all of the drops are spherical in shape. Then the weight of an individual drop is given by:

$$W = \frac{4}{3}\pi R^3 \rho \qquad \text{(E-1)}$$

The resistance (drag) forces may be calculated by one of the three formulae below,[17] since for a spherical particle, it is well known that the resistance R is

$$R = \frac{\pi}{8} C_D \rho_A V^2 D^2 \qquad \text{(E-2)}$$

where

ρ_A = air density, lb/ft^3

$$C_D = \frac{24}{N_{Re}}, N_{Re} < 2$$

$$C_D = 0.4 + \frac{40}{N_{Re}}, 2 < N_{Re} < 500$$

$$C_D = 0.44, N_{Re} > 500.$$

The above relations may be manipulated to give:

$$R = 3\pi\mu V D \qquad N_{Re} < 2 \qquad \text{(E-3)}$$

$$R = \pi(0.05\rho A V^2 D^2 + 5\mu V D) \qquad 2 < N_{Re} < 500 \qquad \text{(E-4)}$$

$$R = 0.055\pi\rho A V^2 D^2 \qquad N_{Re} > 500 \qquad \text{(E-5)}$$

Using Equations (E-3), (E-4) or (E-5), whichever is appropriate, it is a routine calculation to determine the relative value of the ratio of the resistance to the gravity effects. Strictly speaking, Equations (E-3), (E-4) and (E-5) apply only to droplets moving through a quiescent gas stream, and not to a system in which there is a relative air velocity or in which evaporation is significant. The net result of the two effects of evaporation and relative air velocity will likely tend to make the calculated results conservative.

Table XXIV below shows the values of R/W, the ratio of the resistance forces to the gravity forces, for a set of typical drop sizes and velocities. A sample calculation is also given. The data in the table are for water droplets, however similar calculations carried out for Freon 11 showed values of R/W of about the same value for each size of drop.

TABLE XXIV

RATIO OF RESISTANCE TO GRAVITY FORCES

Size Range	Drop Diameter Microns	Typical Drop Velocity (Ft/Sec)	N_{Re}	R/W
2	12.05	6.0	2.07	79.2
3	17.05	7.5	2.76	55.7
4	24.1	11.0	5.73	334
5	34.2	12.0	8.77	189
6	48.2	15.0	15.6	126
7	68.5	25.0	37.0	125
8	96.5	50.0	104.1	188
9	136.5	75.0	221	215
10	193	100	447	245

For size range 2, taking the density of air as 1.29×10^{-3} grams per cubic centimeter and the viscosity of air as 1.79×10^{-4} poise, then

$$R = \pi(0.05 \times 1.293 \times (6.0 \times 30.4)^2 \times (12.05 \times 10^{-4})^2 + 5 \times 1.79 \times 10^{-4} \times 6.0 \times 30.4 \times 12.05 \times 10^{-4})$$

$$= 70.3 \times 10^{-6} \text{ dynes}$$

$$= 71.7 \times 10^{-9} \text{ gms weight}$$

$$W = \frac{\pi D^3}{6}$$

$$= \frac{\pi(12.05 \times 10^{-4})^3(1.0)}{6}$$

$$= 9.05 \times 10^{-10} \text{gms weight}$$

$$R/W = \frac{71.7 \times 10^{-9}}{9.05 \times 10^{-10}} = 79.2$$

APPENDIX F

TABLE XXV

CALCULATED VALUES OF CONSTANTS IN DISTRIBUTION FUNCTIONS

1. Rosin Rammler Equation

Values of Constants in Equation (8.8a)

Run	Location	n	b	Correlation Coefficient
1	1	4.45	4.56×10^{8}	0.929
1	2	4.86	1.18×10^{7}	0.969
1	3	6.44	1.86×10^{12}	0.975
1	4	5.85	1.37×10^{11}	0.986
1	Total	4.94	3.05×10^{9}	0.977
2	1	4.40	7.08×10^{8}	0.961
2	2	3.85	2.01×10^{8}	0.959
2	3	3.74	2.61×10^{7}	0.966
2	4	5.53	3.58×10^{10}	0.985
2	Total	3.67	5.05×10^{7}	0.964
3	1	3.38	1.72×10^{8}	0.982
3	2	3.32	2.03×10^{7}	0.973
3	3	4.82	2.45×10^{9}	0.980
3	4	4.85	2.45×10^{9}	0.980
3	Total	3.35	2.50×10^{8}	0.970
4	1	4.46	3.12×10^{8}	0.965
4	2	3.83	7.27×10^{7}	0.974
4	3	3.86	1.87×10^{8}	0.983
4	4	4.10	2.31×10^{8}	0.977
4	Total	3.81	9.88×10^{7}	0.979
5	1	4.46	3.12×10^{8}	0.965
5	2	3.83	7.27×10^{7}	0.975
5	3	3.87	1.87×10^{8}	0.983
5	4	4.11	2.32×10^{8}	0.977
5	Total	3.81	9.88×10^{7}	0.979
6	1	3.53	1.56×10^{5}	0.977
6	2	3.07	3.55×10^{4}	0.990
6	Total	3.33	8.14×10^{4}	0.982
7	1	4.15	9.42×10^{5}	0.975
7	2	4.11	1.02×10^{6}	0.969
7	3	4.07	8.53×10^{5}	0.985
7	Total	4.08	8.96×10^{6}	0.974
8	1	4.08	3.58×10^{5}	0.986
8	2	3.49	1.05×10^{5}	0.956
8	3	4.58	7.76×10^{5}	0.995
8	Total	3.74	2.46×10^{5}	0.965
9	1	3.80	2.23×10^{5}	0.971
9	2	3.65	2.50×10^{5}	0.925
9	3	3.45	3.50×10^{5}	0.980
9	Total	3.75	2.5×10^{5}	0.977
10	1	6.07	2.23×10^{10}	0.971
10	2	7.22	2.65×10^{12}	0.979
10	3	6.87	7.95×10^{10}	0.977
10	Total	7.33	4.70×10^{12}	0.977

TABLE XXV (CONT'D)

2. Nukiyama Tanasawa Equation

Values of Constants in Equation (8.9)

Run	Location	a ($\times 10^{-3}$)	b	Correlation Coefficient
1	1	2.59	5.91	0.963
1	2	3.36	4.86	0.963
1	3	1.44	4.52	0.986
1	4	1.41	0.971	0.971
1	Total	3.58	4.76	0.956
2	1	7.54	5.23	0.956
2	2	15.0	5.63	0.942
2	3	29.7	6.09	0.950
2	4	2.78	4.68	0.959
2	Total	57.5	6.39	0.948
3	1	7.41	5.19	0.792
3	2	40.5	6.26	0.924
3	3	1.18	4.32	0.941
3	4	1.18	4.42	0.941
3	Total	114.0	6.77	0.940
4	1	3.37	4.93	0.951
4	2	4.56	5.05	0.907
4	3	10.2	5.40	0.900
4	4	.457	3.33	0.908
4	Total	22.8	5.49	0.888
5	1	0.631	3.98	0.634
5	2	9.88	5.38	0.949
5	3	3.15	4.75	0.958
5	4	1.84	4.68	0.982
5	Total	42.5	6.10	0.935
6	1	1.17	4.52	0.962
6	2	.847	4.39	0.937
6	Total	1.015	4.46	0.952
7	1	.610	4.16	0.974
7	2	13.07	5.34	0.947
7	3	.213	3.64	0.970
7	Total	.167	3.48	0.968
8	1	1.51	4.70	0.968
8	2	2.53	4.85	0.971
8	3	.209	3.87	0.966
8	Total	3.11	4.97	0.970
9	1	7.08	5.35	0.953
9	2	16.28	5.57	0.974
9	3	2.58	4.81	0.982
9	Total	22.55	5.74	0.970
10	1	2.78	4.87	0.974
10	2	2.32	4.78	0.974
10	3	0.786	4.28	0.971
10	Total	1.07	4.43	0.973

APPENDIX G

LIST OF REFERENCES

1. Balje, O.E., and Larson, L.V., "The Mechanism of Jet Disintegration," AAF Air Material Command, Report No. MCREXE-664-531B (1949).

2. Bankoff, S.G., and Mikesell, R.D., "Growth of Bubbles in a Liquid of Initially Nonuniform Temperature," Paper No. 58-A-105, Annual Meeting ASME, 1958.

3. Baron, T., Tech. Report No. 4, Eng. Exp. Station, University of Illinois, (1947).

4. Basset, A.B., A Treatise on Hydrodynamics, Deighton, Bell and Co., Cambridge, 1888.

5. Brown Ralph, Ph.D. Thesis, University of Michigan, 1960.

6. Castleman, R.A., Journal Res. Nat. Bur. Standards, 6, (1931), 369.

7. Crowe, Clayton, Ph.D. Thesis, University of Michigan, 1962.

8. Davies, C.N., Symposium on Particle Size Analysis, Inst. Chem. Eng. and Soc. Chem. Ind., London, Feb. 28, 1947.

9. De Juhasz, K.J. (ed.), Spray Literature Abstracts, ASME, New York (1959).

10. Dodd, K.N., Journal of Fluid Mechanics, Vol. 9, Part 2, (Oct. 1960) 175.

11. **E.I. du Pont de Nemours** and Co., "Thermodynamic Properties of Freon 11, Trichloromonofluoromethane."

12. **E.I. du Pont de Nemours** and Co., "Thermodynamic Properties of Freon 113, Trichlorotrifluoroethane."

13. El Wakil, M.M., Uyehara, O.A., and Myers, P.S., Nat. Advisory Comm. Aeronaut. Tech. Note 3179 (1954).

14. Fledderman, R.G., and Hanson, A.R., University of Michigan Eng. Research Report CM667 (June 1951).

15. Forster, H.K., and Zuber, N., Jour. Appl. Physics, 25, No. 4 (1954), 474-478.

16. Frössling, N., Gerlands Beitre Geophys., 52, (1938), 170.

17. Giffen, E., and Mursaszew, A., "The Atomization of Liquid Fuels", John Wiley and Sons Inc., New York, 1953.

18. Gorbatschew, S.W., and Nikiforowa, W.M., Koll. Z., 73,(1935), 14.

19. Griffith, P., Trans. ASME, 80,(1958), 721.

20. Haenlein, A., Forsch. Gebiete Ingenieur Forschungsheft, 2, (1931), 139.

21. Hinze, J.O., AIChE Journal, 1, (1955).

22. Jimze, J.O., "On the Mechanism of Disintegration of High Speed Liquid Jets," Sixth Int. Congress Appl. Mechanics, Paris, 1946.

23. Kesler, G.H., Sc.D. Thesis, Mass. Inst. Tech., 1952.

24. Kottler, F., J. Franklin Inst., 250, (1950), 339, 419.

25. Lamb, Sir Horace, "Hydrodynamics", Dover, 1945.

26. Lane, W.R., Ind. Eng. Chem., 43, (1951), 1312.

27. Liu, Vi-Cheng, Dept. of U.S. Air Force, Project 2160, 1955.

28. Littaye, G., Comptes Rendus, 217, No.4, (1943), 99, 340.

29. Littaye, G., Comptes Rendus, 218, (1944), 440.

30. Lyons, D.B., Thesis McGill Univ., 1951.

31. Manning, W.P., and Gauvin, W.H., AIChE Journal, 6, (1960), 184.

32. Marshall, W.R., Trans. ASME, 77, (1955), 1377.

33. Mehlig, H., A.T.Z., 37, (1934), 411.

34. Miesse,C.C., Ind. Eng. Chem., 47, (1955), 1690.

35. Mirsky, W., Ph.D. Thesis, Univ. of Mich., 1956.

36. Mugele, R.A., and Evans, H.D., Ind. Eng. Chem., 43, (1951), 1317.

37. Nukiyama, S., and Tanasawa, Y., Trans. Soc. Mech. Eng. (Japan), 4, No. 14, (1938), 86 and No. 15, (1938), 138, 5, No. 18, (1939), 63, No. 22, (1940), II-7, and No. 23, (1940), II-8.

38. Ohnesorge, W., Z. Angew. Math. and Mech., 16, (1936), 355.

39. Pearcey, T., and Hill, G.W., Australian Journal of Physics, 9, No. 1, 1956.

40. Plesset, M.S., and Zwick, S.A., J. Appl. Phys., 25, No.4, 1954.

41. Poritsky, H., Proc. of First U.S. National Congress of Applied Mechanics, 1951.

42. Probert, R.P., Phil. Mag., 37, (1946), 94.

43. Putnam, A.A., et al., "Injection and Combustion of Liquid Fuels", WADC Tech. Rept. 56-344, March, 1957.

44. Ranz, W.E., and Binark, H., ASME Paper No. 58-A-284, 1958.

45. Ranz, W.E., and Marshall, W.R., Chem. Eng. Prog., 48, (1952), 141, 173.

46. Rayleigh, Lord, Proc. London Math. Soc., 34, (1892), 153.

47. Rayleigh, Lord, Proc. London Math. Soc., 10, (1978), 4.

48. Richardson, E.G., Appl. Sci. Res., A4, (1954), 374.

49. Sauter, J., NACA Tech. Memo. No. 390, 1926.

50. Schweitzer, P.H., Penn. State Coll. Bull., No.12, November, 1930.

51. Shu, S.S., Proc. of First U.S. National Congress of Appl. Mech., 1951.

52. Siestrunck, R., Comptes Rendus, 215, (1942), 404.

53. Sjenitzer, F., Chem. Eng. Sci., 1, (1952), 101.

54. Soo, S.L., Chem. Eng. Sci., 5, (1956), 57.

55. Steinour, H.I., Ind. Eng. Chem., 36, (1944), 618, 840, 901.

56. Thiemann, A.E., A.T.Z., 37, (1934), 429.

57. Thiemann, A.E., A.T.Z., 38, (1935), 484.

58. Volk, W., "Applied Statistics for Engineers", McGraw-Hill, 1958.

59. Weber, C., Zeit. fuer Angew. Math. und Mech., 11, (1931), 136.

60. York, J.L., Ph.D. Thesis, Univ. of Michigan, 1949.

61. York, J.L., and Stubbs, H.E., Trans. ASME, 74, (1952), 1157.